This manuscript has not been peer reviewed and has not been formally accepted for publication.

This work has been submitted to *Nature Communications* and is currently in review.

Please note that the final peer reviewed version of this manuscript may differ in content from this preprint. An updated, reviewed and revised, version of this manuscript will be made available via a DOI link on this webpage if/when it has been accepted following peer review.

This manuscript comprises the Main Text and Supplementary Information of the article submitted for peer review.

Ediacaran coupling of climate and biosphere dynamics

Thomas W. Wong Hearing[1], Benjamin Tindal[2], Thomas Vandyk[3,4], Lin Na[1,5], Alexandre Pohl[6], Alexander G. Liu[7], Thomas H. P. Harvey[1], and Mark Williams[1]

[1]Centre for Palaeobiology and Biosphere Evolution, School of Geography, Geology and the Environment, University of Leicester, Leicester, LE1 7RH, UK.

[2]Chief Scientist's Directorate, Natural England, 8 City Walk, Leeds, LS11 9AT, UK.

[3]Open University, Gass Building, Walton Hall, Milton Keynes, MK7 6AA, UK.

[4]School of Natural Sciences, Birkbeck University of London, Malet Street, London WC1E 7HX, UK.

[5]State Key Laboratory of Palaeobiology and Stratigraphy, Nanjing Institute of Geology and Palaeontology, Chinese Academy of Sciences, Beijing East Road 39, 210008 Nanjing, China

[6]Biogéosciences, UMR 6282 CNRS, Université de Bourgogne, 6 Boulevard Gabriel, 21000 Dijon, France.

[7]Department of Earth Sciences, Downing Street, University of Cambridge, Cambridge, CB2 3EQ, UK.

Abstract

Throughout the Phanerozoic (538.8 Ma to present), climate change is demonstrably linked to radiations, extinctions, and turnovers in the biosphere. Here, we show that this connection existed in the late Ediacaran (~579 to 538.8 Ma), the first interval in Earth's history to host complex macro-organisms, including early metazoans. Current correlations of glacial sedimentary deposits have been used to argue for either one long (>20 Myr) or up to four short (1 to 5 Myr) ice ages during the mid- to late Ediacaran. Here, we evaluate the dating, correlation, and glaciogenicity of candidate Ediacaran glaciogenic deposits and find evidence for two icehouse intervals (mid-Ediacaran, ~593 to 579 Ma; and late Ediacaran, ~565 to ~550 Ma) alternating with greenhouse intervals (late Ediacaran, ~579 to 565 Ma; and terminal Ediacaran, ~550 Ma to Cambrian). Both icehouse intervals were characterised by high to mid-latitude glaciation of ~10 to 15 Myr duration, with expansion and retreat of ice sheets. These changes in climate state correspond in time with apparent step-changes in the late Ediacaran biosphere, including changes in standing diversity and taxonomic composition of palaeocommunities. Our results support a Phanerozoic-style coupling of global climate and biosphere during the early stages of animal evolution.

Introduction

Changes in Earth's climate and biosphere are closely linked throughout the Phanerozoic Eon, spanning the last ~539 million years. Transitions between globally cooler and warmer conditions are implicated in extinctions, diversifications, and biotic turnovers in the Phanerozoic fossil record (e.g. Erwin 2009; Bond and Grasby 2017; Fenton *et al.* 2023; Woodhouse *et al.* 2023). However, it is unclear whether such relationships existed in Earth's earliest metazoan biosphere, that of the late Ediacaran Period (~580 to 538.8 Ma). Here, we build on recent advances in stratigraphic correlation (e.g. Rooney *et al.* 2020; Yang *et al.* 2021; Bowyer *et al.* 2023, 2024; Busch *et al.* 2023) and palaeobiology (e.g. Boag *et al.* 2016, 2024; Muscente *et al.* 2019; Boddy *et al.* 2021; Surprenant and Droser 2024) to interrogate the co-evolution of physical and biological components of the Earth System through the Ediacaran Period.

The Ediacaran Period follows the Cryogenian Period, supposedly characterised by extreme and long-lasting 'snowball' climate conditions (Hoffman *et al.* 2017), and precedes the prolonged greenhouse climate of the Cambrian Period (Scotese *et al.* 2021; Wong Hearing *et al.* 2021). The Ediacaran Period can therefore be viewed as a transitional interval in Earth's climate history, coincident with the early diversification of animals and major perturbations and reorganisation of the carbon cycle (Butterfield 2009; Wood *et al.* 2019; Xiao and Narbonne 2020).

In recent years abundant evidence for glaciogenic sedimentary deposits of broadly mid- to late Ediacaran age has been recognized (e.g. Hambrey and Harland 1981; Youbi *et al.* 2020; Vandyk *et al.* 2021; Linnemann *et al.* 2022; Retallack 2022; Tindal 2023; Wang *et al.* 2023a, b; Niu *et al.* 2024). Candidate glacial deposits have been variously considered to collectively represent several very short glaciations (e.g. Pu *et al.* 2016; Linnemann *et al.* 2022; Retallack 2022; Niu *et al.* 2024), or one continuous 20 to 40 million year icehouse interval with a shifting locus (e.g. Wang *et al.* 2023a, b). However, each of these studies has included different sets of putative Ediacaran glaciogenic deposits, and compared them within different correlation frameworks (Table 1; Figure S1; Youbi *et al.* 2020; Retallack 2022; Wang *et al.* 2023a, b; Niu *et al.* 2024). The resulting uncertainty (Table 1) over the glaciogenicity and correlations between late Neoproterozoic deposits has hindered assessments of Ediacaran climate evolution during critical biosphere events. For example, it is unclear whether the largest carbon cycle perturbation in the geological record, the Shuram negative carbon isotope excursion (CIE;$\delta^{13}C$ values as low as –12 ‰; ~574 to 566 Ma; Rooney *et al.* 2020; Yang *et al.* 2021; Busch *et al.* 2023), occurred when Earth was in a greenhouse (Shields *et al.* 2019; Bergmann *et al.* 2022) or an icehouse (Wang *et al.* 2023a, b) climate state.

Table 1. Comparison of published literature compilations and correlations of candidate Ediacaran glacial deposits. Each row indicates the total number of Ediacaran glacial deposits identified by the study cited (at left), as well as their proposed association with any 'named' glacial event. For reference, and not shown here for legibility: Tindal (2023) identified 224 potentially glaciogenic deposits with radiometric age constraints compatible with Ediacaran deposition, although poor age constraints for some mean many of these could be Cryogenian; Youbi et al. *(2020) identified 25 candidate glaciogenic deposits of Ediacaran age grouped into 12 predominantly local or regional glaciations and concluded that most were plausibly correlated with a ~580 Ma Gaskiers glaciation. See Figure S1 and Supplementary Data 1 for further details on these compilations.*

Compilation	**Unique deposits**	**Gaskiers[a]**	**Fauquier[b]**	**Bou Azzer[c]**	**Hankalchough[d]**	**GEG[e]**	**Other/ Uncertain**
Retallack (2022)	31	4	5	9	12	–	1
Wang *et al.* (2023a, b)	39	–	–	–	–	39	–
Niu *et al.* (2024)	50	18	3	10	14	–	5

[a]Gaskiers glaciation: 581 to 579 Ma (Retallack 2022; Niu *et al.* 2024).

[b]Fauquier glaciation: 572 to 570 Ma (Retallack 2022), or 571 Ma (Niu *et al.* 2024).

[c]Bou Azzer: 566 to 564 Ma (Retallack 2022), or 565 to 560 Ma (Niu *et al.* 2024).

[d]Hankalchough: 555 to 549 Ma (Retallack 2022), or 563 to 551 Ma (Niu *et al.* 2024).

[e]Great Ediacaran Glaciation: GEG; ~580 to 560 Ma or possibly 594 to 546 Ma (Wang *et al.* 2023a, b).

Here, we combine sedimentological and palaeobiological data in a refined chronostratigraphic framework to evaluate the hypothesis that there is a temporal link between global climate state and biodiversity dynamics (faunal turnovers) in the late Ediacaran geological record. We critically evaluate both the dating and sedimentological evidence for putative mid- to late Ediacaran glaciogenic deposits, focusing on those which could plausibly be younger than 600 Ma. We consider all deposits included in recent compilations (Youbi *et al.* 2020; Retallack 2022; Tindal 2023; Wang *et al.* 2023a, b; Niu *et al.* 2024) as well as other deposits that could reasonably fall into the age bracket, rigorously assess their age constraints within a robust chronostratigraphic framework, and, uniquely, systematically assess the evidence that each deposit was actually formed by ice-related processes, i.e. their likely glaciogenicity, for which we assign a star rating ranging from "unequivocal" (rating five) to "insufficient" evidence (rating zero), following Tindal (2023; Table 2; Methods; Table S1). Hereafter, we distinguish between icehouse and greenhouse climate states by the presence or absence of low altitude continental ice sheets respectively, and note that the presence of sea ice alone is insufficient evidence of icehouse conditions.

Table 2. Summary of the star ratings assigned to candidate Ediacaran glaciogenic deposits included in published literature compilations, presented here as: the number of deposits (percentage of deposits to nearest 1 %) per star rating for each compilation. Most previous compilations include a considerable number of deposits that have weak (two star or less) sedimentological or geomorphological evidence for glacial conditions. See Tindal (2023), Methods, Table S1, and Supplementary Information for methodology and ratings.

Compilation	**Five star**	**Four star**	**Three star**	**Two star**	**One star**	**Zero star**	**Unrated**[a]
Youbi *et al.* (2020)	0	10	11	3	0	0	1
	(0 %)	(40 %)	(44 %)	(12 %)	(0 %)	(0 %)	(4 %)
Retallack (2022)	0	7	8	2	2	1	11
	(0 %)	(23 %)	(26 %)	(6 %)	(6 %)	(3 %)	(35 %)
Tindal (2023)[b]	3	62	84	41	16	18	0
	(1 %)	(28 %)	(38 %)	(18 %)	(7 %)	(8 %)	(0 %)
Wang *et al.* (2023a, b)	0	14	17	3	1	2	2
	(0 %)	(36 %)	(44 %)	(8 %)	(3 %)	(5 %)	(5 %)
Niu *et al.* (2024)	1	15	18	3	2	3	8
	(2 %)	(30 %)	(36 %)	(6 %)	(4 %)	(6 %)	(16 %)

[a]Deposits included in a compilation but not given an explicit rating in Tindal's (2023) Appendix 2.

[b]Tindal's (2023) compilation includes many deposits that are most likely Cryogenian (based on non-radiometric age constraints) in the plausible Ediacaran dataset.

Extrapolating from the Phanerozoic Earth System, we would expect to see in the fossil record a biosphere response to changing climate via changes in standing diversity and/or taxonomic composition (e.g. Erwin 2009; Woodhouse *et al.* 2023). The absence of this pattern in the Ediacaran (the null hypothesis) would indicate (a) that geological and collection biases are obscuring our ability to read the Ediacaran geological record, and/or (b) that our data have insufficient age controls for accurate correlation, and/or (c) that the Ediacaran biosphere had a fundamentally different relationship to the climate system than the Phanerozoic biosphere. Understanding past temporal relationships between the biosphere and climate system is essential for evaluating hypotheses of how animal evolution affected Earth's climate evolution, and *vice versa*.

Results

Recent publications that compile, compare or review candidate Ediacaran glaciogenic deposits (Table 1) can be grouped into three broad categories: (a) those that correlate most glacial evidence to the Gaskiers glaciation (~580 Ma; Youbi *et al.* 2020), (b) those which argue for two to four short-lived (~1 to 5 Myr) glaciations (Linnemann *et al.* 2018, 2022; Retallack 2022; Niu *et al.* 2024), and (c) those that argue for a single, protracted, late Ediacaran icehouse of ~20 to 40 Myr duration (Wang *et al.* 2023a, b). Figure 1 shows our updated compilation of candidate late Ediacaran glaciogenic deposits, following scoring by us to assess the strength of evidence for glaciogenicity. The most parsimonious interpretation of our data identifies two icehouse intervals of 10 to 15 Myr in duration, here termed the mid-Ediacaran icehouse (MEIH; ~593 to 579 Ma) and the late Ediacaran icehouse (LEIH; ~565 to ~550 Ma), separated by greenhouse intervals termed the late Ediacaran greenhouse (LEGH; ~579 to 565 Ma), and the terminal Ediacaran greenhouse (TEGH; ~550 Ma to Cambrian).

126 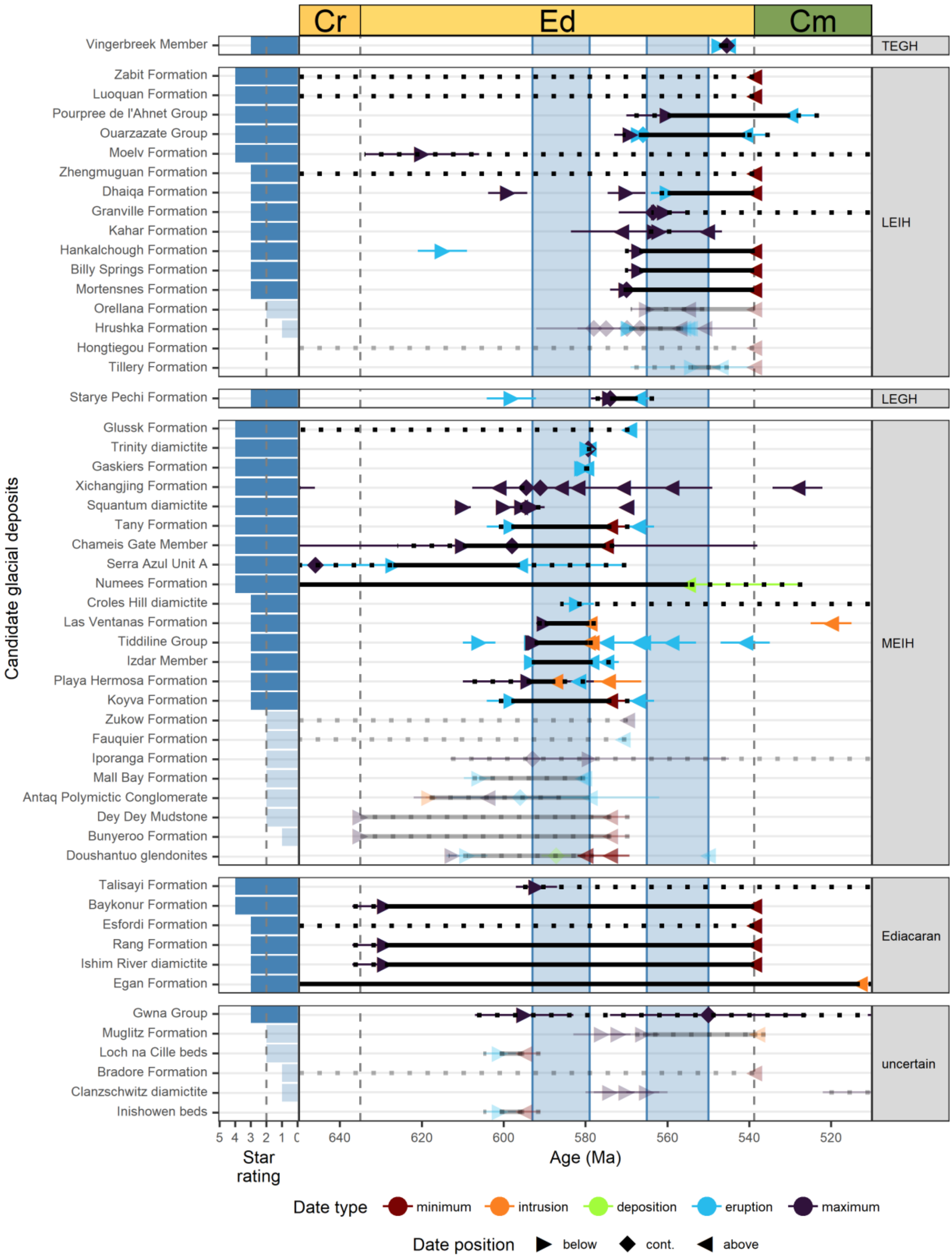

127 *Figure 1. Age constraints on candidate Ediacaran glaciogenic deposits grouped by their likely depositional interval. TEGH:*
128 *terminal Ediacaran greenhouse; LEIH: late Ediacaran icehouse; LEGH: late Ediacaran greenhouse; MEIH: mid-Ediacaran*
129 *greenhouse; Ediacaran: deposits constrained only to the Ediacaran Period; uncertain: deposits that may be Ediacaran in age*
130 *but with questionable constraints. Thick solid lines show the age range of each deposit, which is bracketed by depositional*
131 *age constraints below and above, excluding only "maximum" date type (e.g. detrital zircons); thick dotted lines show the*
132 *full possible age range including analytical uncertainty for each deposit. Age constraints are from radiometric dates, carbon*
133 *isotope stratigraphy, and terminal Ediacaran or Palaeozoic biostratigraphic data (see Methods; Supplementary Data 1).*

Date type: how the age constraint relates to the candidate glaciogenic deposit; Date position: whether the age constraint is stratigraphically below, contemporaneous (cont.) with, or above the candidate glaciogenic deposit. Deposits that were scored less than three stars are faded. Vertical blue regions show the likely intervals of the mid-Ediacaran icehouse (~593 to 579 Ma) and the late Ediacaran icehouse (~565 to 550 Ma). Cr: Cryogenian (pars.); Ed: Ediacaran; Cm: Cambrian (pars.). See also main text Supplementary Figure S2.

593 to 579 Ma: mid-Ediacaran icehouse (MEIH)

Our compilation demonstrates that there is strong support for Earth's climate being in an icehouse state in the mid-Ediacaran between ~593 to 579 Ma (Figure 1), even when candidate glacial deposits of low sedimentological confidence (less than three star) are discounted. This icehouse was previously considered to be a short-lived cold interval of perhaps less than 1 Myr, characterised as the 'Gaskiers glaciation' at ~580 Ma (Pu *et al.* 2016). There is now evidence for icehouse conditions lasting perhaps ~5 Myr on Avalonia (Fitzgerald *et al.* 2024; Mills *et al.* 2024), ~10 Myr on the Rio de Plata craton (Mallmann *et al.* 2007; Oyhantçabal *et al.* 2007), and ~10 to 15 Myr on North African Gondwana (Letsch *et al.* 2018), with a consistent termination age of ~579 Ma (Figure 1). Often called the 'Gaskiers glaciation', here we use the term 'mid-Ediacaran icehouse' (MEIH) to emphasise its broader palaeogeographical and temporal distribution.

Of these deposits, the Gaskiers Formation and Trinity diamictite of Avalonian Newfoundland, both rated four star deposits (Tindal 2023), have the tightest age constraints for the termination of glacial activity. Underlying the Gaskiers Formation in Newfoundland, the Mall Bay Formation is only rated a two star deposit (Supplementary Information) but indicates evidence of cold conditions on Avalonia prior to deposition of the Gaskiers and Trinity diamictites (Fitzgerald *et al.* 2024). Overlying the Gaskiers Formation, turbidites of the Drook Formation were deposited in similar deep water slope settings and contain some of the oldest Ediacaran macrofossils (Matthews *et al.* 2020), but appear to lack evidence of glacial influence. This is despite much palaeontological and stratigraphical research on the upper part of this unit (Hofmann *et al.* 2008; Matthews *et al.* 2020), and may indicate a sharp change in the local climate regime at ~579 Ma (Pu *et al.* 2016). Strata of the lower Drook Formation may offer insights into the climatic transition at the end of the MEIH. Also on Avalonia, the Squantum Member diamictite (Roxbury Conglomerate Formation, Boston Basin, northeast USA) has been radiometrically constrained to between ~595 to 570 Ma (Thompson and Bowring 2000; Thompson *et al.* 2007). Although rated a four star deposit (Tindal 2023), the reliability of reports of striated clasts has been called into question, with some studies concluding there is no strong evidence of glaciogenicity (Dott 1961; Socci and Smith 1990; Carto and Eyles 2012; Supplementary Information). Nevertheless, the glaciomarine Gaskiers and Trinity diamictites provide strong positive evidence for low altitude glaciation on Avalonia, terminating at ~579 Ma.

Across several sections in Morocco (North African Gondwana), candidate glaciogenic strata of the Tiddiline Group and Izdar Member, both rated three star units (Tindal 2023), were deposited between ~593 to 579 Ma (Thomas *et al.* 2002; Inglis *et al.* 2004; Blein *et al.* 2014; Letsch *et al.* 2018). The diamictites are interpreted as both terrestrial and marine tillites, providing evidence for proximal glacial activity, whereas the laminites with dropstones reflect more distal glaciomarine conditions (Letsch *et al.* 2018). The repeated alternation of tillites and laminites evidences local waxing and waning of low altitude land ice on Gondwana (Letsch *et al.* 2018).

The Las Ventanas Formation on the Río de Plata craton, southeast Uruguay, rated as a three star deposit (Tindal 2023), is constrained by radiometric dates to between 590 ± 2 Ma to 579 ± 1.5 Ma (Mallmann *et al.* 2007; Oyhantçabal *et al.* 2007), consistent with less precise radiometric ages and acritarch biostratigraphy (Bossi *et al.* 1993; Sanchez Bettucci and Linares 1996; Gaucher *et al.* 2008; Pecoits *et al.* 2011). The Las Ventanas Formation was deposited in a tectonically active setting with evidence of non-glaciogenic debris flow deposits, but the candidate glaciogenic deposits include diamictites and fine-grained rhythmites hosting outsized clasts with facetted surfaces (Pecoits 2003; Gaucher *et al.* 2008; Pecoits *et al.* 2008, 2011).

On the Baltic craton, the Tany and Koyva formation diamictites (Serebryanka Group, central Urals, Russia), were deposited between 598.1 ± 6.0 Ma and the EN2 carbon isotope excursion (~579 Ma; Chumakov 2011; Grazhdankin *et al.* 2011; Chumakov *et al.* 2013; Maslov *et al.* 2013). Although rated four and three star deposits (Tindal 2023) respectively, the Tany and Koyva formations were deposited in an outer shelf to slope setting and the diamictites are interbedded with various gravity-driven mass flow-derived deposits including flysch, conglomerates, breccias, and turbidites (Chumakov 2011). Further sedimentological research is needed to fully assess whether these deposits are glaciogenic or gravitationally derived (Supplementary Information).

579 to 565 Ma: late Ediacaran greenhouse (LEGH)

The late Ediacaran experienced a major perturbation to the carbon cycle, as recorded by the Shuram negative CIE (Xiao and Narbonne 2020; Yang *et al.* 2021; Busch *et al.* 2022), which began no earlier than 575 Ma (Rooney *et al.* 2020; Yang *et al.* 2021) and terminated after 566.9 ± 3.5 Ma (Busch *et al.* 2023). The Shuram CIE has been studied in globally distributed sections and a wide range of depositional settings (e.g. Yang *et al.* 2021; Bergmann *et al.* 2022; Busch *et al.* 2022; Cantine *et al.* 2024), yet only a single unit preserves a possible Shuram-correlative CIE alongside potential glacial evidence: the lower Starye Pechi Formation diamictite (Sylvitsa Group, central Urals, Russia), rated a three star deposit (Tindal 2023) and radiometrically constrained to between 598.1 ± 6.0 Ma (Maslov *et al.* 2013) and 567.2 ± 3.9 Ma (Grazhdankin *et al.* 2011; Figure 1). Very negative (typically –10 to –

15 ‰) carbon isotope values were reported from carbonate olistoliths in the upper Starye Pechi Formation and from the underlying Buton and Kernos formations, where they were interpreted as either diagenetic or resulting from methane or carbon dioxide seeps (Chumakov *et al.* 2013). An alternative interpretation would be that the very negative carbon isotope values reflect deposition during the Shuram CIE. The Starye Pechi Formation diamictites are interbedded with massive quartz-feldspar sandstones (Grazhdankin *et al.* 2009; Chumakov 2011) and the under- and overlying strata include conglomerates, breccias, turbidites, flysch, and olistoliths with substantial syn-sedimentary slumping (Chumakov 2011; Chumakov *et al.* 2013; Maslov *et al.* 2013), all consistent with mass transport-derived deposition on the outer shelf and continental slope (Chumakov 2011). Overall, the interpretation of the Starye Pechi diamictite as glaciogenic rather than debris flow-derived is contingent on rare Ipat'eva *in* ref(Maslov *et al.* 2013) outsized and striated clasts: improved documentation of both the age constraints and sedimentology of this unit are required to assess whether this is a glacially-derived or gravitationally-derived deposit, contemporary with or older than the Shuram excursion. If the original interpretation (Chumakov *et al.* 2013) of the very negative carbon isotope values is correct, the Starye Pechi Formation may predate the Shuram CIE and be contemporaneous with the MEIH. On current evidence, we consider that both pre-Shuram (MEIH) and syn-Shuram (LEGH) age assignments are plausible, but a glaciogenic origin is unlikely.

There are no further candidate glaciogenic deposits with reasonable depositional age constraints that could plausibly have been deposited between ~579 to 565 Ma (Figure 1). In sections with near-continuous sedimentation, there is no evidence for glaciation after ~579 Ma and before ~565 Ma, including in Avalonian sections where glacial deposits were well developed prior to ~579 Ma and there is no substantial change in depositional setting (Carto and Eyles 2011; Pu *et al.* 2016; Fitzgerald *et al.* 2024; Mills *et al.* 2024). Because of the lack of well-constrained evidence for glaciation, we term this interval the 'late Ediacaran greenhouse' (LEGH).

565 to 550 Ma: late Ediacaran icehouse (LEIH)

At around ~565 to 560 Ma, a concentration of reliable evidence for land ice returns (Figure 1) on Gondwana and peri-Gondwanan terranes (Linnemann *et al.* 2018, 2022). This icehouse interval has been known by various names, but particularly as the 'Hankalchough glaciation', or the 'Upper Ediacaran Glacial Period' (Linnemann *et al.* 2022). Here, we use the term 'late Ediacaran icehouse' (LEIH) to avoid tying the climate interval to specific deposits.

In North African Gondwana, the Pourprée de l'Ahnet Group diamictite (Algeria), rated a four star unit (Tindal 2023), was deposited between 560 ± 10 Ma and 530 ± 7 Ma (Caby and Fabre 1981; Bertrand-Sarfati *et al.* 1995; Chumakov 2009). Also on North African Gondwana (Morocco) are the

Ouarzazate Group diamictites and glacial surfaces, rated a four star deposit (Supplementary Information), with a maximum depositional age of 566 ± 4 Ma (Blein *et al.* 2014), therefore likely post-dating the recovery of the Shuram CIE. The Kahar Formation diamictite (Gondwanan Iran), rated a three star deposit (Tindal 2023), has a radiometrically constrained depositional age between 563.1 ± 3.9 Ma and 550.3 ± 3.6 Ma (Etemad-Saeed *et al.* 2016). The Dhaiqa Formation diamictite (Saudi Arabia, Arabian Shield, Gondwana), rated a three star deposit (Tindal 2023), is younger than 560 ± 4 Ma and underlies candidate Ediacaran fossils (Miller *et al.* 2008; Vickers-Rich *et al.* 2013).

Several candidate glaciogenic deposits in the palaeo-terranes of present-day northern China have poor age constraints but were likely deposited between ~565 to 550 Ma (Xiao *et al.* 2004; Shen *et al.* 2007, 2010; Le Heron *et al.* 2019; Zhou *et al.* 2019; Wang *et al.* 2021a, 2023b). On the North China craton, the likely correlative (Le Heron *et al.* 2019; Wang *et al.* 2021a) Luoquan, four star (Tindal 2023), and Zhengmuguan, three star (Supplementary Information) formations were deposited below the first occurrences of the late Ediacaran tubular taxon *Shaanxilithes* in the conformably overlying Dongpo and Tuerkeng formations respectively (Shen *et al.* 2007; Zhou *et al.* 2019; Wang *et al.* 2021a). Similarly, on the Qaidam Block, the poorly documented Hongtiegou Formation diamictite (Supplementary Information) was deposited below occurrences of *Charnia* and *Shaanxilithes* in the Zhoujieshan Formation (Shen *et al.* 2010; Pang *et al.* 2021; Wang *et al.* 2022). The Luoquan, Zhengmuguan, and Hongtiegou formations unconformably overlie Mesoproterozoic sedimentary deposits but are conformable with their overlying, Ediacaran fossil-bearing, units (Shen *et al.* 2007, 2010; Wang *et al.* 2021a). On the Tarim block, the Hankalchough Formation, rated a three star deposit (Supplementary Information), is at least 65 m stratigraphically above the recovery limb of an extreme negative CIE in the Shuiquan Formation that has been correlated with the Shuram CIE (Xiao *et al.* 2004; Wang *et al.* 2023a). The maximum depositional age of the Hankalchough Formation is therefore taken as the minimum age of the Shuram CIE recovery: 566.9 ± 3.5 Ma (Busch *et al.* 2023). The overlying Xishanblaq Formation hosts earliest Cambrian acritarchs, which provide a minimum age constraint on the Hankalchough Formation (Xiao *et al.* 2004; Yao *et al.* 2005).

On the Baltic Shield, the Mortensnes Formation diamictite (Norway), a three star deposit (Tindal 2023), lacks precise radiometric dates but is similarly constrained by a possible Shuram-equivalent CIE beneath (Halverson *et al.* 2005; Rice *et al.* 2011) and Ediacaran macrofossils above (Högström *et al.* 2013; McIlroy and Brasier 2017; Jensen *et al.* 2018; Agić *et al.* 2024). It is likely that the Mortensnes Formation was deposited between the Shuram CIE and the terminal Ediacaran.

Four candidate glaciogenic deposits have been identified across peri-Gondwanan Cadomia (Linnemann *et al.* 2018, 2022). Diamictites from the Müglitz Formation (Weesenstein Group) and

Clanschwitz Group Member 3 (both Germany) are rated two and one star deposits respectively (Supplementary Information) and were considered to be likely younger than 562 ± 5 Ma (Linnemann *et al.* 2018). However, recent work has indicated a non-glacial origin for these units as well as a considerably revised depositional age of late Cambrian to Ordovician based on U-Th-Pb monazite dates (Kühnemann *et al.* 2024) and ichnofossil evidence (Meinhold *et al.* 2025). The Granville Formation (France) diamictites, rated a three star deposit (Tindal 2023), are younger than 562.1 ± 3.1 Ma, with the upper diamictite younger than 560.6 ± 3.3 Ma (Linnemann *et al.* 2022). The Orellana Formation (Spain), rated a two star deposit (Tindal 2023) and not universally regarded as glaciogenic (Palacios 2024), is younger than 565 ± 4 Ma (Linnemann *et al.* 2018) and is found unconformably below Ediacaran fossil-bearing carbonates (Álvaro *et al.* 2019; Palacios 2024). Overall, the evidence for late Ediacaran glaciation across Cadomia in the ~565 to 550 Ma interval is weak in comparison to that on palaeocontinental Gondwana and the terranes of northern China.

Where there is depositional continuity above the LEIH candidate glaciogenic deposits, Ediacaran fossils are commonly found in the overlying strata (Shen *et al.* 2007, 2010; Högström *et al.* 2013; Vickers-Rich *et al.* 2013; Jensen *et al.* 2018; Wang *et al.* 2021a, 2022; Agić *et al.* 2024), demonstrating that this icehouse terminated before the end of the Ediacaran. Less well constrained than the MEIH, the LEIH probably commenced after the Shuram CIE recovery, likely between 565 to 560 Ma, and terminated before the end of the Ediacaran Period, likely about ~550 Ma (Xiao *et al.* 2004; Miller *et al.* 2008; Chumakov 2009; Vickers-Rich *et al.* 2013; Etemad-Saeed *et al.* 2016; Linnemann *et al.* 2018, 2022; Agić *et al.* 2024).

550 to 539 Ma: terminal Ediacaran greenhouse (TEGH)

There is scant evidence of glaciation in the terminal Ediacaran after ~550 Ma. The only temporally well-constrained candidate glaciogenic deposit known from this interval is the Vingerbreek Member (Nudaus Formation, Nama Group, southern Namibia and northwest South Africa) and its associated basal Vingerbreek Unconformity (Schwellnus 1941; Kröner and Germs 1971; Kröner 1981; Germs and Gaucher 2012; Zieger-Hofmann *et al.* 2022), together rated as a three star unit (Tindal 2023) and radiometrically constrained to between 547.36 ± 0.23 Ma (Bowring *et al.* 2007) to 545.27 ± 0.11 Ma (Nelson *et al.* 2022).

The Vingerbreek Unconformity has only been found in parts of the southern Nama Basin (the Zaris and possibly the Vioolsdrif sub-basins), not in the Witputs sub-basin to the north (Kröner 1981; Germs and Gaucher 2012; Zieger-Hofmann *et al.* 2022). The Vingerbreek Member basal diamictite was deposited in wide channels in the unconformity surface, which have been interpreted as deriving from fluvial or submarine mass flow erosion processes; both far-field glacioeustasy and tectonism have been proposed as potentially responsible for lowering base level (Martin 1965; Kröner 1981; Germs and Gaucher 2012). The grooves and surface polish on some channel flanks have been interpreted as deriving from glacier-rock (Schwellnus 1941; Germs and Gaucher 2012; Zieger-Hofmann *et al.* 2022) or sea ice-rock (Martin 1965; Kröner 1981) interactions, though similar features also form from mass flow and rock avalanche erosion processes (Hambrey and Harland 1981; Hu and McSaveney 2018). The diamictite deposits are better described as conglomerates and breccias (Germs and Gaucher 2012) and have been interpreted as fluvial or submarine current-derived deposits, including in studies that found glacial action at least partly responsible for the unconformity (Kröner 1981; Germs and Gaucher 2012). In northwest South Africa, the diamictite grades into turbidites (Zieger-Hofmann *et al.* 2022). The Vingerbreek Member and Unconformity therefore provide only circumstantial, stratigraphically and spatially isolated evidence for glacial ice. Further field work is required to determine the depositional context of the Vingerbreek Unconformity and Vingerbreek Member, and it stands as a test of our hypothesis that the ~550 to 545 Ma interval was characterized by a greenhouse climate.

Elsewhere the terminal Ediacaran lacks any signs of glaciation, and we therefore use the term ‘terminal Ediacaran greenhouse’ (TEGH) for this interval. Similar to previous compilations of climatically sensitive lithologies (Boucot *et al.* 2013; Wong Hearing *et al.* 2021), we do not find evidence of well-dated glacial sedimentary deposits in either the terminal Ediacaran or early Cambrian periods.

Climate and the Ediacaran biosphere

Our analysis indicates that the mid- to late Ediacaran climate is characterised by two icehouse intervals (~593 to 579 Ma and ~565 to 550 Ma) and two greenhouse intervals (~579 to 565 Ma and ~550 to 539 Ma). Independent of our analysis, the late Ediacaran biosphere has been characterised by three distinct marine biotic assemblages (Figure 2; Figure 3; Table 3), governed by some combination of environmental and evolutionary control (Waggoner 2003; Grazhdankin 2004b; Gehling and Droser 2013; Boag *et al.* 2016; Muscente *et al.* 2019; Evans *et al.* 2022). To test whether biotic turnover is coincident with climatic shifts, we examine diversity dynamics over this interval, mindful that the assemblages are typically found in different palaeogeographic regions and depositional settings, as well as time intervals (Waggoner 2003; Boag *et al.* 2016, 2024; Muscente *et al.* 2019; Boddy *et al.* 2021; Bowyer *et al.* 2022, 2024; Evans *et al.* 2022). Because of the substantial contribution of geological and societal biases in the current Ediacaran fossil record (taxonomic richness largely follows sampling intensity; Figure 4; Bowyer *et al.* 2024), it is generally more instructive to consider taxonomic composition than taxonomic richness, though some biodiversity signals do appear to be robust to sampling biases (Figure 4).

Table 3. Summary of the main late Ediacaran biotic assemblages.

Assemblage	Age range	Depositional setting(s)	Morpho-groups and innovations
Avalon	>575 Ma to 565 Ma	Deep marine basin to shelf (Narbonne *et al.* 2014; Noble *et al.* 2015; Matthews *et al.* 2020), lacking shallow marine occurrences (Boag *et al.* 2024).	Complex macroscopic organisms; mostly frondose morphologies; no tubular taxa.
	565 Ma to <560 Ma	Deep marine shelf to basin (Narbonne *et al.* 2014; Carbone *et al.* 2015; Noble *et al.* 2015; Matthews *et al.* 2020; Boag *et al.* 2024), and shallow marine, above storm wave base (Cope 1977, 1983; Pauley 1991; Liu 2011; Clarke *et al.* 2024).	Complex macroscopic organisms; frondose morphologies; discoidal fossils both of probable frond holdfasts and individual discoidal organisms; rare simple surface trace fossils; candidate cnidarians; no or very few tubular taxa (Carbone *et al.* 2015); matgrounds in shallower settings.
White Sea	<560 Ma to >550 Ma	Marine offshore shelf to shallow shoreface (Grazhdankin 2004b; Boag *et al.* 2016; McMahon *et al.* 2020; Boag *et al.* 2024), most likely spanning all settings from near storm weather wave base to the intertidal zone (McMahon *et al.* 2020).	Bilaterialomorphs; first erniettomorphs; various radialomorphs; abundant non-mineralised tubular fossils (Surprenant and Droser 2024); increasingly diverse simple trace fossils; fewer frondose fossils.
Nama	<550 Ma to 538.8 Ma	Marine offshore (open marine) inner shelf to reef (Boag *et al.* 2016, 2024; Amorim *et al.* 2020; Xiao *et al.* 2021; Wood *et al.* 2023; O'Connell *et al.* 2024), includes sites in shallow settings above storm weather wave base (Boag *et al.* 2016, tbl. S6; Xiao *et al.* 2020).	Biomineralized and soft bodied tubular fossils (Surprenant and Droser 2024); increasingly diverse and complex trace fossils; few new frondose fossils; erniettomorphs become more prominent; candidate sponges.

Figure 2. Representative late Ediacaran fossils of the ***Avalon****,* ***White Sea****, and* ***Nama*** *biotic assemblages. Scale bars = 10 mm unless otherwise stated; photographed scale bar increments are cm and mm.* ***Nama (left to right):*** Charnia masoni*, NIGP 161628, Shibantan Member (Dengying Formation), Wuhe, South China, scale bar = 10 cm;* Helicolocellus cantori*, NIGP 176531, Shibantan Member (Dengying Formation), Wuhe, South China;* Pteridinium*, Aar Member, Farm Aar, Namibia;* Namacalathus*, Urusis Formation, Farm Swartpunt, Namibia;* Corumbella werneri*, Tamengo Formation, Corumba region, Brazil; burrows in carbonates, Shibantan Member (Dengying Formation), Wuhe, South China.* ***White Sea (left to right):*** Charnia masoni *(incomplete), Verkhovka Formation, Solza River, Russia;* Dickinsonia costata*, SAM P49355, Ediacara Member (Rawnsley Quartzite), Flinders Ranges, South Australia;* Kimberella quadrata*, PIN 3993/5106, Vendian Group, Zimnie Gory locality, White Sea coast, Russia;* Tribrachidium*, SAM P12898, Ediacara Member (Rawnsley Quartzite), Flinders Ranges, South Australia;* Funisia dorothea*, Ediacara Member, South Australia;* Helminthoidichnites *trace fossils, SAM P42142, Ediacara Member, Flinders Ranges (Rawnsley Quartzite), South Australia.* ***Avalon (left to right):*** Charnia masoni *(holotype), New Walk Museum, Leicester, Bradgate Formation, Charnwood Forest, UK;* Haootia quadriformis *(holotype), NFM F-994, Fermeuse Formation, Bonavista Peninsula, Newfoundland, Canada;* Bradgatia*, ROM 36500, Conception Group, Mistaken Point Ecological Reserve (MPER), Newfoundland, Canada;* Fractofusus andersoni*, Briscal Formation, MPER, Newfoundland, Canada; surface locomotory trace fossil, Mistaken Point Formation, MPER, Newfoundland, Canada. Abbreviations: NIGP = Nanjing Institute of Geology and Palaeontology; ROM = Royal Ontario Museum; NFM = The Rooms Provincial Museum, St. John's, Newfoundland; SAM = South Australia Museum; PIN = Palaeontological Institute, Moscow.*

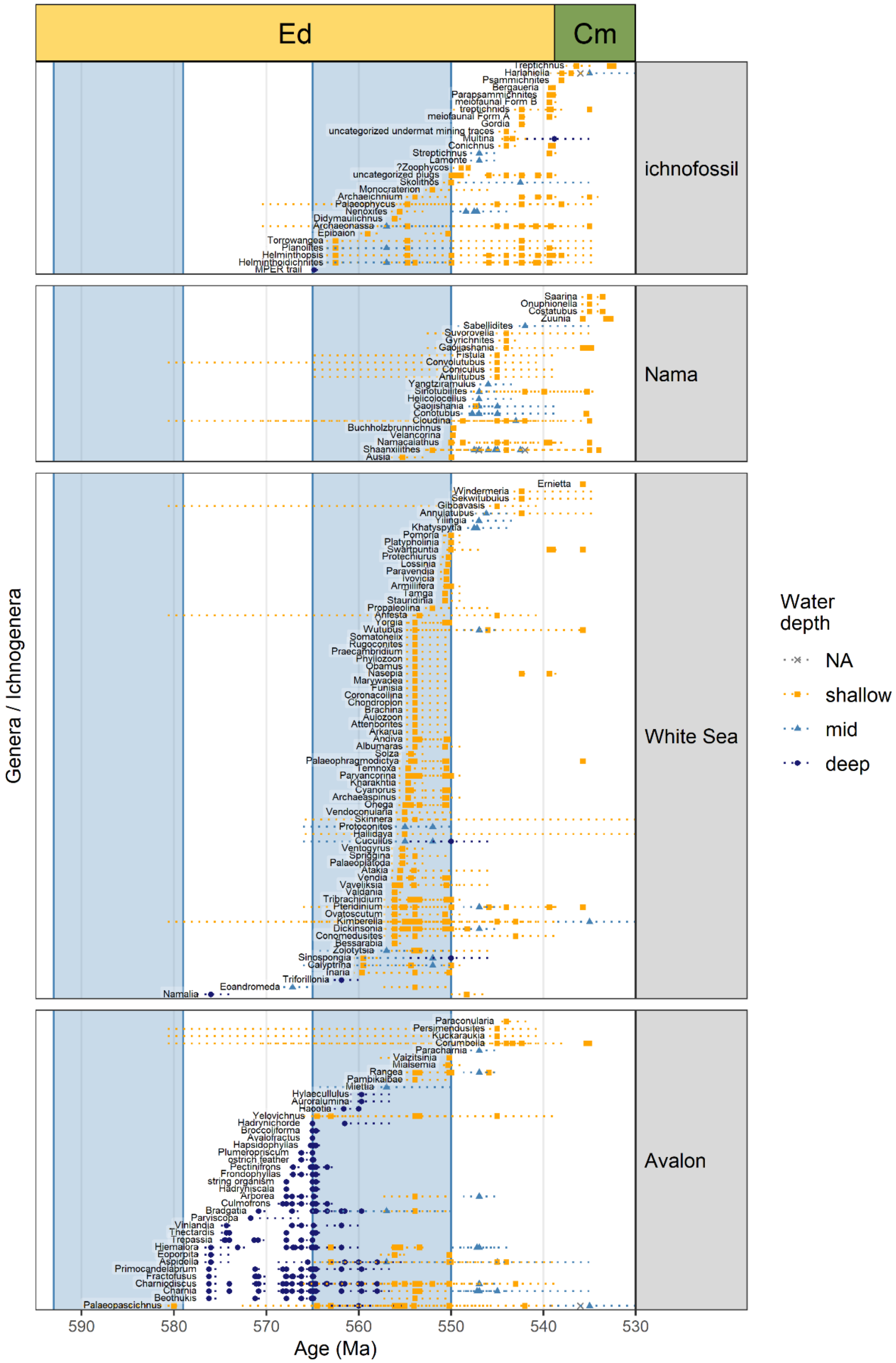

Figure 3. Temporal distribution of Ediacaran fossil occurrences excluding those from South Australia, with blue-shaded MEIH and LEIH icehouse climate states as inferred from well-dated glaciogenic deposits (Figure 1). Palaeobiological data after: Matthews (2015); Matthews et al. *(2020); Boddy* et al. *(2021); Bowyer* et al. *(2023, 2024); Surprenant and Droser (2024); and references therein (see Supplementary Data 2). Taxa grouped into assemblages following their morphogroup*

assignments (see Supplementary Data 2). Colours and shapes represent inferred water depth of each occurrence. Ed: Ediacaran; Cr: Cambrian. Dashed lines show the age uncertainty of each occurrence.

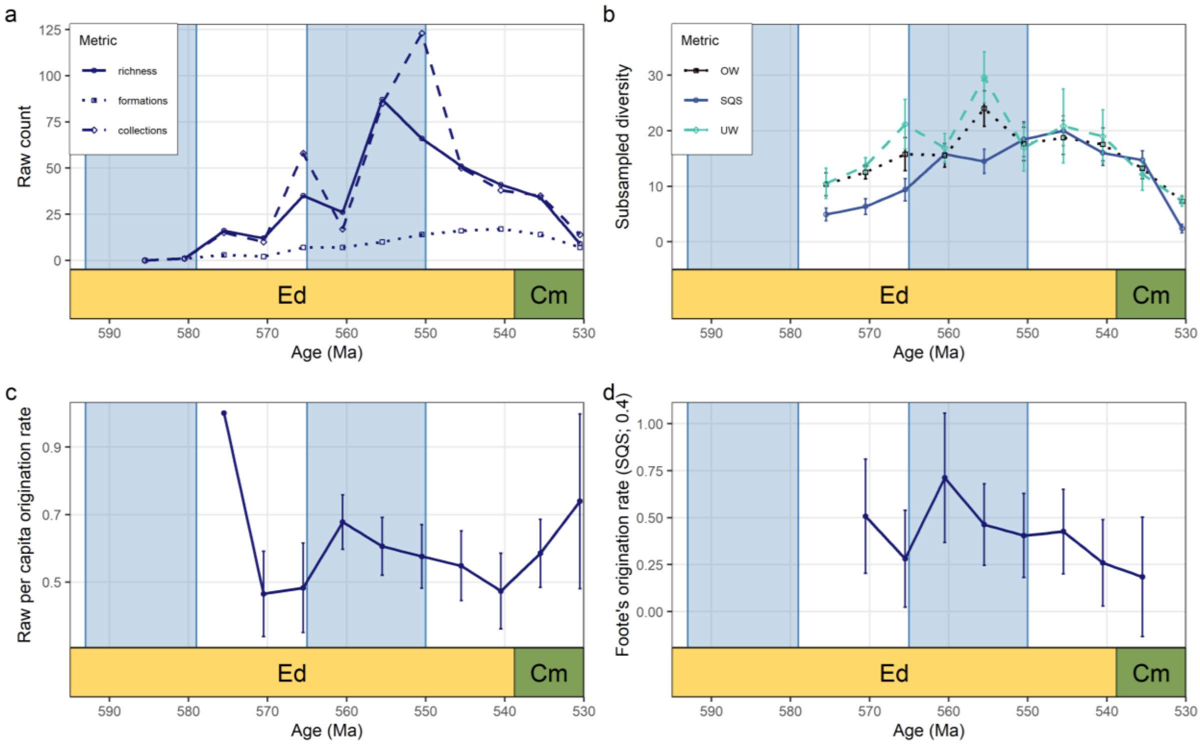

Figure 4. Palaeobiodiversity metrics for the late Ediacaran biosphere. (a) Raw taxonomic richness (circles; solid lines) plotted alongside number of collections (diamonds; dashed lines) and number of formations (squares; dotted lines). (b) Subsampled taxonomic richness following Shareholder Quorum subsampling (SQS; quota = 0.4), unweighted collection-based classical rarefaction (UW; quota = 8 collections), and occurrence-weighted subsampling (OW; quota = 14 occurrences). (c) Raw per capita origination rate for 1 Myr and 5 Myr bins. (d) SQS (quota = 0.4) subsampled Foote's origination rate for 1 Myr and 5 Myr bins. The decline in values across the Ediacaran–Cambrian boundary is an artefact of our palaeobiology data compilation which focused on taxa with first occurrences in the Ediacaran Period. Data from Supplementary Data 2. See Figure S5 for sensitivity to the loose correlation of sites in South Australia.

The Avalon assemblage

The oldest diverse assemblages of the Ediacaran macrobiota, belonging to the Avalon biotic assemblage, first appear in deep marine siliciclastic deposits between ~579 to 575 Ma (Figure 3), after the MEIH and before the Shuram CIE (Pu *et al.* 2016; Matthews *et al.* 2020; Yang *et al.* 2021; Boag *et al.* 2024; Bowyer *et al.* 2024). This assemblage reaches an apparent acme in diversity in deep marine settings around 565 Ma (Matthews *et al.* 2020; Boag *et al.* 2024), coincident with the end of the LEGH and the transition into the LEIH (Figure 3), and persists in deep water settings until at least 560 Ma (Wilby *et al.* 2011; Noble *et al.* 2015; Kenchington *et al.* 2018). The post-560 Ma fate of the deep water Ediacaran biota remains unknown due to the scarcity of deep marine siliciclastic deposits after this time (Bowyer *et al.* 2024).

Depauperate communities of the Avalon biotic assemblage are known from shallow marine settings on Avalonia (Cope 1977, 1983) and Laurentia (Hofmann *et al.* 1983; Narbonne and Hofmann 1987; Pyle *et al.* 2004; Moynihan *et al.* 2019) after, but not before or during, the Shuram CIE (~574 to 566 Ma; Boag *et al.* 2024; Clarke *et al.* 2024). The majority of Avalon assemblage taxa are thought to belong to a deep- and/or cool-water biotope (Boag *et al.* 2016, 2024; Bowyer *et al.* 2024). Here we suggest that a ~565 to 560 Ma interval of global cooling at the onset of the LEIH allowed some elements of the otherwise deep water adapted Avalon assemblage to colonise cooling shallow marine environments.

The White Sea assemblage

In situ palaeocommunities of White Sea biotic assemblage taxa are found in shallow marine settings, above storm weather wave base and predominantly above fair weather wave base (e.g. Grazhdankin 2004b; McMahon *et al.* 2020) from before 557 Ma until at least 553 Ma (Martin *et al.* 2000; Fedonkin *et al.* 2012; Grazhdankin 2014; Yang *et al.* 2021; Bowyer *et al.* 2022, 2024). Our analysis places this range within the LEIH. The White Sea assemblage is defined by the appearance of new morphogroups, including bilaterialomorphs, radialomorphs, and tubular forms, which occur alongside a few persistent Avalon-type taxa (Figure 3; Table 3; Martin *et al.* 2000; Narbonne 2005; Fedonkin *et al.* 2012; Grazhdankin 2014; Muscente *et al.* 2019; Surprenant and Droser 2024). The first step-change in trace fossil diversity is associated with this interval: rare trace fossils older than 560 Ma are stratigraphically isolated simple surface traces (Liu *et al.* 2010, 2014a), but from at least 557 Ma a range of horizontal burrows and trails created by candidate bilaterians are found in shallow marine deposits (Figure S4). Novel White Sea morphogroups are found in shallow marine strata deposited during the latter part of the LEIH (~560 to 550 Ma) but not before ~560 Ma (Boag *et al.* 2024; Clarke *et al.* 2024). By raw taxonomic richness, the White Sea is the most diverse of the three biotic assemblages and, although the Ediacaran fossil record is strongly affected by sampling biases, the White Sea diversity peak may be robust to some subsampling methods designed to mitigate such biases (Figure 4).

The Nama assemblage

The Nama is the youngest of the three biotic assemblages, and is found in shallow marine carbonate and siliciclastic deposits younger than ~550.5 Ma (Darroch *et al.* 2015; Muscente *et al.* 2019; Xiao *et al.* 2021; Wood *et al.* 2023; Boag *et al.* 2024) up to the base of the Cambrian (Linnemann *et al.* 2019; Bowyer *et al.* 2022, 2023, 2024; Nelson *et al.* 2022; Wood *et al.* 2023; Runnegar *et al.* 2024). It is characterised by the diversification of trace fossils, particularly vertical burrows, and the appearance of biomineralized tubular taxa, which are found only in deposits younger than ~550.5 Ma (Wood *et al.* 2023; Surprenant and Droser 2024). The Nama assemblage is coincident with the TEGH. Some

White Sea-type taxa, including dickinsoniomorphs and erniettomorphs (Wang *et al.* 2021c; Xiao *et al.* 2021; Wood *et al.* 2023), and Avalon-type taxa, including arboreomorphs and rangeomorphs (Xiao *et al.* 2021; Wu *et al.* 2022), are found alongside novel Nama morphogroups in shallow marine deposits from this interval.

Recent re-analyses of the depositional context of White Sea and Nama assemblage sites have demonstrated substantial facies overlap, thereby reducing the likelihood that the change in faunal composition over this interval is exclusively an artefact of sampling different depositional settings, and increasing the likelihood that it reflects a real biotic change (McMahon *et al.* 2020; Evans *et al.* 2022; O'Connell *et al.* 2024). The oldest known fossils in the Nama Group have recently been reported from shallow, subtidal medium to fine-grained sandstones attributed to the lower Mara Member (Dabis Formation) in the Tsaus Mountains, Namibia (Wood *et al.* 2023). These fossils have been interpreted to reflect a low diversity community of taxa that persisted from earlier White Sea and Avalon assemblages, with new Nama morphogroups being absent, perhaps representing a syn- or immediately post-extinction community (Wood *et al.* 2023). The broadly similar shallow marine depositional settings in the typical White Sea assemblage deposits of South Australia and the lower Mara Member in the Tsaus Mountains (Wood *et al.* 2023), lend support to the hypothesis of an extinction separating the White Sea and Nama assemblages, with some time-gap before the biosphere recovered and new morphogroups, in particular biomineralized tubular forms, appearing. However, detailed sedimentological research in the Tsaus Mountains is required to confirm the precise depositional settings of that locality, while the differences in assemblage composition could feasibly result from other (e.g. geochemical) environmental or palaeogeographical factors.

Summary

The Ediacaran biota was initially restricted to deep marine settings during the LEGH (Avalon assemblage, ~575 to 565 Ma) (Boag *et al.* 2024); it was not until the beginning of the LEIH, from ~565 Ma, that elements of the Avalon assemblage appear to have colonised shallow water settings. The first step-change in high-level taxonomic composition of the Ediacaran biosphere, including the advent of bilaterians and unmineralized tubes, occurred early in the LEIH interval (before 557 Ma) with the appearance of White Sea assemblage morphogroups. This step-change is underlined by the Ediacaran peak origination rate across the Avalon-White Sea transition, and the subsequent White Sea peak in taxonomic richness (Figure 4). A second step-change in high-level taxonomic composition accompanied the transition from the LEIH to the TEGH at ~550 Ma, with the appearance of biomineralizing taxa and vertical burrowing in shallow marine settings.

The majority of taxonomic elements of the Avalon assemblage are not found in White Sea and Nama communities, and similarly the majority of White Sea assemblage taxa are not found in Nama communities (Boag *et al.* 2016; Muscente *et al.* 2019; Evans *et al.* 2022; Wood *et al.* 2023; Bowyer *et al.* 2024) (Figure 3). Considering only shallow water occurrences (from strata deposited above storm-weather wave base), the small numbers of taxa shared between the shallow water Avalon, White Sea, and Nama communities support discrete episodes of faunal turnover (extinctions and radiations) in the shallow marine realm across the late Ediacaran (Figure 3). There appear to be distinct assemblages of morphogroups (Waggoner 2003; Boag *et al.* 2016; Muscente *et al.* 2019; Evans *et al.* 2022) that are separated in time, demarcated by the prevailing climate regime.

Discussion

The timing of Ediacaran climate change

The glacial sedimentary record provides evidence of low altitude grounded ice for two ~15 Myr intervals in the mid and late Ediacaran (~593 to 579 Ma and ~565 to 550 Ma; Figure 1). The termination of the mid-Ediacaran icehouse (MEIH) is well constrained to ~579 Ma by radiometrically dated deposits in North Africa (Thomas *et al.* 2002; Inglis *et al.* 2004; Blein *et al.* 2014; Letsch *et al.* 2018; Youbi *et al.* 2020), the Rio de Plata craton (Mallmann *et al.* 2007; Oyhantçabal *et al.* 2007), and Avalonia (Pu *et al.* 2016; Mills *et al.* 2024). In Oman, and elsewhere on the palaeo-Gondwanan margin, the pre-Shuram CIE interval is characterised by condensed sedimentary successions, with a marked increase in depositional rates between ~580 to 560 Ma (Cantine *et al.* 2024). On the tropical palaeolatitude South China craton, stratigraphically constrained glendonite occurrences (indicative of cool or cold water conditions) in the Doushantuo Formation also indicate cooler ocean temperatures between ~600 to 579 Ma (Wang *et al.* 2017, 2020; Zhou *et al.* 2017), with conditions in the basin changing after ~579 Ma and during the EN3/Shuram CIE (Supplementary Information).

The late Ediacaran icehouse (LEIH) is more loosely temporally constrained than the MEIH, with the radiometrically dated Kahar Formation diamictite (Alborz Mountains, northern Iran; Etemad-Saeed *et al.* 2016) being an exceptionally well-dated unit. Most candidate glaciogenic deposits of this age are broadly bracketed by the Shuram CIE below and terminal Ediacaran or Cambrian fossils above. However, indirect evidence from the broader geological record also supports a climate state transition before the terminal Ediacaran, likely at ~550 Ma. Bowyer *et al.* (2024) identified, from a global rock record compilation, declining proportions of carbonate and increasing proportions of silicate rocks by area and volume from ~565 to 550 Ma, including a total absence of carbonate rocks from ~555 to 550 Ma. There is a substantial hiatus in deposition on the South China craton between the uppermost Doushantuo Formation and the lowermost Dengying and Liuchapo formations that is younger than EN3/Shuram CIE recovery (~566 Ma) and older than 550.1 ± 0.6 Ma (Yang *et al.* 2021), coincident with the global sea level lowstand that reached a nadir at ~550.5 Ma (Bowyer *et al.* 2024), and with the end of the LEIH identified here. The carbonate-barren interval is followed by a marine transgression and increasing contribution of carbonates to the global rock record after ~550 Ma (Bowyer *et al.* 2024). Segessenman and Peters (2024) identified a contemporaneous approximately two-fold increase in sediment volume flux across Laurentia from ~550.5 Ma, persisting until at least 545 Ma. The marine transgression (Bowyer *et al.* 2024) and increased sediment flux (Segessenman and Peters 2024) may therefore reflect eustatic sea level rise driven by melting land ice during the transition from the LEIH to the TEGH, with associated increased weathering intensity and/or the flushing of glacial regolith into the oceans.

Above the ~550.5 Ma lowstand, Bowyer *et al.* (2024) next identified global transgressive surface is at the Ediacaran-Cambrian boundary, arguably the best known marine transgression in the stratigraphic record (Peters and Gaines 2012), though of debated origin (Keller *et al.* 2019; Tasistro-Hart and Macdonald 2023). In light of the emerging climate record through this interval, the lack of reported glaciogenic deposits of terminal Ediacaran (see above) or early Cambrian age (Boucot *et al.* 2013; Johnson *et al.* 2019; Wong Hearing *et al.* 2021; Álvaro *et al.* 2022) supports a tectono-eustatic rather than glacioeustatic driver for this transgression (e.g. Tasistro-Hart and Macdonald 2023).

What drove the changes in Ediacaran climate state is an open question. Shields *et al.* (2019) described how the oxidation of a large oceanic reservoir of dissolved organic carbon (DOC) could lead to elevated $p\mathrm{CO_2}$ levels and global temperatures through the Shuram CIE, with a temperature-enhanced silicate weathering feedback drawing down $p\mathrm{CO_2}$ after the ocean DOC reservoir was exhausted. This temporally constrained mechanism would account for a Shuram interval greenhouse and post-Shuram cooling over several million years (Shields *et al.* 2019), as we infer from the Ediacaran glacial sedimentary record. Another potential driver of Ediacaran climate is the Central Iapetus Magmatic Province (CIMP) associated with Rodinian break-up and the opening of the Iapetus Ocean (Youbi *et al.* 2020). Pulsed emplacement of large quantities of mafic igneous rock drives $p\mathrm{CO_2}$ up from volcanic outgassing and then down via the silicate weathering feedback effect (Berner 2004, 2006; Mills *et al.* 2019). Whatever the principal drivers of Ediacaran climate, our analysis provides a more tightly constrained framework for evaluation.

Coupling of climate and biosphere dynamics

Our analysis consolidates global evidence for step-changes in the Ediacaran biosphere coincident with changes in climate state at ~579 Ma, ~565 to 560 Ma, and ~550 Ma (Figure 1; Figure 3; Figure 4). Considering more proximate potential drivers of biotic change, Evans *et al.* (2022) found evidence for abiogenic influence, potentially oxygen availability, on Ediacaran biodiversity patterns, and Boag *et al.* (2024) related the ecophysiology of Ediacaran organisms to potential global temperature regimes, suggesting that high temperatures may have prevented the colonisation of shallow water settings during the Shuram CIE. Bowyer *et al.* (2024) linked Ediacaran biodiversity dynamics to long-term sea level variation and potentially environmental oxygen availability. We suggest that first-order climate shifts are the underlying drivers of the observed large-scale patterns in sea level variation, oxygen availability and ocean temperature, with the fossil record recording responses in the biosphere.

Sea level change has been implicated in shaping both apparent and real Ediacaran biodiversity dynamics by controlling available habitat space and the preserved rock record (Evans *et al.* 2022; Bowyer *et al.* 2024). In the Phanerozoic, marine transgressions and sea level highstands, associated with warmer climate states, increased both shallow marine habitat area and preservation potential of the shallow marine shelf (Hallam and Wignall 1999; Alroy 2010b). Conversely, cooler intervals are associated with steeper latitudinal diversity gradients (LDGs) driven by increased thermal niche partitioning in the tropics, whereas warmer intervals are associated with flatter LDGs and lower taxonomic richness (Song *et al.* 2020; Fenton *et al.* 2023; Woodhouse *et al.* 2023). Despite sampling limitations, it is notable that the highest Ediacaran taxonomic richness is found during the LEIH (~560 to 550 Ma; Figure 4), an interval characterised by low rock volume, a marine regression, and a sea level lowstand (Bowyer *et al.* 2024), in agreement with climatically-driven diversity trends in the Phanerozoic (Song *et al.* 2020; Fenton *et al.* 2023; Woodhouse *et al.* 2023).

Ediacaran biosphere dynamics have been closely associated with ocean oxygenation as well as sea level (Evans *et al.* 2018, 2022; Wood *et al.* 2019; Bowyer *et al.* 2024). Because an increase in temperature depresses oxygen solubility but elevates metabolic demand, the combination of temperature and ocean oxygenation is crucial for understanding marine habitability (Deutsch *et al.* 2015; Boag *et al.* 2018; Penn *et al.* 2018; Stockey *et al.* 2021). In this context, higher temperatures of the LEGH and TEGH intervals would have increased ecological stress by reducing thermal niche partitioning and oxygen availability. A resulting prediction is that generalist organisms with tolerance to low oxygen conditions would fare better during icehouse to greenhouse transitions. Evans *et al.* (2022) found a positive correlation between organisms’ surface area to volume ratio and survivorship through the White Sea to Nama transition, and speculated that a high surface area to volume ratio would be beneficial to surviving in lower oxygen environments. Our analysis suggests a potential mechanism for environmentally-derived selectivity in the Ediacaran biosphere via global temperature change reflecting icehouse/greenhouse transitions.

We suggest that a ~565 to 560 Ma interval of global cooling at the beginning of the late Ediacaran icehouse made it possible for some elements of the otherwise deep- and cold-water adapted Avalon assemblage to colonise cooling shallow marine environments (Boag *et al.* 2024). This is similar to the 'polar emergence' pattern observed in the Antarctic fossil record during late Pliocene and early Pleistocene cooling episodes (Berkman *et al.* 2004), the inverse of the present-day response to global heating (e.g. Perry *et al.* 2005). Cooling temperatures with associated increasing thermal gradients (Song *et al.* 2020; Fenton *et al.* 2023; Woodhouse *et al.* 2023), increasing oxygen availability, and decreasing metabolic oxygen demand (Deutsch *et al.* 2015; Boag *et al.* 2018; Penn *et al.* 2018; Stockey *et al.* 2021) at the beginning of the LEIH may have increased niche availability across the greenhouse to icehouse transition, similar to the thermally-driven polar diversity pump of the Cenozoic (Clarke and Crame 1992; Griffiths *et al.* 2023).

Overall, the close correspondence between changes in Ediacaran palaeobiology and palaeoclimate supports the hypothesis that coupling of the biosphere and climate was established at least by the middle Ediacaran Period. Notably, the radiation of bilaterians appears to occur in shallower water settings during a cold interval, and metazoan biomineralization and deep burrowing seem to coincide with a transition from cold to warm conditions. This coupling is evident in spite of uncertainties in global correlation and the known biases of both rock and fossil records (e.g. Bowyer *et al.* 2024), suggesting that it was a first-order property of the Ediacaran Earth System, as it is for the Phanerozoic.

Concluding remarks

Late Ediacaran climate appears to be characterized by two discrete intervals of icehouse conditions (MEIH: ~593 to 579 Ma, and LEIH: ~565 to 550 Ma) and two discrete intervals of greenhouse conditions (LEGH: ~579 to 565 Ma, and TEGH: ~550 Ma into the early Cambrian) (Figure 1), the transitions between which are coincident with turnovers in the biosphere (Figure 3). There is wide scope for further work: the causal mechanisms of these climate changes require greater investigation; the known Ediacaran fossil record is particularly unevenly sampled; and the glacial record requires work to constrain both the depositional ages and potential glaciogenicity of many of its deposits. Nevertheless, there is a clear first-order signal in the mid- to late Ediacaran rock record of two discrete intervals of glaciation separated by a greenhouse interval, and there is no robust evidence for icehouse climate conditions immediately preceding the Phanerozoic Eon. We encourage rigorous testing of the climatic and biotic framework we propose here, which from available evidence supports a Phanerozoic-style coupling of metazoan life and climate since the Ediacaran Period.

Methods

Ediacaran glacial deposits

Our Ediacaran glaciogenic deposits dataset (Supplementary Data 1) is derived from the compilations of Youbi *et al.* (2020), Retallack (2022), Tindal (2023), Wang *et al.* (2023a, b), and Niu *et al.* (2024), with additional data drawn from references cited in those studies, notably Hambrey and Harland (1981) and Arnaud *et al.* (2011), as well as more recent publications. All deposits included in the compilations of Youbi *et al.* (2020), Retallack (2022), Wang *et al.* (2023a, b), and Niu *et al.* (2024) were considered. Deposits not included in these compilations but that were included in Tindal's (2023) Appendix 2 were considered where:

1) their glaciogenicity score was greater than one star (see below; Tindal 2023), AND
2) an Ediacaran depositional age was plausible, meaning that:
    a) neither age constraint contradicts an Ediacaran age, AND
    b) at most one of the maximum and minimum age constraints is missing (“NA”), AND
        i) the maximum age constraint is not older than 635 Ma, OR
        ii) the minimum age constraint is older than 485.4 Ma AND younger than 600 Ma

    (i.e. maximum age is Ediacaran or the minimum age is mid-Ediacaran to Cambrian).

After this screening process, many of the remaining deposits from Tindal (2023) are still more likely of Cryogenian rather than Ediacaran age.

Determining depositional age

There is substantial circularity in the dating and correlation of Neoproterozoic putative glaciogenic deposits (Tindal 2023), which is partly responsible for the discrepancies between previous compilations(Table 1; Table 2; Figure S1; Supplementary Information). Putative Neoproterozoic glaciogenic deposits tend to be correlated together on lithostratigraphic grounds (‘glaciostratigraphy’; Tindal 2023). Independent age constraints are therefore crucial for testing potential patterns and quantifying temporal uncertainty in global palaeoclimate data.

Literature searches were performed to make rigorous assessments of depositional age for each potentially glaciogenic deposit. Where available, radiometric age constraints are preferred. Radiometric dates were included only if they possess a well-documented stratigraphic relationship with a putative glaciogenic deposit. Chemostratigraphic evidence is considered where there is good evidence for regional and global chemostratigraphic correlation. Biostratigraphic age constraints are a valuable independent dating method for candidate glaciogenic deposits. In particular, biostratigraphy is useful where Ediacaran fossils are found overlying a diamictite deposit, for example in northern China, Arabia, and the Baltic region, where the overlying units contain fossils like *Shaanxilithes* that are known to be restricted to the terminal Ediacaran or older (~550 to 538.8 Ma (Vickers-Rich *et al.* 2013; Wang *et al.* 2021a; Agić *et al.* 2024); Supplementary Information). Where late Ediacaran macrofossils are used to provide a conservative minimum age constraint, this is taken as the current age of the Ediacaran–Cambrian boundary, 538.8 Ma (Cohen *et al.* 2013; Linnemann *et al.* 2019), though it is likely that the true minimum age constraint is younger.

Assessing glaciogenicity

Putative glaciogenic deposits readily enter the literature, but are very difficult to excise from it if originally misinterpreted, as shown by the number of low-scoring deposits and the variable range of deposits included or excluded from previous Ediacaran compilations (Table 1; Table 2; Figure S1; Tindal 2023). Neoproterozoic diamictite deposits are frequently interpreted as glaciogenic, even when the sedimentology and geotectonic context make a non-glacial origin more parsimonious (Kennedy *et al.* 2019; Kennedy and Eyles 2021; Molén 2023; Palacios 2024). To mitigate for this, we followed the glaciogenicity assessments of Tindal (2023), who devised a semi-quantitative logarithmic five-star rating scheme to assess the strength of evidence for glaciogenicity of deposits, and applied it consistently across the pre-Pleistocene glacial record.

Tindal's (2023) scheme weights individual lines of sedimentological and geomorphological evidence alongside consideration of the depositional and tectonic context on a one to five star logarithmic scale on which a rating of five indicates unequivocal evidence for glaciation, and a rating of one means that a broad range of ice-free depositional processes could be responsible for producing the assembled characteristics (Supplementary Information; Table S1). The summary rating for each deposit is an exponential combination of all individual depositional characteristics, such that two lines of evidence at one level equate to one line of evidence at the next (higher) level. Because the scoring system incorporates multiple lines of evidence of varying individual strengths, it should be used to guide interpretations of the potentially glacial origins of a deposit but not as a strict diagnostic test.

In our compilation, we included all deposits following the criteria outlined above, meaning that all deposits cited in the compilations of Youbi *et al.* (2020), Retallack (2022), Wang *et al.* (2023a, b), and Niu *et al.* (2024) were included here regardless of score. However, we consider unreliable those deposits that score less than three out of five stars, meaning that for reliable units there is ‘circumstantial’ or better evidence that the deposit was formed under glacial influence(Tindal 2023, tbl. 2.1). For some deposits rated less than three stars, it may be that the level of described evidence does not accurately reflect the evidence that is available in the field, and so they may be upgraded in the future when further data come to light. Where a deposit was not included by Tindal (2023) and/or where substantial new evidence has been published since the initial assessment, BHT has reviewed the currently available evidence and provided updated ratings for these deposits (Supplementary Information).

Ediacaran palaeobiological data

Our palaeobiological dataset is primarily based on the compilations of Boddy *et al.* (2021) and Bowyer *et al.* (2024), with additional data from Surprenant and Droser (2024), Muscente *et al.* (2019), and other primary sources (Supplementary Data 2). The primary age model used to calibrate the palaeobiology dataset is Bowyer *et al.*'s (2023, 2024) age model K; for deposits older than ~550 Ma the age model primarily follows Yang *et al.* (2021). For Mistaken Point Ecological Reserve (MPER) data, we follow the original age model of Matthews *et al.* (2020). Where further radiometric or carbon isotope age controls are available, these have also been included within an updated age model (Supplementary Data 2).

We follow Wood *et al.* (2023) in considering each late Ediacaran biotic assemblage to be characterised by the novel morphotypes or major groups that first appear in that assemblage (Supplementary Data 2). For example, this makes the rangeomorph *Rangea* a component of the Avalon assemblage because rangeomorphs first appeared as a key part of the Avalon assemblage, even though *Rangea* itself is only known from deposits younger than ~557 Ma.

Palaeobiodiversity analyses were performed in *R* (R Core Team 2021) using the package *divDyn* (Kocsis *et al.* 2019). We examined raw genus richness and subsampled genus richness using inexact Shareholder Quorum subsampling (SQS; Alroy 2010a, 2014) with a quota of 0.4, unweighted collection-based classical rarefaction (UW) with a quota of eight collections, and occurrence-weighted by-list subsampling (OW) with a quota of 14 occurrences. Analyses were performed on the full dataset (Figure 4) and on the full dataset excluding South Australia due to the lack of precise dating of the South Australian sections (see below; Figure S5).

Water depth and the Avalon assemblage

The Avalon biotic assemblage is widely considered to be the oldest of the three Ediacaran biotic assemblages, and comprises predominantly sessile benthic taxa including frondose and non-frondose morphologies, some of which likely stood up in the water column whereas others reclined on the sea floor (Gehling and Narbonne 2007), alongside candidate cnidarians (e.g. Liu *et al.* 2014b, 2015; Dunn *et al.* 2022), and rare trace fossils (Liu *et al.* 2010, 2014a). The oldest occurrences of the Avalon assemblage are typically found between the end of the Gaskiers glaciation (~579 Ma) and the onset of the Shuram CIE (~575 Ma; Pu *et al.* 2016; Matthews *et al.* 2020; Boddy *et al.* 2021; Yang *et al.* 2021; Boag *et al.* 2024; Bowyer *et al.* 2024). The majority of Avalon assemblage occurrences are known from deep water siliciclastic depositional settings (Hofmann *et al.* 2008; Wilby *et al.* 2011; Narbonne *et al.* 2014; Boag *et al.* 2016, 2024; Matthews *et al.* 2020). However, a few shallow marine sites are now known.

Shallow marine Ediacaran fossil assemblages have been known from the Long Mynd (Welsh Borderland, UK) for over a century, but these are now largely regarded as either microbial or algal fossils, or microbially-induced sedimentary structures (McIlroy and Walter 1997; Liu 2011; Menon *et al.* 2015, 2017; McMahon *et al.* 2022). All of the Long Mynd fossil occurrences are younger than 566.6 ± 2.9 Ma, and reach an acme around 555.9 ± 3.5 Ma (Compston *et al.* 2002; Liu 2011). Shallow marine Ediacaran body fossils have been recovered from the Coomb Volcanic Formation (Llangynog Inlier, southeast Wales, UK), and include typical Avalon assemblage taxa like the palaeopascichnids *Palaeopascichnus* and *Yelovichnus*, as well as the holdfast discs *Aspidella sensu lato* and *Hiemalora* (Cope 1977, 1983; Clarke *et al.* 2024). The Llangynog Inlier fossil occurrences are all younger than 566.53 ± 0.72 Ma, and only the palaeopascichnids have been found in levels older than 564.09 ± 0.70 Ma (Clarke *et al.* 2024).

The upper Fermeuse Formation (Avalon Peninsula, eastern Newfoundland, Canada) was likely deposited on a shallow marine prograding delta slope, possibly above storm weather wave base (Gehling *et al.* 2000) or a little below it (Wood *et al.* 2003) and possibly within the photic zone (Hawco *et al.* 2021), and is considered to be younger than 564.13 ± 0.65 Ma (Matthews *et al.* 2020). The fossil assemblage in the uppermost Fermeuse Formation comprises discoidal forms, including *Aspidella terranovica* alongside probable holdfast discs, palaeopascichnids, and simple trace fossils (Gehling *et al.* 2000; Menon *et al.* 2013; Menon 2015; Hawco *et al.* 2021).

Boag *et al.* (2024) described soft-bodied Avalon assemblage Ediacaran fossils from shelf facies of the Blueflower Formation in the Goz A and Goz B sections, Wernecke Mountains, northwest Canada, including specimens of *Beltanelliformis* (which may be a pseudofossil; Menon *et al.* 2015), the holdfast disc *Aspidella s.l.*, and juvenile fronds with an external stem that could plausibly reflect *Arborea*, *Charniodiscus*, or *Trepassia* specimens. Regarding the possible affinities of the frondose forms, only *Charniodiscus* has been reported from older deep water facies in northwest Canada (Narbonne *et al.* 2014). No tubular fossils have yet been found in the shallow water facies of the Blueflower Formation, despite their presence in the deep water facies there (Carbone *et al.* 2015; Boag *et al.* 2024), and candidate bilaterian trace fossils are present but rare (Boag *et al.* 2024). The Blueflower Formation conformably overlies the Gametrail Formation, which contains a Shuram-correlative negative CIE, the termination of which has been dated as younger than 566.9 ± 3.5 Ma (Busch *et al.* 2023).

All shallow marine Avalon assemblage sites are younger than the termination of the Shuram CIE. The post-Shuram CIE shallow marine Avalon assemblages are differentiated from the shallow marine White Sea biotic assemblages more by the absence of taxa rather than their presence. There are no taxa exclusive to the Avalon assemblage in these shallow water deposits: palaeopascichnids and holdfast discs from both Avalonia and Laurentia, as well as the two indeterminate fronds from Laurentia, could all plausibly belong to taxa that are known to persist through both White Sea and Nama assemblages (e.g. *Charniodiscus*). However, tubular fossils, dickinsoniomorphs, bilaterialomorphs, and the various radial morphogroups that are ubiquitous in younger White Sea assemblage deposits are absent from the shallow marine Avalon assemblage sites that closely follow the Shuram CIE, as well as from coeval, post-Shuram, deeper marine Avalon assemblage sites (Narbonne *et al.* 2014; Noble *et al.* 2015; Kenchington *et al.* 2018; Boag *et al.* 2024; Clarke *et al.* 2024). The shallow marine northwest Canada occurrences of the problematic *Windermeria* alongside various annulated tubes and rare indeterminate trace fossils in the upper Blueflower Formation are thought to be considerably younger than the immediate post-Shuram interval (Narbonne 1994; Carbone *et al.* 2015; Boag *et al.* 2024).

The low number and diversity of shallow water occurrences of the Avalon biotic assemblage could be an artefact of environmental specificity, preservation or collection bias, but it is notable that no macrofossils have been recovered from shallow marine rocks in Laurentia deposited before the termination of the Shuram (Gametrail) negative CIE (Boag *et al.* 2024). This includes searches of barren sites where (a) the sedimentology appears suitable for such fossil preservation, (b) significant research time has been spent looking for these fossils by teams with a track record of finding them, and (c) coeval deep-water strata do preserve typical Avalon assemblage taxa (Boag *et al.* 2024). Moreover, although the scarcity of deep marine siliciclastic deposits after ~560 Ma may explain the apparent loss of the deep water Avalon biotic assemblage, there is no concomitant absence of shallow and mid-depths marine carbonate and siliciclastic deposits prior to the termination of the Shuram CIE (Bowyer *et al.* 2024) – there are pre- and syn-Shuram deposits which could have preserved a shallower water fauna if it was present (e.g. the shallow marine facies of the Nadaleen and Gametrail formations of northwest Canada (Boag *et al.* 2024), or the Wonoka Formation of South Australia). This observation lends support to the idea that the majority of Avalon assemblage taxa belonged to a deep-water biotope, with some components (e.g. *Charnia*) being more environmentally tolerant generalist taxa that were capable of inhabiting shallower marine settings in the later Ediacaran (Grazhdankin 2014; Boag *et al.* 2024), perhaps facilitated by post-Shuram global cooling into the late Ediacaran icehouse.

White Sea assemblage: correlating South Australia

The Ediacaran White Sea biotic assemblage is primarily known from localities in the Baltic Shield, where it has been dated to between >557 Ma and <553 Ma (e.g. Yang *et al.* 2021), and from South Australia (East Gondwana), where it is poorly constrained in age. The depositional age of the South Australia White Sea assemblage fossils is constrained below by the negative CIE in the Wonoka Formation, which is a likely correlative of the Shuram excursion and therefore provides a maximum depositional age for the Rawnsley Quartzite of ~566 Ma (Yang *et al.* 2021; Busch *et al.* 2022, 2023). The upper age constraint on the Rawnsley Quartzite is the unconformably overlying Uratanna and Parachilna formations. The Uratanna Formation has little in the way of age controls, but is widely regarded as being early Cambrian in age (Fortunian to Age 2), and trace and skeletal fossils in the Parachilna Formation indicate deposition during Cambrian Age 2 (Betts *et al.* 2018). The Ediacara Member fossiliferous deposits are typically correlated with those of the White Sea region on the East European Platform on the basis of taxonomic similarity of the South Australia and European White Sea assemblages (Waggoner 2003; Boag *et al.* 2016; Muscente *et al.* 2019; Boddy *et al.* 2021; Bowyer *et al.* 2022, 2023, 2024; Evans *et al.* 2022).

In the Baltic Shield, the northeast Russia White Sea deposits have yielded zircon U-Pb ages of 552.96 ± 0.66 Ma (sample WhiteSeaAsh, basal Zimnie Gory Formation) and 557.28 ± 0.63 Ma (sample 9607-1601-1, basal Verkhovka Formation), respectively (Yang *et al.* 2021). The Verkhovka and Erga (=Yorga) formations are the most fossiliferous of the four named late Ediacaran formations in the White Sea region (Grazhdankin 2004a), with fossil occurrences primarily reported from the upper Verkhovka and lower Erga formations, though sparser occurrences are also known from the Lyamsta (=Lamsta) and Zimnie Gory (=Zimnegory) formations (Fedonkin *et al.* 2012). The older radiometric date derives from a tuff that underlies the majority of occurrences of White Sea taxa in Russia (Fedonkin *et al.* 2012), providing a likely maximum age for the White Sea assemblage in its type area of ~558 Ma (Yang *et al.* 2021). However, the younger of the two dates derives from a horizon within the acme of White Sea taxonomic richness (Fedonkin *et al.* 2012; Yang *et al.* 2021). Potentially major sequence boundaries at the base and top of the Zimnie Gory Formation (Grazhdankin 2004b; Fedonkin *et al.* 2012) make it impractical to develop an age model above the lower Zimnie Gory tuff, and this is a source of uncertainty for a minimum age for the White Sea assemblage (Bowyer *et al.* 2023, 2024). On the East European Platform, a radiometric date of 556.82 ± 0.2 Ma from the middle of the discoidal and trace fossil-bearing horizons of the Mohylivska (=Mogilev; =Mohyliv) Formation, Podolya Basin, southeast Ukraine (Soldatenko *et al.* 2019), provides good correlative evidence for essentially synchronous existence of the White Sea assemblage across palaeogeographical Baltica.

In the Baltic Shield, the White Sea biotic assemblage is found in sedimentary deposits interpreted as lower to upper shoreface, deltaic, and distributary mouth bar (Grazhdankin 2004b) – i.e., shallow marine settings above fair-weather wave base). Following Boag *et al.* (2016, 2024) and Evans *et al.* (2022), the majority of the White Sea biotic assemblage fossils occur in strata deposited at or above storm-weather wave base, with only two very low diversity sites likely deposited below storm-weather wave base. The depositional context of the Ediacara Member fossiliferous rocks may be slightly different to that of other White Sea biotic assemblage sites, with facies discrepancies masked by regional differences in terminology (Gehling and Droser 2013; McMahon *et al.* 2020; Reid *et al.* 2020a, b). East Gondwanan Ediacara Member fossils are typically found in lower and middle shoreface facies, and less commonly in upper shoreface, lagoonal, and mixed-flat settings, all above fair weather wave base and in contrast to more mud-rich (possibly slightly deeper) occurrences on palaeogeographical Baltica (Grazhdankin 2004b; McMahon *et al.* 2020).

In summary, organisms of the White Sea biotic assemblage predominantly resided above storm weather wave base (Grazhdankin 2004b; Boag *et al.* 2016; McMahon *et al.* 2020; Reid *et al.* 2020a; Evans *et al.* 2022), and were typically younger than 558 Ma and older than 550 Ma (e.g. Soldatenko *et al.* 2019; Yang *et al.* 2021; Bowyer *et al.* 2023; Środoń *et al.* 2023), though the minimum age constraints plausibly allow slightly younger depositional ages. The age of the classic sites in South Australia is only loosely constrained without recourse to Ediacaran macrofossil biostratigraphy. To mitigate the potential circularity of using biostratigraphic age constraints in our study, we conducted sensitivity analyses by evaluating the palaeontological dataset both with (Figure 3; Figure 4) and without (Figure S3; Figure S5) occurrences from South Australia. Our patterns in both faunal composition (Figure 3; Figure S3) and taxonomic richness (Figure 4; Figure S5) are robust to the removal of all South Australia fossil occurrences.

Acknowledgements

We gratefully acknowledge funding from The Leverhulme Trust, grant RPG-2022-233 to MW, THPH, AGL and AP (Earth System dynamics at the dawn of the animal-rich biosphere), and the NERC C-CLEAR DTP (supporting the PhD studentship of BHT).

Supplementary Information

1. Summary of Ediacaran glaciation in the literature

Since 2020, several publications have compiled, compared, and tried to untangle various lines of evidence for putatively glaciogenic Ediacaran deposits (Table 1; Table 2; Figure S1). Linnemann *et al.* (2018, 2022) provided new radiometric age constraints for several peri-Gondwanan putative glaciogenic deposits and concluded that there were at least two episodes of mid- to late Ediacaran glaciation, at ~579 Ma and ~567–559 Ma respectively. Linnemann *et al.* (2018) further correlated these two intervals with the early and late stages of the Shuram negative carbon isotope excursion (CIE). Youbi *et al.* (2020) reviewed the likely depositional ages and palaeolatitudes of 25 candidate Ediacaran glaciogenic deposits, concluding that most were plausibly correlatable to the ~579 Ma Gaskiers glaciation of Newfoundland, and considered that Central Iapetus Magmatic Province (CIMP) volcanism around ~579 Ma may have contributed to termination of the Gaskiers glaciation. Vandyk *et al.* (2021) reviewed 20 Neoproterozoic striated pavements, including both Cryogenian and Ediacaran examples. Retallack (2022) reviewed 31 putative Ediacaran glaciogenic deposits and sedimentary structures, with a view to providing a glacial subdivision of the Ediacaran System. Tindal (2023) reviewed all putative pre-Pleistocene glacial deposits, including 224 of potentially Ediacaran age, and found good support for a discrete Gaskiers-interval glaciation terminating at ~579 Ma, but noted that there were significant and variable age uncertainties on almost all pre-Pleistocene glacial deposits. Wang *et al.* (2023a, b) reviewed 39 Ediacaran glaciogenic deposits and proposed a 'Great late Ediacaran ice age' (GEG in Figure S1) spanning approximately 20 Myrs from the Gaskiers glaciation at 580 Ma to the Hankalchough glaciation at 560 Ma, and noted that the GEG may possibly extend from 590 to 550 Ma. Niu *et al.* (2024) also reviewed Ediacaran glaciation evidence, broadly building on the dataset and correlations of Retallack (2022)but expanded to a total of 50 deposits, and reinterpreted many deposits as deriving from a 'Cordilleran-type mountain ice sheet' (CMIS) setting.

Despite including similar numbers of deposits overall (main text Table 1; main text Table 2), these previous compilations (Youbi *et al.* 2020; Retallack 2022; Wang *et al.* 2023a, b; Niu *et al.* 2024) included different sets of putative Ediacaran glaciogenic deposits and provided different correlation frameworks for them (Figure S1). In this contribution, we consider all of the global deposits included in these publications, and provide further discussion of several of them below (section 3) to clarify our views on their evidence for glacial conditions.

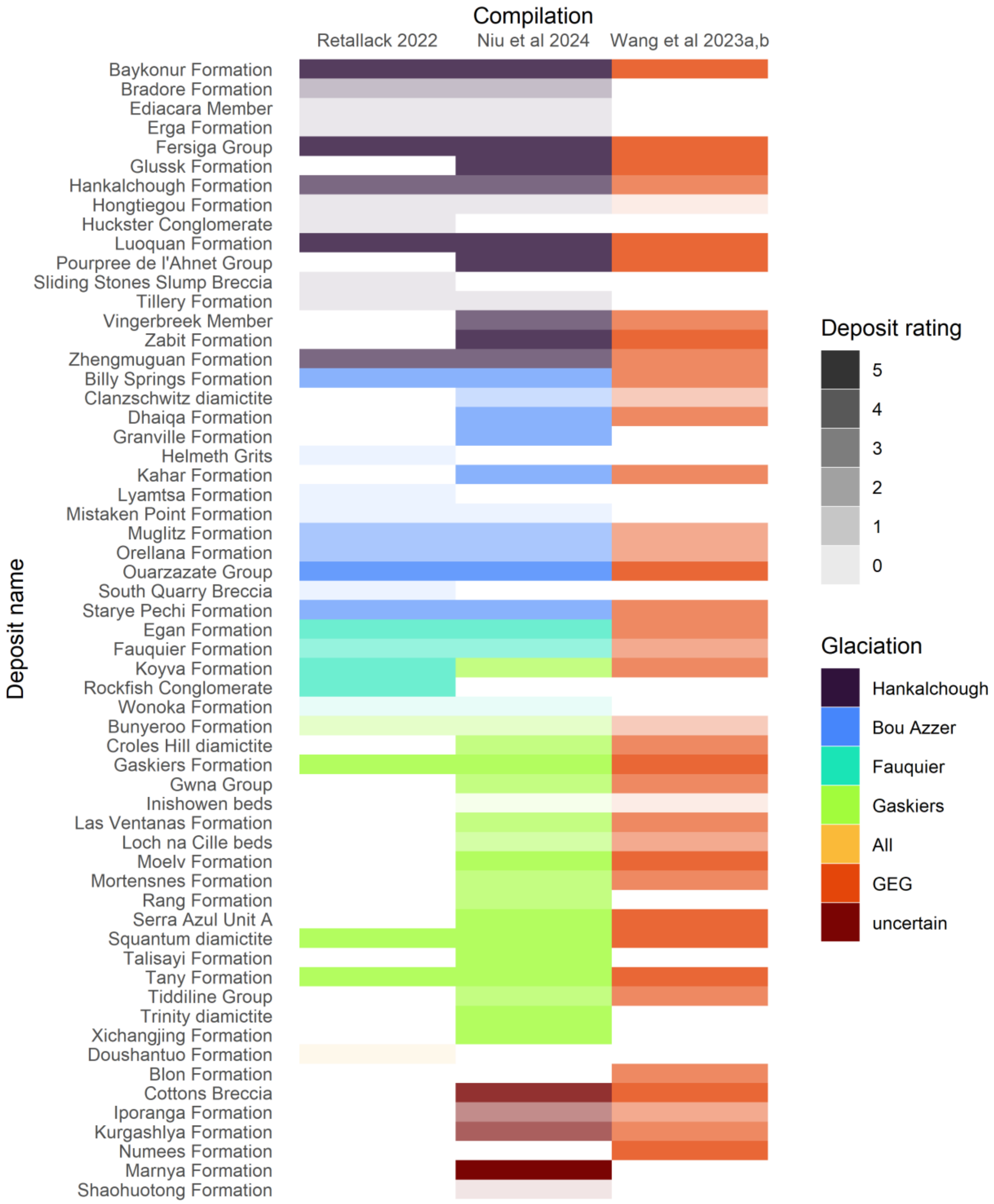

Figure S1. Deposits included in four recent compilations (Retallack 2022; Wang et al. *2023a, b; Niu* et al. *2024) of candidate glaciogenic deposits, coloured by the glaciations they were assigned to in each compilation and faded according to their star rating (this study and Tindal 2023). Note that Retallack (2022) interpreted glacioeustasy in the Doushantuo Formation as relevant to all four identified glaciations.*

845 ## 2. Age constraints on putative Ediacaran glaciogenic deposits

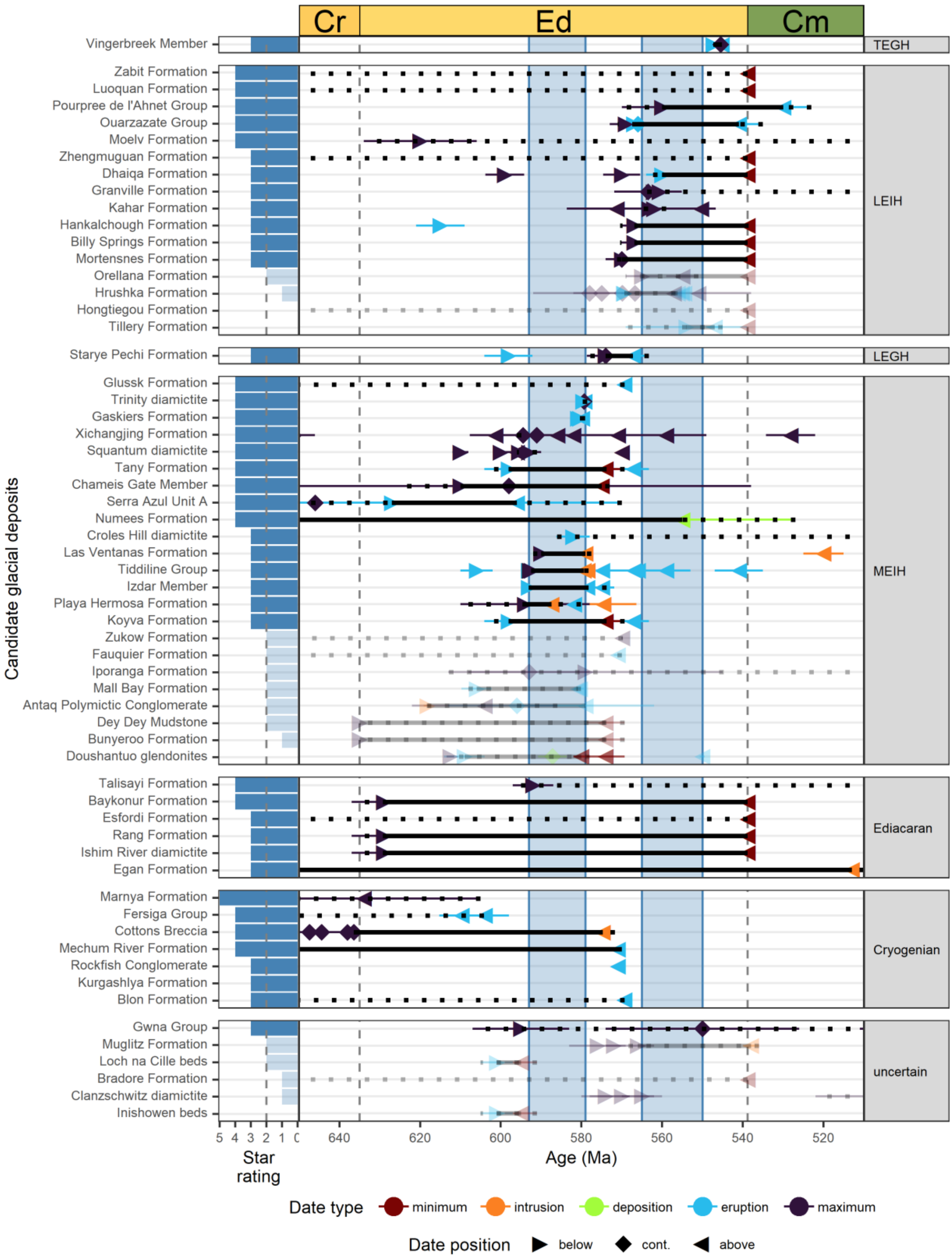

846

847 *Figure S2. Age constraints on all candidate Ediacaran glaciogenic deposits included in our Supplementary Data 2, grouped*
848 *by their likely depositional interval, and arranged by the strength of evidence for glacial influence on their deposition (the*
849 *star rating score). TEGH: terminal Ediacaran greenhouse; LEIH: late Ediacaran icehouse; LEGH: late Ediacaran greenhouse;*
850 *MEIH: mid-Ediacaran greenhouse; Ediacaran: deposits constrained only to the Ediacaran Period; Cryogenian: deposits more*

likely of Cryogenian than Ediacaran age; uncertain: deposits that may be Ediacaran in age but with questionable constraints. Thick solid lines show the age range of each deposit which is bracketed by depositional age constraints below and above, not including maximum age constraints (e.g. detrital zircons); thick dotted lines show the full possible age range including analytical uncertainty for each deposit. Age constraints are from radiometric dates, carbon isotope stratigraphy, and terminal Ediacaran or Palaeozoic biostratigraphic data (see Methods; Supplementary Data 1). Date type: how the age constraint has been interpreted with respect to its source; Date position: whether the age constraint is stratigraphically below, contemporaneous (cont.) with, or above the candidate glaciogenic deposit. Deposits that were scored two stars or less are faded. Vertical blue regions show the likely intervals of the mid-Ediacaran icehouse (~593 to 579 Ma) and the late Ediacaran icehouse (~565 to 550 Ma). Cr: Cryogenian; Ed: Ediacaran; Cm: Cambrian; cont.: contemporaneous. See also main text Figure 1 which excludes the likely Cryogenian deposits.

3. Rating likely glaciogenicity

Here we briefly describe the potential glaciogenicity star rating system devised by Tindal (2023, ch. 2); readers are referred to the thesis for a fuller description and explanation. The five star exponential rating scheme (Table S1) can be used to assess the likelihood that any particular sedimentary deposit had a glacial origin (Tindal 2023). This scheme incorporates the diversity of possible sedimentological and depositional setting evidence for glaciogenicity, much of which can also result from non-glacial origins.

Five qualitatively-defined categories of confidence are used, with individual lines of evidence being given a rating of zero to five stars (Tindal 2023). Each deposit may have multiple different lines of evidence, all of which contribute to an overall rating for the whole deposit. In this way, a deposit may be confidently considered glaciogenic if it has either one five star “unequivocal” line of evidence or several weaker (four star: “strong”; three star: “circumstantial”; two star: “weak”; one star: “equivocal”) lines of evidence (Tindal 2023). An additional zero star “insufficient” category is added here (Table S1), which was used but not defined for some deposits that fail to meet the evidence threshold of one (Tindal 2023).

Tindal's (2023) approach to semi-quantitatively combining lines of evidence was to make two lines of evidence from one category equivalent to one line of evidence from the next category. For example, two three-star (“circumstantial”) lines of evidence in one deposit would be equivalent to one four-star (“strong”) line of evidence. It is therefore possible to have a ‘greater-than-five-star’ deposit, though in practice this is not a concern for the candidate Ediacaran glaciogenic deposits examined here.

Table S1. Adaptation of Tindal's (2023) table 2.1 describing the five-star rating scheme for assessing the potential glaciogenicity of a given sedimentary deposit. Here we have added an "insufficient" zero star rating for deposits that have been interpreted as glaciogenic in the literature but do not meet the one star evidential threshold following Tindal's (2023) method.

Strength	Stars	Definition
Unequivocal	★★★★★	No realistic ice-free depositional environment could produce this evidence.
Strong	★★★★	No realistic ice-free depositional environment is likely to produce this evidence.
Circumstantial	★★★	This evidence could be produced by specific, but rare, ice-free depositional environments.
Weak	★★	Some ice-free depositional environments could produce this evidence.
Equivocal	★	Many ice-free depositional environments could produce this evidence.
Insufficient		Many ice-free depositional environments could produce this evidence, and an ice-related origin of the observed features is not supported by the evidence.

4. Notes on specific deposits

We do not discuss all potential glaciogenic deposits here. Instead we focus on deposits:

a. that were not explicitly rated in Tindal's (2023) original compilation and/or the availability of new evidence means their ratings have been reviewed since the initial compilation;
b. where there is uncertainty about their glaciogenicity that is not captured in the rating scheme; or
c. where there is uncertainty about their depositional age that affects their interpretation in this study.

4.1. Deposits with revised star ratings

All deposits with new or revised glaciogenicity ratings were assessed by BHT following his original methodology.

4.1.1. Four star: Ouarzazate Group, Morocco

The Ouarzazate Group, as distinct from the Izdar Member, was not included in Tindal (2023) and is given a four star rating here following data presented in Vernhet *et al.* (2012).

Ouarzazate Group: ★★★★☆ Small striated surfaces with crescentic gouges, and diamictite with subangular to subrounded clasts from 3 lithological groups, some of which are striated.

4.1.2. Four star: Xichangjing Formation, China

The Xichangjing Formation was included in the Niu *et al.* (2024) compilation. Originally grouped by Tindal (2023) with the Shaohuotonggou Group, Gansu Province, China, new evidence presented in Niu *et al.* (2024) now allows an independent assessment of the Xichangjing Formation. This revised assessment provides a four star rating for the Xichangjing Formation.

Xichangjing Formation: ★★★★☆ Deformed beds interpreted as glaciotectonism, and diamictite with subangular to rounded clasts from 4 lithological groups, some of which are facetted or striated.

4.1.3. Three star: Hankalchough Formation, China

The Hankalchough Formation was originally rated a two star deposit (Tindal 2023). The addition of dropstones (Xiao *et al.* 2004) makes the Hankalchough Formation a three star deposit.

Hankalchough Formation: ★★★☆☆ diamictite and dropstones with angular clasts from 3 lithological groups.

4.1.4. Three star: Zhengmuguan Formation, China

The Zhengmuguan Formation was originally rated a two star deposit (Tindal 2023). The addition of angular clasts and smoothed surfaces (Wang *et al.* 2021b) makes the Zhengmuguan Formation a three star deposit.

Zhengmuguan Formation: ★★★☆☆ Small smooth surfaces, and diamictite and dropstones with angular to rounded clasts from 2 lithological groups.

4.1.5. Two star: Iporanga Formation, Brazil

The Iporanga Formation has been included in the Wang *et al.* (2023a, b) and Niu *et al.* (2024) compilations. The Iporanga Formation has not been uniformly interpreted as glaciogenic, with diamictite units hosting mostly locally-sourced pebbles interbedded with turbidites (Campanha *et al.* 2008). The Iporanga Formation was excluded from the Tindal (2023) compilation because the publications with sedimentological data did not interpret the unit as glaciogenic (but rather as a basal conglomerate and breccia (Campanha *et al.* 2008)). The Iporanga Formation is rated here because of its inclusion in recent compilations (Wang *et al.* 2023a, b; Niu *et al.* 2024) and published mention of glaciogenic interpretation (Campanha *et al.* 2008), and is given a two star rating.

Iporanga Formation: ★★☆☆☆ Basal conglomerate with clasts of unreported roundness from 3 lithological groups.

4.1.6. Two star: Mall Bay Formation, Canada

Evidence of glaciogenicity was assessed for the Mall Bay Formation following the recent publication of Fitzgerald *et al.* (2024). Rare dropstones have previously been reported from the uppermost part of the formation (Pu *et al.* 2016), but Fitzgerald *et al.* (2024) recorded evidence of cold climate conditions in the Mall Bay Formation at least 500 m below its top, and therefore substantially below the pre-Gaskiers Formation date of 580.34 ± 0.52 Ma (Pu *et al.* 2016). As well as potentially glaciogenic deposits in the Mall Bay Formation, Fitzgerald *et al.* (2024) also reported the occurrence of glendonites which provide further support for cold water conditions. Based on the new evidence presented by Fitzgerald *et al.* (2024), the Mall Bay Formation is rated a two star deposit.

Mall Bay Formation: ★★☆☆☆ subrounded dropstones from 2 lithological groups, some of which are facetted.

4.1.7. Two star and one star: Weesenstein Group Müglitz Formation and Clanzschwitz Group Member 3, Germany

The Clanzschwitz Group Member 3 and Weesentein Group Müglitz Formation diamictites were originally given a combined rating in Tindal (2023). Here, we assess each on its own merits following the revised Cambro-Ordovician age assignment for both units and questions about their potential glaciogenicity (Kühnemann *et al.* 2024; Meinhold *et al.* 2025). The Clanzschwitz and Weesenstein diamictites are now rated one and two stars, respectively.

Clanzschwitz Group Member 3: ★☆☆☆☆ loose stones found in a field containing diamictite with clasts of unreported roundness from one lithological group, some of which are facetted.

Weesenstein Group Müglitz Formation: ★★☆☆☆ diamictite and dropstones with rounded clasts from 2 lithological groups, some of which are facetted.

Of the Cadomian candidate Ediacaran glaciogenic deposits, only the Granville Formation (Normandy, France) is considered a three star deposit, and sea ice-derived dropstones remains a plausible interpretation for that unit (Doré 1981).

4.1.8. Zero star: Doushantuo Formation, China

The Retallack (2022) compilation included the Doushantuo Formation as evidence for each of the four glaciations he identified. Retallack (2022, p. 227) states in the text that the evidence of glaciogenicity this refers to is glacioeustasy inferred from hiatuses in the Doushantuo Formation stratigraphy, in the form of "*three glacioeustatic disconformities marked by paleokarst*", with the evidence and stratigraphic positions of these disconformities not being specified. Tindal (2023) explicitly discounted evidence that relates to glacioeustasy, considering it not to reflect evidence of proximal glaciation. We follow the same argument here and do not consider the Doushantuo Formation to contain evidence of glaciation. Because it was included in a compilation, here we assign it a zero star rating, rather than simply removing it.

4.1.9. Zero star: English conglomerates, UK

The Retallack (2022) compilation included the Huckster Conglomerate (Portway Formation), the Helmeth Grits (Stretton Shale), South Quarry Breccia Member (Beacon Hill Formation), and Sliding Stones Slump Breccia Member (Ives Head Formation). As noted by Tindal (2023, pp. 187-188), these deposits have never previously been considered glaciogenic and are generally interpreted as shallow marine conglomerates or volcaniclastic marine slump breccias. A.G.L. has examined all of these deposits and also favours a non-glaciogenic interpretation. Here, we follow the widely accepted non-glaciogenic interpretations for all of these units and do not include them in our compilation.

4.1.10. Zero star: Tillery Formation, USA

The Tillery Formation was not interpreted as potentially glaciogenic before its inclusion in the Retallack (2022) and Niu *et al.* (2024) compilations. The Tillery Formation is generally regarded as having been deposited by volcanic and submarine gravitational processes by researchers who have published primary sedimentological data (Gibson and Teeter 1984). We discuss it here because it was included in two recent compilations (Retallack 2022; Niu *et al.* 2024) but, following Tindal (2023), we assign a zero star rating to the Tillery Formation because it has not been interpreted as potentially glaciogenic by researchers who have published primary sedimentological data.

4.2. Uncertainty in depositional context

4.2.1. Vingerbreek Member and Unconformity, Namibia

The Vingerbreek Member (Nudaus Formation, basal Schwarzrand Subgroup, Nama Group), Namibia, is a putative glaciogenic deposit from the terminal Ediacaran interval (~551 to 540 Ma; Kröner and Germs 1971; Kröner 1981). Reported glaciogenic deposits of the Vingerbreek Member have been studied in the Klein Karas Mountains, Namibia, and can be seen on Farms Tierkloof, Zukoms, and Steinfeld, as well as near the Orange River in South Africa (Schwellnus 1941; Martin 1965; Kröner and Germs 1971; Kröner 1981; Germs and Gaucher 2012; Zieger-Hofmann *et al.* 2022). The basal Vingerbreek Member and Vingerbreek Unconformity are younger than 547.36 ± 0.23 Ma (Bowring *et al.* 2007), possibly as young as 545.27 ± 0.11 Ma (Nelson *et al.* 2022), with a likely age of ~545.5 Ma (Bowyer *et al.* 2023), though the scarcity of carbon isotope data in this part of the Nama Group stratigraphy hampers more precise correlation. Nevertheless, it is clearly younger than the LEIH identified here as terminating at ~550 Ma.

In the Zaris and Vioolsdrif sub-basins, the Vingerbreek Member includes a basal diamictite resting on an erosional unconformity (Kröner 1981; Germs and Gaucher 2012; Zieger-Hofmann *et al.* 2022). In the Klein Karas Mountains, the Vingerbreek Member diamictites are sporadic and typically thin (~1 to 3 m thick), though they exceptionally reach up to 11 m in the Orange River region (Kröner 1981). Clasts reach a diameter of approximately 0.5 m and sit in a matrix of ferruginous and calcareous shale (Kröner 1981). The Vingerbreek Member was originally described as a “limestone conglomerate”, with clasts comprising the boulders and pebbles of the underlying “Schwarzkalk” limestone (Kröner and Germs 1971). Kröner (1981, p. 176) stated that the diamictite comprises “an obviously reworked boulder bed” with some facetted and striated clasts ranging from 0.02 to 1 m diameter comprising sandy and silty shales, dolostones, quartzite, schist, and granite, and most subsequent work has focused on the Vingerbreek Unconformity rather than the ‘diamictite’. The Vingerbreek Member ‘diamictite’ may thus be better described as a clast-supported conglomerate or breccia, and has even been interpreted as fluvial or current-derived in origin in studies that determined a glacial origin for the unconformity beneath (Kröner 1981).

Similar to the striated and polished surfaces reported for the Vingerbreek Unconformity, the (rare) striated clasts supposedly found in the Vingerbreek diamictite (Martin 1965; Kröner 1981) can also be explained by debris flow deposition rather than glacial action (e.g. Winterer and Von der Borch 1968; Kennedy and Eyles 2021; Tindal 2023). Striated clasts have not been found in the southern outcrops near the Orange River (Zieger-Hofmann *et al.* 2022) and none have been figured from the more northerly outcrops in the Zaris sub-basin. Significantly, in the Orange River area, the diamictite grades into turbidites (Zieger-Hofmann *et al.* 2022), consistent with a non-glaciogenic mass flow interpretation for these deposits.

Possible glacial geomorphology has been reported in the form of a polished and striated surface (with seemingly random orientations of striations) with channels up to 20 m deep and 1.6 km wide that exhibit grooves on their flanks (Kröner 1981; Zieger-Hofmann *et al.* 2022). Early reports of *roches moutonées* (Schwellnus 1941) have been refuted by subsequent work (Martin 1965). This basal Vingerbreek Unconformity has only been found in the southern part of the Nama Basin (the Zaris and possibly Vioolsdrif sub-basins), where up to 30 metres of stratigraphy may have been lost (Kröner 1981; Germs and Gaucher 2012; Zieger-Hofmann *et al.* 2022). The unconformity has not been reported in the northern Witputs sub-basin.

The Vingerbreek unconformity has been interpreted to result from one or more of tectonic, glacial, proglacial, and fluvial mechanisms (Schwellnus 1941; Kröner 1981; Germs and Gaucher 2012; Zieger-Hofmann *et al.* 2022). Even if there was no ice present in the Nama Basin during its formation, glacioeustasy has been invoked as the driving mechanism for the erosion (Germs and Gaucher 2012). The channels have largely been interpreted as fluvial in origin, however, with the infill deposit and flank grooves discussed as potentially caused by glacial or sea ice (Martin 1965; Kröner 1981; Germs and Gaucher 2012; Zieger-Hofmann *et al.* 2022). Rock avalanche and mass flow processes are also known to produce similar polished and striated surfaces (Hambrey and Harland 1981; Huang and Fan 2013; Massey *et al.* 2013; Hu and McSaveney 2018), and such non-glacial explanations have been debated in case of the Vingerbreek Member and Unconformity since early studies of the area (Sandberg 1928; Schwellnus 1941). There exists uncertainty even in publications that confidently conclude a glacial interpretation of the Vingerbreek unconformity, with Germs and Gaucher (2012, p. 100) ascribing the formation of the unconformity in the Zaris sub-basin to both far-field glacioeustasy and near-field subglacial action, whilst also acknowledging that "*tectonism in the Nama foreland basin probably played a role in the formation of the Vingerbreek Unconformity*".

Kröner (1981) interpreted the Vingerbreek as recording a short-lived mountain glaciation. The short time interval is consistent with the plausible depositional age range of ~1.5 to 4 Myr (Bowyer *et al.* 2023), but this is inconsistent with a mountain glacier interpretation, which would require rapid uplift and subsidence, without concomitant erosion, of only the southern sub-basins to account for the surrounding marine deposits.

A glaciogenic interpretation is implausible, but not impossible. The diamictite and surfaces require further study and documentation to properly assess this hypothesis. Perhaps more plausible than a glaciogenic interpretation is a combination of glacioeustatic sea level fall driving erosion (although this is not seen in the rest of the Nama Basin (Bowyer *et al.* 2024)) with a final cold pulse at the end of the LEIH facilitating the formation of sea ice in the Zaris and Vioolsdrif sub-basins, as proposed by Martin (1965). Support for this may be found in the rock volume and area record (Bowyer *et al.* 2024), which in addition to the major step-change at 550.5 Ma witnesses a second, smaller, step-change at ~547 Ma with an increase in the relative proportion of carbonate rocks (mostly limestones). If the Vingerbreek Unconformity is dated to the maximum end of its possible age constraints, it may indeed reflect a final glacioeustatic sea level fall related to the LEIH (main text Figure 1; **Error! Reference source not found.**), possibly with the development of sea ice around the Nama Basin. However, it is not clear why this would not have left some signal in the northern part of the Nama Basin as well. Fundamentally, further sedimentological work is required to address the glaciogenicity of the Vingerbreek Member and Unconformity, but its depositional and palaeoclimatic context currently argue against a glacial interpretation.

4.2.2. Squantum Member (Roxbury Conglomerate Formation), USA

The Squantum Member (Roxbury Conglomerate Formation) crops out in the Boston Basin, northeast USA, and was deposited on the Avalonian palaeoplate in the late Neoproterozoic. It is reasonably well-constrained in age by radiometric dates to between 595.8 ± 1.2 Ma (from the underlying Lynn-Mattapan volcanic complex; Thompson *et al.* 2007) and ~568 Ma (from the overlying Cambridge Argillite; Thompson and Bowring 2000).

The Boston Basin in the Ediacaran was a back-arc basin setting within the Avalon Terrane, the modern extent of which is strongly demarcated by faults (Carto and Eyles 2012). The Ediacaran stratigraphy in the Boston Basin is organized into the Boston Bay Group, which comprises two formations: the lower Roxbury Conglomerate and upper Cambridge Argillite. The Roxbury Conglomerate is divided into three members. The lower Brookline Member is predominantly composed of conglomerates, the middle Dorchester Member is primarily fine-grained (argillaceous) turbidites with minor conglomerates, and the upper Squantum Member is mostly diamictite facies interbedded with sandstones and siltstones (Carto and Eyles 2012). The Cambridge Argillite comprises approximately 5.5 km of tuff-rich finely laminated to thinly bedded fine-grained (argillaceous) turbidites (Carto and Eyles 2012). Three primary and conformably associated facies are recognized across the Roxbury Conglomerate (Carto and Eyles 2012): (1) conglomerate and sandstone, (2) diamictite, and (3) mudrock.

The conglomeratic and sandstone facies (1) are common in the Brookline Member, which can be up to approximately 1.3 km thick (Tierney *et al.* 1968) and comprises massive clast- and matrix-supported conglomerates with erosive bases that grade up to normally graded sandstones (Carto and Eyles 2012). The conglomerate clasts are pebble- to boulder-sized, moderately to well sorted, subrounded to rounded, and are predominantly of lithologies found within the Boston Basin, including rhyolites, dacites, basalts, diorites, and granites (Carto and Eyles 2012). The sandstones which grade out of the conglomerates are mostly massive but some develop low-angle cross-lamination, whilst laminated normally graded sandstones also occur and may have soft sediment deformation structures including convolute laminae and ‘dish-and-pillar’ structures (Carto and Eyles 2012). The conglomerate and sandstone facies are often interbedded diamictites and thick mudrocks (Carto and Eyles 2012). The conglomerate and sandstone facies is interpreted as the result of the rapid deposition from cohesionless gravelly debris flows representing T_a (conglomerate) to $T_{b\text{-}c}$ (sandstone) divisions of the Bouma sequence (Bouma 1962) with a likely fluvial origin of the clasts (Carto and Eyles 2012). Rapid deposition is supported by soft sediment deformation structures observed in the sandstone bodies (Carto and Eyles 2012).

The diamictite facies (2), typically associated with the upper Squantum Member, comprises massive or chaotic matrix-supported polymict diamictites with pebble- to boulder-sized, moderately to well sorted subrounded to angular clasts of predominantly local lithologies (felsic and mafic volcanics, granodiorite, quartzite, siltstone, and sandstone), similar to the clasts of the conglomerate facies (Carto and Eyles 2012). The diamictites vary in thickness from approximately 8 m in outcrop to 215 m in the subsurface (Tierney *et al.* 1968; Carto and Eyles 2012). The diamictite facies is typified by sharp, erosive basal contacts and transitional upper boundaries as the diamictites grade into sandstones or conglomerates (Carto and Eyles 2012). The chaotic diamictites can show crude stratification with large rafts of conglomerate, sandstone, and mudrock poorly mixed through the diamictite (Carto and Eyles 2012). Facetted clasts have not been found, and striated clasts identified by earlier workers (Sayles 1914) were not found by subsequent investigators (Carto and Eyles 2012). Carto and Eyles (2012) note that the distinction between the Roxbury Conglomerate diamictite and conglomerate facies is the proportion of matrix (10 vol.% to 30 vol.% in the conglomerates and 80 vol.% in the diamictites) with other characteristics, particularly clast composition and form, being remarkably similar – a similarity noted by previous workers who were also dubious of a glaciogenic origin (Dott 1961; Socci and Smith 1990). The diamictite facies is interpreted as the result of the earlier stages of downslope mixing of conglomeratic and muddy material deriving from primary fan or slope-deposited conglomerates, an interpretation that is supported by the conformable, interbedded, relationship between the diamictite facies with coarse- and fine-grained turbidites (Carto and Eyles 2012).

The argillite facies (3) refers to "rhythmically laminated (0.1 to 1 mm thick) muddy-siltstones that grade subtly into mudstone" (Carto and Eyles 2012, p. 8). The argillite facies is typical of the Cambridge Argillite but is found interbedded with both the conglomerate and diamictite facies throughout the Boston Bay Group on scales of centimetres to hundreds of metres thickness (Carto and Eyles 2012). Sedimentary structures include parallel to wavy laminations, cross-lamination, and both large- and small-scale slump folds which occur throughout the unit in argillite interbedded with conglomerate and diamictite facies as well as with discrete tuff horizons (Carto and Eyles 2012). The argillite facies has been consistently interpreted as a deep marine (below storm wave base) low-density turbidite (Dott 1961; Thompson and Bowring 2000; Carto and Eyles 2012)

A fourth facies, or perhaps a sub-facies of the argillite facies, is also considered: the pebbly argillite (Carto and Eyles 2012). Stratigraphically and geographically limited to approximately 0.5 m in total directly underlying diamictites at Squantum Head is a laminated argillite with matrix-supported pebbles (approximately 75 vol.% matrix) that is interbedded with non-pebbly laminated and graded argillites (Carto and Eyles 2012). The clasts are all small, typically gravel-size or smaller, rounded to subrounded, and composed of the same local lithologies as the conglomerate and diamictite facies (Carto and Eyles 2012). The pebbly layers form couplets with overlying thin laminae of massive pebble-free argillite (Carto and Eyles 2012). The 'diamictite-argillite couplets' have been interpreted as ice-rafted debris or dropstones – and this remains possible – but an interpretation as debrite-turbidite couplets where finer material is sheared off the top of a dilute debris flow as a turbidity current and settles out onto the deposited debrite is more parsimonious with the surrounding facies (Carto and Eyles 2012). Important to this non-glaciogenic origin is the apparent absence of any larger (cobble- or boulder-sized) clasts from the pebbly argillite (Carto and Eyles 2012). The pebbly argillite is interpreted as a slightly more distal equivalent of the diamictite facies, representing part of a debris flow that ran away from or further than the main flow resulting in a more dilute flow (Carto and Eyles 2012).

The weight of evidence reviewed in Carto and Eyles (2012) argues against a primary glaciogenic origin for the 'Squantum Tillite'. However, it does still fulfil several criteria for consideration as being somewhat glaciogenic and is given a four star rating under Tindal's 2023) scheme. The most parsimonious interpretation for the depositional context of the Squantum Member diamictite facies may be as part of a continuum of deposits resulting from downslope remobilization of fan or slope sediments including sandstones, mudstones, and conglomerates. The conglomerates may have an originally glaciogenic origin, but that is not certain and could equally, or perhaps more plausibly given the absence of strongly facetted or striated clasts, have a fluvial origin.

4.2.3. Glendonites as cold climate indicators in the Doushantuo Formation, China

Although not a glaciogenic deposit, support for a generally cold climate between 600 to 579 Ma comes from glendonites deposited in the Doushantuo Formation, South China. Situated in low (tropical) latitudes during the Ediacaran (Scotese 2016; Merdith *et al.* 2021; Li *et al.* 2023), South China would have avoided glaciation in all but the most extreme of icehouse climate conditions. Although there is no direct evidence for mid-Ediacaran glaciation known from South China, the Doushantuo Formation includes stratigraphically restricted occurrences of glendonites (Wang *et al.* 2017, 2020), which are geologically stable pseudomorphs of the hydrous calcium carbonate mineral ikaite that preferentially precipitates from cold (<4°C, possibly up to 10°C) sea water with high alkalinity, organic content, and perhaps phosphorous concentrations (e.g. Suess *et al.* 1982; Stein and Smith 1986; Bischoff *et al.* 1993; Zhou *et al.* 2015; Field *et al.* 2017).

Glendonites are restricted to the middle Doushantuo Formation, approximately coincident with the exceptionally preserved Weng'an biota (Wang *et al.* 2017, 2020). The lowest Doushantuo Formation glendonite occurrences are reported from slightly above a small negative CIE between EN1 and EN2 (Wang *et al.* 2017, 2020) that has a detrital zircon age of <612.5 ± 0.9 Ma (Zhou *et al.* 2017; Yang *et al.* 2021), and is tentatively correlated with horizons dated at 599 ± 4 Ma (zircon U-Pb; Barfod *et al.* 2002; Wang *et al.* 2017, 2020) and 587.2 ± 3.6 Ma (shale Re-Os; Yang *et al.* 2021). No glendonites have been found above the EN2 carbon isotope excursion (Wang *et al.* 2017, 2020), which has been correlated with the terminal Gaskiers glaciation at ~580 Ma and is below the EN3 (Shuram) CIE (e.g. Yang *et al.* 2021).

The abundant and temporally-restricted glendonites in the low latitude deep marine Doushantuo Formation may reflect a cooler ocean compared to the intervals before and after. The glendonite occurrences are constrained by radiometric dating and carbon isotope stratigraphy to between ~600 and ~579 Ma (Wang *et al.* 2017, 2020; Zhou *et al.* 2017), during the MEIH interval identified here.

4.3. Uncertainty in depositional age

4.3.1. Hankalchough Formation, China

The Hankalchough Formation is reliably constrained by radiometric dates and chemostratigraphy to a late Ediacaran age. The upper Zhamoketi Formation, considerably stratigraphically below the Hankalchough Formation, has yielded a detrital zircon U-Pb date of 616.5 ± 5.9 Ma (He *et al.* 2014), providing a firm maximum age constraint. The Hankalchough Formation was deposited at least 65 m stratigraphically above the recovery limb of an extreme negative CIE in the Shuiquan Formation (stratigraphically above the dated Zhamoketi Formation); this extreme negative CIE has been correlated with the Shuram excursion globally (Xiao *et al.* 2004; Wang *et al.* 2023a). The maximum depositional age of the Hankalchough Formation is therefore taken as the minimum depositional age of the Shuram isotope excursion recovery (younger than 566.9 ± 3.5 Ma; Busch *et al.* 2023). The unconformably overlying Xishanblaq Formation has yielded Cambrian microfossils (Xiao *et al.* 2004; Yao *et al.* 2005), providing a minimum depositional age of 538.8 Ma for the Hankalchough Formation. The relatively close stratigraphic proximity of the negative CIE below the Hankalchough Formation makes a late but not terminal Ediacaran age most likely, though better age constraints are required to be certain.

4.3.2. *Shaanxilithes* age constraints in northern China

Three major candidate glaciogenic diamictites of Neoproterozoic age in present-day northern China lack radiometric or chemostratigraphic constraints: the Hongtiegou Formation (Qaidam block), the Zhengmuguan Formation (North China craton), and the Luoquan Formation (North China craton). Radiometric age constraints for all of these deposits are poor or non-existent, with all of the diamictites resting unconformably on rocks with Mesoproterozoic zircon dates (Wang *et al.* 2021a). Biostratigraphy provides the primary age constraint on these deposits, which are overlain by strata containing successively Ediacaran and Cambrian fossils, notably the non-biomineralised tubular cloudinomorph *Shaanxilithes* (Wang *et al.* 2021a).

Shaanxilithes is documented to have a short, terminal Ediacaran stratigraphic range in North China (Wang *et al.* 2021a, b; Surprenant and Droser 2024), and possibly pre-dates *Cloudina* fossils in South China and Siberia (Wang *et al.* 2021a). Importantly, *Shaanxilithes* has not been reliably reported from above the Ediacaran-Cambrian boundary, making it a candidate terminal Ediacaran index fossil (Chai *et al.* 2021; Wang *et al.* 2021b). Although generally reported from deposits known to be younger than 550 Ma (Psarras *et al.* 2023), stratigraphic uncertainty would allow a longer, older range of dates to be possible on the East European Platform (Surprenant and Droser 2024). Here, we apply a conservative approach and use occurrences of *Shaanxilithes* to provide a minimum age constraint of 538.8 Ma (Ediacaran-Cambrian boundary) on deposits that otherwise lack a clear minimum age constraint.

On the Qaidam Block (northern China), the Hongtiegou Formation diamictite is considered to be glaciogenic, with a minimum depositional age constrained by the occurrence of *Shaanxilithes* and *Charnia* in the overlying Zhoujieshan Formation (Shen *et al.* 2010; Pang *et al.* 2021; Wang *et al.* 2022). Both *Shaanxilithes* and *Charnia* are known from the terminal Ediacaran but not the Cambrian, and therefore provide a hard minimum age constraint of 538.8 Ma on the Hongtiegou Formation. It is likely that the unit is older than this, and possibly older than 550 Ma due to the delayed first appearance of *Shaanxilithes* above the diamictite. The maximum depositional age of the Hongtiegou Formation is less well constrained, but has been considered to be likely younger than 560 Ma following inconclusive carbon isotope data from the underlying Hongzaoshan Formation that show a recovery from a negative excursion of at least -6 ‰ near the base of that unit(Shen *et al.* 2010). Supposedly, *Redkinia* specimens have been recovered from the underlying Heitupo Formation (Wang *et al.* 1980; cited in Shen *et al.* 2010), which would indicate a likely maximum depositional age of ~555 Ma.

On the North China craton the minimum depositional age of the Luoquan and Zhengmuguan formations is constrained to a late Ediacaran (550 to 538.8 Ma) age by the occurrence of *Shaanxilithes* in the overlying Dongpo and Tuerkeng formations, respectively (Wang *et al.* 2021a), though the maximum depositional age is unconstrained. Both the Luoquan and Zhengmuguan formations provide extensive evidence for glaciation, including the repeated advance and retreat of glaciers or grounded ice sheets (Le Heron *et al.* 2018; Wang *et al.* 2021a, b). The conformable contact between the diamictites and overlying fossiliferous strata likely precludes an early or middle Ediacaran age for glaciation evidence. Similar to the Hontiegou and Zhoujieshan formations, the delayed first appearance of *Shaanxilithes* until near the top of the non-glacial unit likely indicates a minimum depositional age closer to 550 Ma than 538.8 Ma, following the suspected range of *Shaanxilithes* (Wang *et al.* 2021a, b; Surprenant and Droser 2024).

Here, we consider it likely that the Hongtiegou, Luoquan, and Zhengmuguan formations are of similar age (Wang *et al.* 2021a, b) and were probably deposited before ~550 Ma. However, we consider that the only robust minimum age constraint is the minimum likely age of *Shaanxilithes* occurrences at 538.8 Ma.

4.3.3. Starye Pechi Formation, Russia

The Serebryanka and Sylvitsa groups in the Central Urals, Russia (Baltica) include three candidate glaciogenic units (e.g. Chumakov 2011; Maslov *et al.* 2013). Stratigraphically, the Tany Formation is the lowest member of the Serebryanka Group and rests unconformably on likely Cryogenian-age (though poorly dated) siliciclastic and volcaniclastic deposits. The Koyva (=Koiva) Formation occurs in the middle of the Serebryanka Group and includes diamictites, volcaniclastics, and possible dropstones. The Starye Pechi Formation is the basal unit of the Sylvitsa Group, which both conformably and unconformably overlies the Serebryanka Group in different parts of the region (Chumakov 2011).

The maximum depositional age of all three formations is constrained by a zircon date of 598.1 ± 6.0 Ma from pillow basalts at the base of the Tany Formation, underlying all of the potentially glaciogenic strata (Maslov *et al.* 2013). Grazhdankin *et al.* (2011) provided a minimum depositional age of 567.2 ± 3.9 Ma for all three formations from a tuff bed zircon date in the Perevalok Formation, which overlies the Starye Pechi Formation. The Serebryanka and Sylvitsa groups underlie the White Sea assemblage fossils of the East European Platform (Grazhdankin *et al.* 2011), which also indicates deposition before ~557 Ma (Yang *et al.* 2021).

Carbon isotope data may further constrain the minimum age of the Tany and Koyva formations and the maximum age of the Starye Pechi Formation (Chumakov *et al.* 2013). Specifically, $\delta^{13}C$ data from the uppermost Serebryanka Group (Buton and Kernos formations) have yielded extreme negative carbon isotope values of typically –10 to –15 ‰ (Chumakov *et al.* 2013). Very negative carbon isotope values of –12 to –14 ‰ have also been recovered from carbonate olistoliths in the upper Starye Pechi Formation, above the diamictite at the base (Chumakov *et al.* 2013). These values are within the typical range of the Shuram CIE, but were originally interpreted as reflecting either diagenetic alteration or precipitation of carbonate from methane or carbon dioxide seeps (Chumakov *et al.* 2013). The radiometric age constraints and the range of $\delta^{13}C$ values make a Shuram-equivalent age for the Buton, Kernos, and Starye Pechi formations plausible, and would make the Tany and Koyva formations older than the Shuram CIE. No similarly negative carbon isotope values have been recovered below the Buton Formation, though the upper Koyva Formation carbonates record negative values as low as –9.3 ‰, with a mean ± one standard deviation of –5.4 ± 1.8 ‰; Chumakov *et al.* 2013), more typical of the post-Gaskiers CIE (Yang *et al.* 2021). Radiometric and chemostratigraphic age constraints therefore allow for these units to have been deposited between 598 to 567 Ma, with the Tany and Koyva formations likely deposited before the Shuram excursion (older than 575 Ma) and the Starye Pechi Formation deposited during the excursion, before 567.2 ± 3.9 Ma (Grazhdankin *et al.* 2011; Rooney *et al.* 2020; Yang *et al.* 2021; Busch *et al.* 2023).

There is also some uncertainty about the glaciogenicity of these units. All three units include diamictites interbedded with definitively gravitationally-driven mass flow deposits (Grazhdankin *et al.* 2009; Chumakov 2011; Maslov *et al.* 2013). The Tany Formation is up to 800 m thick and comprises two diamictite members separated by a sandstone and shale member (Chumakov 2011). In the Lower Member, diamictites alternate with “schists” (presumably mudstones or shales), limestones and dolomites, slump breccias, and mafic volcanic rocks, the lower pillow basalts of which have yielded a radiometric date (Chumakov 2011; Maslov *et al.* 2013). The Lower Member diamictite matrix is dark grey and hosts clasts of quartz sandstone, felsic igneous rock, gneiss, and carbonate, which can be up to 3.5 m diameter and may occur as clusters of clasts (Chumakov 2011). Rare shale beds include outsized clasts (Chumakov 2011). In places, there is a dolostone bed at the top of the Lower Member (Chumakov 2011). The Middle Member comprises quartz-feldspar sandstone beds (Chumakov 2011). The Upper Member comprises massive and stratified diamictites interbedded with laminated shales hosting outsized clasts, and has a sharp but conformable transition into the overlying Garevka Formation, which consists of interbedded shales and sandstones (Chumakov 2011).

The Koyva Formation composition is regionally variable (250 m to 600 m thick), and predominantly consists of laminated claystones, siltstones, clay-silt shales, limestones, and dolomites, with either conglomerates (Maslov *et al.* 2013) and/or diamictites present north of the Sylvitsa River but none to the south (Chumakov 2011). Where present, the diamictites or conglomerates occur in the upper part of the formation and are interbedded with shales which may, but do not all, have outsized clasts, as well as alkali basalt flows in the northern outcrops (Chumakov 2011; Maslov *et al.* 2013). Rhythmically laminated shales are described from throughout the formation which, in the uppermost part, can contain rare small outsized clasts and dolomite interbeds (Chumakov 2011; Maslov *et al.* 2013).

The Starye Pechi Formation is up to 500 m thick and predominantly comprises thinly bedded yellow-green grey siltstones and mudstones, with massive and stratified diamictites interbedded with sandstones and shales with outsized clasts in its lower part (Grazhdankin *et al.* 2009; Chumakov 2011; Maslov *et al.* 2013). The diamictite deposits are geographically restricted to the southern part of the Kvarkush-Kamennogorsk Meganticlinorium (Grazhdankin *et al.* 2009) and found in the lower part of the formation, interbedded with coarse grained sandstones with parallel to wavy bedding, unidirectional cross stratification, rippled tops, and erosive bases with load casts (Grazhdankin *et al.* 2009). The sandstones also occasionally host isolated rounded floating pebbles (Grazhdankin *et al.* 2009). The diamictite is chaotic, with a matrix of dark grey sandy siltstone that hosts clasts of unreported roundness but which “vary in size and shape”, including some striated and grooved, and predominantly comprise lithologies of the underlying strata alongside some quartz, quartzite, chert, and plagioclase-rich granites (Grazhdankin *et al.* 2009; Chumakov 2011, p. 292). However Ipat'eva (in Maslov *et al.* 2013) pointed out that striated clasts are rare. The diamictite facies grades into siltstones and shales (Grazhdankin *et al.* 2009). The upper part of the Starye Pechi Formation includes carbonate olistoliths from which carbon isotope data have been obtained (Chumakov *et al.* 2013).

Grazhdankin *et al.* (2009) interpreted the Starye Pechi Formation diamictite clasts as ice-rafted stones dropped into a slope setting on which turbidites were being deposited. Chumakov *et al.* (2013) interpret some of the dolostones associated with the diamictites and other lithologies in the Tany and Koyva formations to be cap carbonates related to the end of a glaciation. The precise stratigraphic relationships of various lithologies, including the carbonates supposedly overlying the diamictites within the Koyva Formation are not clear, as the original stratigraphy has been disrupted by syn-sedimentary slumping and much later faulting (e.g. see Chumakov *et al.* 2013).

Alongside diamictites, the Serebryanka and Sylvitsa group strata include conglomerates, carbonate breccias, turbidites, flysch, and slumps (Chumakov 2011; Chumakov *et al.* 2013; Maslov *et al.* 2013), all consistent with deposition on the outer shelf and continental slope (Chumakov 2011). The upper Starye Pechi Formation, as well as the underlying Kernos and Buton formations, include large carbonate olistoliths (Chumakov *et al.* 2013), which are also indicative of gravity-driven deposition on a slope. The presence of scratched and outsized clasts, including very large blocks, in finer grained sediment can be the result of debris flow deposition as well as glacial action (e.g. Winterer and Von der Borch 1968; Kennedy and Eyles 2021; Tindal 2023).

In summary, the glaciogenicity of all three formations is plausible but questionable: the Tany, Koyva, and Starye Pechi deposits were rated weak or circumstantial, two, three, and three star deposits, respectively (Tindal 2023). In particular, there is abundant evidence for contemporaneous non-glaciogenic gravity-driven mass flow deposition and syn-sedimentary faulting. It is possible that all or some of these diamictites were also the result of gravitational rather than glacial processes, as the features that most strongly indicate glaciogenicity are rare (Ipat'eva in Maslov *et al.* 2013). The case for glaciogenicity of the Starye Pechi Formation is further undermined because the diamictites are interbedded with massive sandstones indicative of significant immature downslope deposition, supported by the presence of substantial olistoliths in both the underlying (Buton and Kernos formations) and overlying (upper Starye Pechi Formation) strata. We consider that further evidence is required to properly assess the depositional context of the Starye Pechi Formation.

5. Ediacaran palaeobiology data

Ediacaran taxa were grouped into biotic assemblages following the approach suggested by Wood *et al.* (2023) for Ediacaran biotic assemblages, whereby each assemblage is characterised by the major morphogroups that have their first appearances in this interval. See Supplementary Data 2 for a table of all assigned morphogroups.

We have made two exceptions to this approach in assigning morphogroups to biotic assemblages, both for morphogroups assigned to the White Sea biotic assemblage: erniettomorphs and radialomorphs. The radialomorphs are typically associated with the White Sea biotic assemblage (Boag *et al.* 2016, 2024; Muscente *et al.* 2019; Wood *et al.* 2023; Bowyer *et al.* 2024) but the radial *Triforillonia* and *Eoandromeda* are known from older strata in Newfoundland (Gehling *et al.* 2000) and China (Zhao *et al.* 2004; Tang *et al.* 2008; Zhu *et al.* 2008), respectively. The erniettomorphs have generally been regarded as part of the Nama biotic assemblage (Boag *et al.* 2016, 2024; Muscente *et al.* 2019) but have also been considered part of the White Sea biotic assemblage (Wood *et al.* 2023; Bowyer *et al.* 2024). The sole candidate Avalon-age erniettomorph is *Namalia*, reported from the deep-water Nadaleen Formation, northwest Canada (Narbonne *et al.* 2014). Here, we follow Wood *et al.* (2023) in assigning erniettomorphs to the White Sea biotic assemblage, but note that this is a choice.

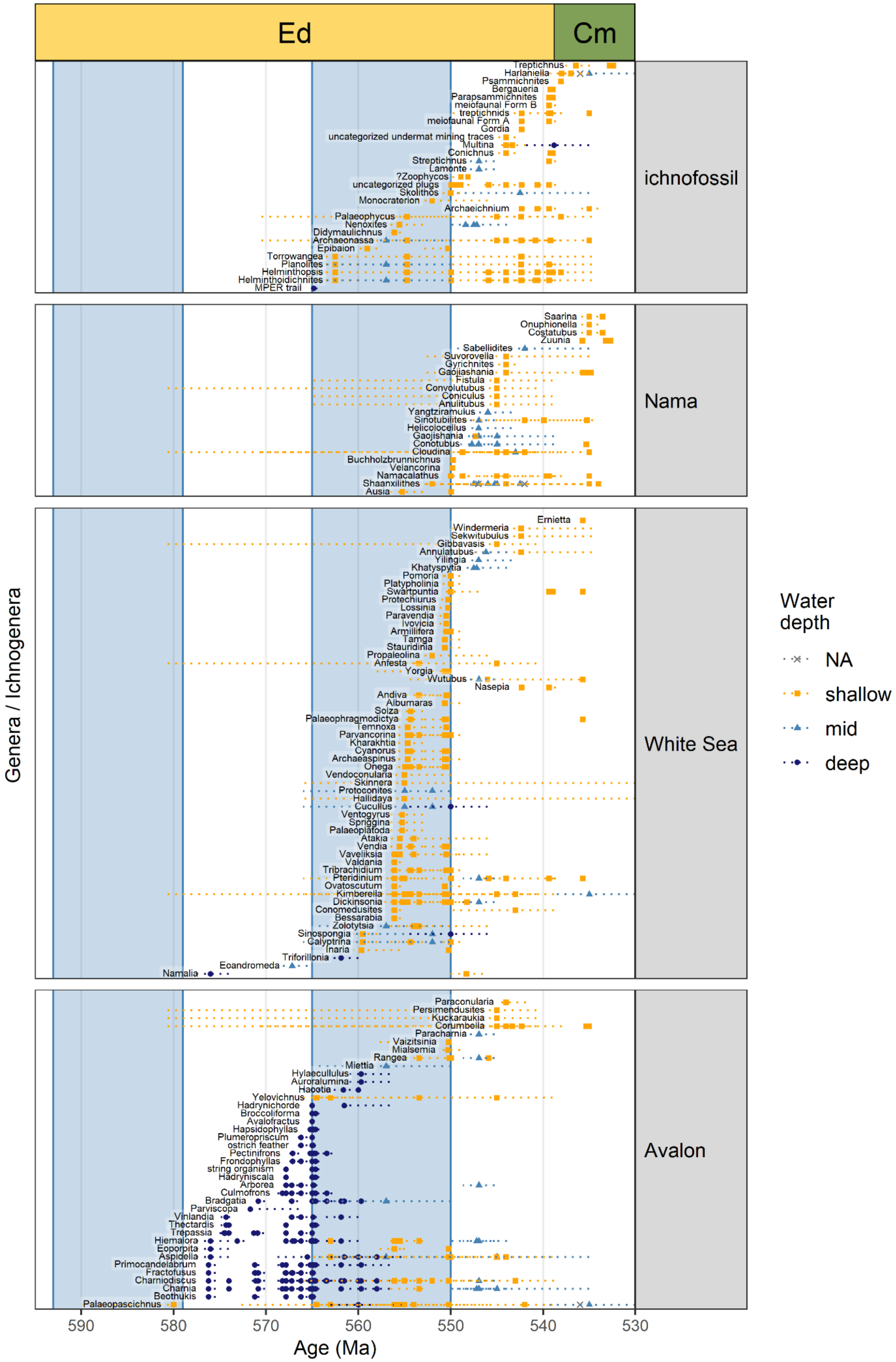

Ed
Cm
ichnofossil
Treptichnus
Harlaniella
Psammichnites
Bergaueria
Parapsammichnites
meiofaunal Form B
treptichnids
meiofaunal Form A
Gordia
uncategorized undermat mining traces
Multina
Conichnus
Streptichnus
Lamonte
?Zoophycos
uncategorized plugs
Skolithos
Monocraterion
Archaeichnium
Palaeophycus
Nenoxites
Didymaulichnus
Archaeonassa
Epibaion
Torrowangea
Planolites
Helminthopsis
Helminthoidichnites
MPER trail
Nama
Saarina
Onuphionella
Costatubus
Zuunia
Sabellidites
Suvorovella
Gyrichnites
Gaojiashania
Fistula
Convolutubus
Coniculus
Anulitubus
Yangtziramulus
Sinotubulites
Helicolocellus
Gaojishania
Conotubus
Cloudina
Buchholzbrunnichnus
Velancorina
Namacalathus
Shaanxilithes
Ausia
White Sea
Erniettia
Windermeria
Sekwitubulus
Gibbavasis
Annulatubus
Yilingia
Khatyspytia
Pomoria
Platypholinia
Swartpuntia
Protechiurus
Lossinia
Paravendia
Ivovicia
Armillifera
Tamga
Staurinidia
Propaleolina
Anfesta
Yorgia
Wutubus
Nasepia
Andiva
Albumares
Solza
Palaeophragmodictya
Temnoxa
Parvancorina
Kharakhtia
Cyanorus
Archaeaspinus
Onega
Vendoconularia
Skinnera
Protoconites
Hallidaya
Cuculus
Ventogyrus
Spriggina
Palaeoplatoda
Atakia
Vendia
Vaveliksia
Valdainia
Tribrachidium
Pteridinium
Ovatoscutum
Kimberella
Dickinsonia
Conomedusites
Bessarabia
Zolotytsia
Sinospongia
Calyptrina
Inaria
Triforillonia
Eoandromeda
Namalia
Avalon
Paraconularia
Persimedusites
Kuckaraukia
Corumbella
Paracharnia
Vaizitsinia
Mialsemia
Rangea
Miettia
Hylaecullulus
Auroralumina
Haootia
Yelovichnus
Hadrynichorde
Broccoliforma
Avalofractus
Hapsidophyllas
Plumeropriscum
ostrich feather
Pectinifrons
Frondophyllas
string organism
Hadryniscala
Arborea
Culmofrons
Bradgatia
Parviscopa
Vinlandia
Thectardis
Trepassia
Hiemalora
Eoporpita
Aspidella
Primocandelabrum
Fractofusus
Charniodiscus
Charnia
Beothukis
Palaeopascichnus
Genera / Ichnogenera
590
580
570
560
550
540
530
Age (Ma)
Water depth
NA
shallow
mid
deep

Figure S3. Occurrences and stratigraphic ranges of Ediacaran macrofossil genera and ichnogenera including all sites in our Supplementary Data 2 grouped by assigned biotic assemblage. Compare with main text Figure 3 which has all "South Australia" occurrences removed. Removing all South Australia occurrences does not alter the fundamental patterns of taxonomic ranges in this dataset. Ed: Ediacaran pars.; Cm: Cambrian pars.

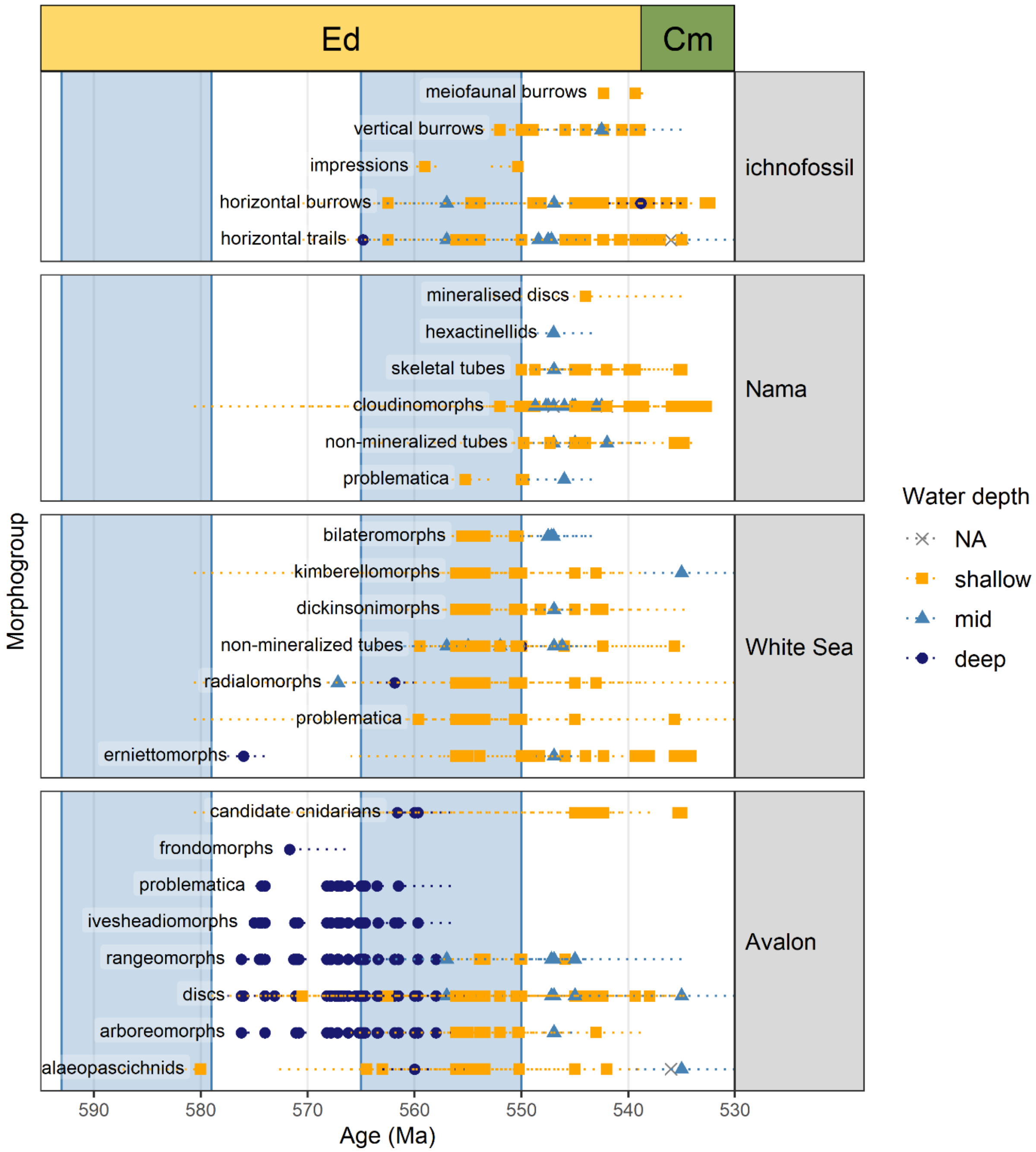

Figure S4. Occurrences and stratigraphic ranges of Ediacaran macrofossil morphogroups used in this study (Supplementary Data 2). Body fossil morphogroups are defined in Supplementary Data 2. Ed: Ediacaran pars.; Cm: Cambrian pars.

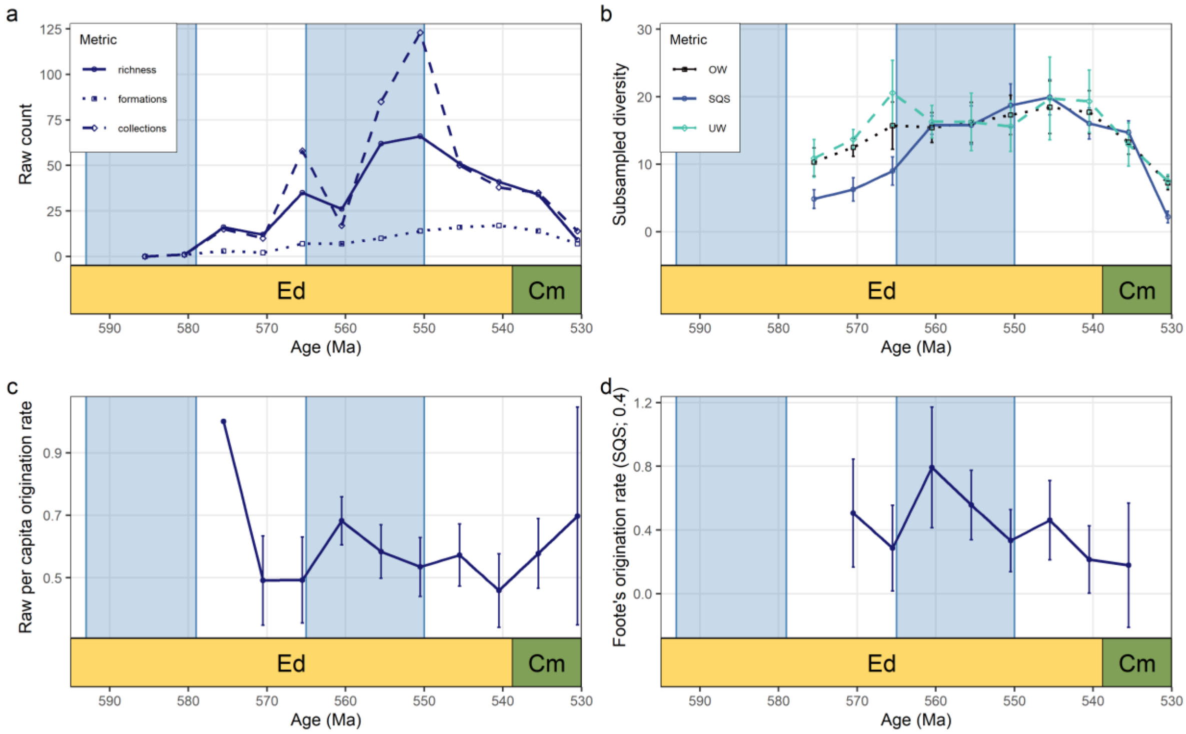

Figure S5. Palaeobiodiversity metrics for the late Ediacaran biosphere excluding the loosely constrained South Australia sites. See main text Figure 4 for plots of the full dataset. (a) Raw taxonomic richness (circles; solid lines) plotted alongside number of collections (diamonds; dashed lines) and number of formations (squares; dotted lines). (b) Subsampled taxonomic richness following Shareholder Quorum subsampling (SQS; quota = 0.4), unweighted collection-based classical rarefaction (UW; quota = 8 collections), and occurrence-weighted subsampling (OW; quota = 14 occurrences). (c) Raw per capita origination rate for 1 Myr and 5 Myr bins. (d) SQS (quota = 0.4) subsampled Foote's origination rate for 1 Myr and 5 Myr bins. The decline in values across the Ediacaran–Cambrian boundary is an artefact of our palaeobiology data compilation which focused on taxa with first occurrences in the Ediacaran Period. Data from Supplementary Data 2.

Combined reference list: Main Text and Supplementary Information

Agić, H., Jensen, S., et al. 2024. Life through an Ediacaran glaciation: Shale- and diamictite-hosted organic-walled microfossil assemblages from the late Neoproterozoic of the Tanafjorden area, northern Norway. *Palaeogeography, Palaeoclimatology, Palaeoecology*, **635**, 111956, https://doi.org/10.1016/j.palaeo.2023.111956.

Alroy, J. 2010a. Fair Sampling of Taxonomic Richness and Unbiased Estimation of Origination and Extinction Rates. *The Paleontological Society Papers*, **16**, 55–80, https://doi.org/10.1017/S1089332600001819.

Alroy, J. 2010b. Geographical, environmental and intrinsic biotic controls on Phanerozoic marine diversification. *Palaeontology*, **53**, 1211–1235, https://doi.org/10.1111/j.1475-4983.2010.01011.x.

Alroy, J. 2014. Accurate and precise estimates of origination and extinction rates. *Paleobiology*, **40**, 374–397, https://doi.org/10.1666/13036.

Álvaro, J.J., Cortijo, I., Jensen, S., Lorenzo, S. and Pieren, A.P. 2019. Updated stratigraphic framework and biota of the Ediacaran and Terreneuvian in the Alcudia-Toledo Mountains of the Central Iberian Zone, Spain. *Estudios Geológicos*, **75**, e093–e093, https://doi.org/10.3989/egeol.43620.548.

Álvaro, J.J., Johnson, S.C., Barr, S.M., Jensen, S., Palacios, T., van Rooyen, D. and White, C.E. 2022. Unconformity-bounded rift sequences in Terreneuvian–Miaolingian strata of the Caledonian Highlands, Atlantic Canada. *GSA Bulletin*, **135**, 1225–1242, https://doi.org/10.1130/B36402.1.

Amorim, K.B., Afonso, J.W.L., et al. 2020. Sedimentary facies, fossil distribution and depositional setting of the late Ediacaran Tamengo Formation (Brazil). *Sedimentology*, **67**, 3422–3450, https://doi.org/10.1111/sed.12749.

Arnaud, E., Halverson, G.P. and Shields-Zhou, G. 2011. *The Geological Record of Neoproterozoic Glaciations*, https://doi.org/10.1144/M36.

Barfod, G.H., Albarède, F., Knoll, A.H., Xiao, S., Télouk, P., Frei, R. and Baker, J. 2002. New Lu–Hf and Pb–Pb age constraints on the earliest animal fossils. *Earth and Planetary Science Letters*, **201**, 203–212, https://doi.org/10.1016/S0012-821X(02)00687-8.

Bergmann, K., Osburn, M.R., et al. 2022. The Shuram excursion: A response to climate extremes at the dawn of animal life, https://doi.org/10.1002/essoar.10511917.1.

Berkman, P.A., Cattaneo-Vietti, R., Chiantore, M. and Howard-Williams, C. 2004. Polar emergence and the influence of increased sea-ice extent on the Cenozoic biogeography of pectinid molluscs in Antarctic coastal areas. *Deep Sea Research Part II: Topical Studies in Oceanography*, **51**, 1839–1855, https://doi.org/10.1016/j.dsr2.2004.07.017.

Berner, R.A. 2004. *The Phanerozoic Carbon Cycle: CO2 and O2*.

Berner, R.A. 2006. Inclusion of the Weathering of Volcanic Rocks in the GEOCARBSULF Model. *American Journal of Science*, **306**, 295–302, https://doi.org/10.2475/05.2006.01.

Bertrand-Sarfati, J., Moussine-Pouchkine, A., Amard, B. and Ahmed, A.A.K. 1995. First Ediacaran fauna found in western Africa and evidence for an Early Cambrian glaciation. *Geology*, **23**, 133–136, https://doi.org/10.1130/0091-7613(1995)023<0133:FEFFIW>2.3.CO;2.

Betts, M.J., Paterson, J.R., et al. 2018. Early Cambrian chronostratigraphy and geochronology of South Australia. *Earth-Science Reviews*, **185**, 498–543, https://doi.org/10.1016/j.earscirev.2018.06.005.

Bischoff, J.L., Fitzpatrick, J.A. and Rosenbauer, R.J. 1993. The Solubility and Stabilization of Ikaite ($CaCO_3 \cdot 6H_2O$) from 0° to 25°C: Environmental and Paleoclimatic Implications for Thinolite Tufa. *The Journal of Geology*, **101**, 21–33, https://doi.org/10.1086/648194.

Blein, O., Baudin, T., et al. 2014. Geochronological constraints on the polycyclic magmatism in the Bou Azzer-El Graara inlier (Central Anti-Atlas Morocco). *Journal of African Earth Sciences*, **99**, 287–306, https://doi.org/10.1016/j.jafrearsci.2014.04.021.

Boag, T.H., Darroch, S.A.F. and Laflamme, M. 2016. Ediacaran distributions in space and time: testing assemblage concepts of earliest macroscopic body fossils. *Paleobiology*, **42**, 574–594, https://doi.org/10.1017/pab.2016.20.

Boag, T.H., Stockey, R.G., Elder, L.E., Hull, P.M. and Sperling, E.A. 2018. Oxygen, temperature and the deep-marine stenothermal cradle of Ediacaran evolution. *Proceedings of the Royal Society B: Biological Sciences*, **285**, 20181724, https://doi.org/10.1098/rspb.2018.1724.

Boag, T.H., Busch, J.F., Gooley, J.T., Strauss, J.V. and Sperling, E.A. 2024. Deep-water first occurrences of Ediacara biota prior to the Shuram carbon isotope excursion in the Wernecke Mountains, Yukon, Canada. *Geobiology*, **22**, e12597, https://doi.org/10.1111/gbi.12597.

Boddy, C.E., Mitchell, E.G., Merdith, A. and Liu, A.G. 2021. Palaeolatitudinal distribution of the Ediacaran macrobiota. *Journal of the Geological Society*, https://doi.org/10.1144/jgs2021-030.

Bond, D.P.G. and Grasby, S.E. 2017. On the causes of mass extinctions. *Palaeogeography, Palaeoclimatology, Palaeoecology*, **478**, 3–29, https://doi.org/10.1016/j.palaeo.2016.11.005.

Bossi, J., Cingolani, C.A., Llambías, E.J., Varela, R. and Campal, N. 1993. Características del magmatismo post-orogénico finibrasiliano en el Uruguay: formaciones Sierra de Ríos y Sierra de Ánimas. *Brazilian Journal of Geology*, **23, no. 3**, https://doi.org/10.5327/rbg.v23i3.469.

Boucot, A.J., Xu, C., Scotese, C.R. and Morley, R.J. 2013. *Phanerozoic Paleoclimate: An Atlas of Lithologic Indicators of Climate*, 1st ed. SEPM Concepts in Sedimentology and Paleontology**11**.

Bouma, A.H. 1962. *Sedimentology of Some Flysch Deposits: A Graphic Approach to Facies Interpretation*.

Bowring, S.A., Grotzinger, J.P., Condon, D.J., Ramezani, J., Newall, M.J. and Allen, P.A. 2007. Geochronologic constraints on the chronostratigraphic framework of the Neoproterozoic Huqf Supergroup, Sultanate of Oman. *American Journal of Science*, **307**, 1097–1145, https://doi.org/10.2475/10.2007.01.

Bowyer, F.T., Zhuravlev, A.Y., et al. 2022. Calibrating the temporal and spatial dynamics of the Ediacaran - Cambrian radiation of animals. *Earth-Science Reviews*, **225**, 103913, https://doi.org/10.1016/j.earscirev.2021.103913.

Bowyer, F.T., Uahengo, C.-I., et al. 2023. Constraining the onset and environmental setting of metazoan biomineralization: The Ediacaran Nama Group of the Tsaus Mountains, Namibia. *Earth and Planetary Science Letters*, **620**, 118336, https://doi.org/10.1016/j.epsl.2023.118336.

Bowyer, F.T., Wood, R.A. and Yilales, M. 2024. Sea level controls on Ediacaran-Cambrian animal radiations. *Science Advances*, **10**, eado6462, https://doi.org/10.1126/sciadv.ado6462.

Busch, J.F., Hodgin, E.B., et al. 2022. Global and local drivers of the Ediacaran Shuram carbon isotope excursion. *Earth and Planetary Science Letters*, **579**, 117368, https://doi.org/10.1016/j.epsl.2022.117368.

Busch, J.F., Boag, T.H., Sperling, E.A., Rooney, A.D., Feng, X., Moynihan, D.P. and Strauss, J.V. 2023. Integrated Litho-, Chemo- and Sequence Stratigraphy of the Ediacaran Gametrail Formation Across a Shelf-Slope Transect in the Wernecke Mountains, Yukon, Canada. *American Journal of Science*, **323**, 4, https://doi.org/10.2475/001c.74874.

Butterfield, N.J. 2009. Macroevolutionary turnover through the Ediacaran transition: ecological and biogeochemical implications. *Geological Society, London, Special Publications*, **326**, 55–66, https://doi.org/10.1144/SP326.3.

Caby, R. and Fabre, J. 1981. A22. Late Proterozoic to Early Cambrian diamictites, tillites and associated glaciogenic sediments in the Série Pourprée of Western Ahaggar, Algeria. *In*: Hambrey, M. J. and Harland, W. B. (eds) *Earth's Pre-Pleistocene Glacial Record*. 140–145.

Campanha, G.A.C., Basei, M.S., Tassinari, C.C.G., Nutman, A.P. and Faleiros, F.M. 2008. Constraining the age of the Iporanga Formation with SHRIMP U-Pb zircon: Implications for possible Ediacaran glaciation in the Ribeira Belt, SE Brazil. *Gondwana Research*, **13**, 117–125, https://doi.org/10.1016/j.gr.2007.05.010.

Cantine, M.D., Rooney, A.D., Knoll, A.H., Gómez-Pérez, I., al Baloushi, B. and Bergmann, K.D. 2024. Chronology of Ediacaran sedimentary and biogeochemical shifts along eastern Gondwanan margins. *Communications Earth & Environment*, **5**, 1–9, https://doi.org/10.1038/s43247-024-01630-1.

Carbone, C.A., Narbonne, G.M., Macdonald, F.A. and Boag, T.H. 2015. New Ediacaran fossils from the uppermost Blueflower Formation, northwest Canada: disentangling biostratigraphy and paleoecology. *Journal of Paleontology*, **89**, 281–291, https://doi.org/10.1017/jpa.2014.25.

Carto, S.L. and Eyles, N. 2011. Chapter 42 The deep-marine glaciogenic Gaskiers Formation, Newfoundland, Canada. *Geological Society, London, Memoirs*, **36**, 467–473, https://doi.org/10.1144/M36.42.

Carto, S.L. and Eyles, N. 2012. Sedimentology of the Neoproterozoic (c. 580 Ma) Squantum 'Tillite', Boston Basin, USA: Mass flow deposition in a deep-water arc basin lacking direct glacial influence. *Sedimentary Geology*, **269–270**, 1–14, https://doi.org/10.1016/j.sedgeo.2012.03.011.

Chai, S., Wu, Y. and Hua, H. 2021. Potential index fossils for the Terminal Stage of the Ediacaran System. *Journal of Asian Earth Sciences*, **218**, 104885, https://doi.org/10.1016/j.jseaes.2021.104885.

Chumakov, N.M. 2009. The Baykonurian glaciohorizon of the Late Vendian. *Stratigraphy and Geological Correlation*, **17**, 373–381, https://doi.org/10.1134/S0869593809040029.

Chumakov, N.M. 2011. Chapter 24 The Neoproterozoic glacial formations of the North and Middle Urals. *In*: Arnaud, E., Halverson, G. P. and Shields-Zhou, G. (eds) *The Geological Record of Neoproterozoic Glaciations*. Geological Society, London, Memoirs**36**, 289–296., https://doi.org/10.1144/M36.23.

Chumakov, N.M., Pokrovskii, B.G. and Maslov, A.V. 2013. Stratigraphic position and significance of carbonate rocks related to neoproterozoic glacial horizons of the Urals. *Stratigraphy and Geological Correlation*, **21**, 573–591, https://doi.org/10.1134/S0869593813060038.

Clarke, A. and Crame, J.A. 1992. The Southern Ocean benthic fauna and climate change: a historical perspective. *Philosophical Transactions of the Royal Society of London. Series B: Biological Sciences*, **338**, 299–309, https://doi.org/10.1098/rstb.1992.0150.

Clarke, A.J.I., Kirkland, C.L., Menon, L.R., Condon, D.J., Cope, J.C.W., Bevins, R.E. and Glorie, S. 2024. U–Pb zircon–rutile dating of the Llangynog Inlier, Wales: constraints on an Ediacaran shallow-marine fossil assemblage from East Avalonia. *Journal of the Geological Society*, **181**, jgs2023-081, https://doi.org/10.1144/jgs2023-081.

Cohen, K.M., Finney, S.C., Gibbard, P.L. and Fan, J.-X. 2013. The ICS International Chronostratigraphic Chart v 2023/09. *Episodes*, **36**, 199–204, https://doi.org/10.18814/epiiugs/2013/v36i3/002.

Compston, W., Wright, A.E. and Toghill, P. 2002. Dating the Late Precambrian volcanicity of England and Wales. *Journal of the Geological Society*, **159**, 323–339, https://doi.org/10.1144/0016-764901-010.

Cope, J.C.W. 1977. An Ediacara-type fauna from South Wales. *Nature*, **268**, 624–624, https://doi.org/10.1038/268624a0.

Cope, J.C.W. 1983. Precambrian faunas from the Carmarthen district. *Nature in Wales*, **1**, 11–16.

Darroch, S.A.F., Sperling, E.A., et al. 2015. Biotic replacement and mass extinction of the Ediacara biota. *Proceedings of the Royal Society B: Biological Sciences*, **282**, 20151003, https://doi.org/10.1098/rspb.2015.1003.

Deutsch, C., Ferrel, A., Seibel, B., Pörtner, H.-O. and Huey, R.B. 2015. Climate change tightens a metabolic constraint on marine habitats. *Science*, **348**, 1132–1135, https://doi.org/10.1126/science.aaa1605.

Doré, F. 1981. E21 Late Precambrian tilloids of Normandy (Armorican Massif). *In*: Hambrey, M. J. and Harland, W. B. (eds) *Earth's Pre-Pleistocene Glacial Record*. 643–648.

Dott, R.H., Jr. 1961. Squantum "Tillite", Massachusetts—Evidence of Glaciation or Subaqueous Mass Movements? *GSA Bulletin*, **72**, 1289–1305, https://doi.org/10.1130/0016-7606(1961)72[1289:STMOGO]2.0.CO;2.

Dunn, F.S., Kenchington, C.G., Parry, L.A., Clark, J.W., Kendall, R.S. and Wilby, P.R. 2022. A crown-group cnidarian from the Ediacaran of Charnwood Forest, UK. *Nature Ecology & Evolution*, **6**, 1095–1104, https://doi.org/10.1038/s41559-022-01807-x.

Erwin, D.H. 2009. Climate as a Driver of Evolutionary Change. *Current Biology*, **19**, R575–R583, https://doi.org/10.1016/j.cub.2009.05.047.

Etemad-Saeed, N., Hosseini-Barzi, M., Adabi, M.H., Miller, N.R., Sadeghi, A., Houshmandzadeh, A. and Stockli, D.F. 2016. Evidence for ca. 560 Ma Ediacaran glaciation in the Kahar Formation, central Alborz Mountains, northern Iran. *Gondwana Research*, **31**, 164–183, https://doi.org/10.1016/j.gr.2015.01.005.

Evans, S.D., Diamond, C.W., Droser, M.L. and Lyons, T.W. 2018. Dynamic oxygen and coupled biological and ecological innovation during the second wave of the Ediacara Biota Lyons, T. W., Droser, M. L., Lau, K. V. and Porter, S. M. (eds). *Emerging Topics in Life Sciences*, **2**, 223–233, https://doi.org/10.1042/ETLS20170148.

Evans, S.D., Tu, C., et al. 2022. Environmental drivers of the first major animal extinction across the Ediacaran White Sea-Nama transition. *Proceedings of the National Academy of Sciences*, **119**, e2207475119, https://doi.org/10.1073/pnas.2207475119.

Fedonkin, M.A., Vickers-Rich, P., Swalla, B.J., Trusler, P. and Hall, M. 2012. A new metazoan from the Vendian of the White Sea, Russia, with possible affinities to the ascidians. *Paleontological Journal*, **46**, 1–11, https://doi.org/10.1134/S0031030112010042.

Fenton, I.S., Aze, T., Farnsworth, A., Valdes, P. and Saupe, E.E. 2023. Origination of the modern-style diversity gradient 15 million years ago. *Nature*, 1–5, https://doi.org/10.1038/s41586-023-05712-6.

Field, L.P., Milodowski, A.E., et al. 2017. Unusual morphologies and the occurrence of pseudomorphs after ikaite (CaCO3·6H2O) in fast growing, hyperalkaline speleothems. *Mineralogical Magazine*, **81**, 565–589, https://doi.org/10.1180/minmag.2016.080.111.

Fitzgerald, D.M., Narbonne, G.M., Pufahl, P.K. and Dalrymple, R.W. 2024. The Mall Bay Formation (Ediacaran) and the protracted onset of the Gaskiers glaciation in Newfoundland, Canada. *Precambrian Research*, **405**, 107369, https://doi.org/10.1016/j.precamres.2024.107369.

Gaucher, C., Blanco, G., Chiglino, L., Poiré, D. and Germs, G.J.B. 2008. Acritarchs of Las Ventanas Formation (Ediacaran, Uruguay): Implications for the timing of coeval rifting and glacial events in western Gondwana. *Gondwana Research*, **13**, 488–501, https://doi.org/10.1016/j.gr.2007.05.008.

Gehling, J.G. and Droser, M.L. 2013. How well do fossil assemblages of the Ediacara Biota tell time? *Geology*, **41**, 447–450, https://doi.org/10.1130/G33881.1.

Gehling, J.G. and Narbonne, G.M. 2007. Spindle-shaped Ediacara fossils from the Mistaken Point assemblage, Avalon Zone, Newfoundland. *Canadian Journal of Earth Sciences*, **44**, 367–387, https://doi.org/10.1139/e07-003.

Gehling, J.G., Narbonne, G.M. and Anderson, M.M. 2000. The first named Ediacaran body fossil, *Aspidella terranovica*. *Palaeontology*, **43**, 427–456, https://doi.org/10.1111/j.0031-0239.2000.00134.x.

Germs, G.J.B. and Gaucher, C. 2012. Nature and extent of a late Ediacaran (ca. 547 Ma) glacigenic erosion surface in southern Africa. *South African Journal of Geology*, **115**, 91–102, https://doi.org/10.2113/gssajg.115.91.

Gibson, G.G. and Teeter, S.A. 1984. *A Stratigrapher's View of the Carolina Slate Belt, Southcentral North Carolina*. Carolina Geological Society Field Trip Guidebook.

Grazhdankin, D. 2004a. Late Neoproterozoic sedimentation in the Timan foreland. *Geological Society, London, Memoirs*, **30**, 37–46, https://doi.org/10.1144/GSL.MEM.2004.030.01.04.

Grazhdankin, D. 2004b. Patterns of distribution in the Ediacaran biotas: facies versus biogeography and evolution. *Paleobiology*, **30**, 203–221, https://doi.org/10.1666/0094-8373(2004)030<0203:PODITE>2.0.CO;2.

Grazhdankin, D. 2014. Patterns of Evolution of the Ediacaran Soft-Bodied Biota. *Journal of Paleontology*, **88**, 269–283, https://doi.org/10.1666/13-072.

Grazhdankin, D.V., Maslov, A.V. and Krupenin, M.T. 2009. Structure and depositional history of the Vendian Sylvitsa Group in the western flank of the Central Urals. *Stratigraphy and Geological Correlation*, **17**, 476–492, https://doi.org/10.1134/S0869593809050025.

Grazhdankin, D.V., Marusin, V.V., Meert, J., Krupenin, M.T. and Maslov, A.V. 2011. Kotlin regional stage in the South Urals. *Doklady Earth Sciences*, **440**, 1222–1226, https://doi.org/10.1134/S1028334X11090170.

Griffiths, H.J., Whittle, R.J. and Mitchell, E.G. 2023. Animal survival strategies in Neoproterozoic ice worlds. *Global Change Biology*, **29**, 10–20, https://doi.org/10.1111/gcb.16393.

Hallam, A. and Wignall, P.B. 1999. Mass extinctions and sea-level changes. *Earth-Science Reviews*, **48**, 217–250, https://doi.org/10.1016/S0012-8252(99)00055-0.

Halverson, G.P., Hoffman, P.F., Schrag, D.P., Maloof, A.C. and Rice, A.H.N. 2005. Toward a Neoproterozoic composite carbon-isotope record. *GSA Bulletin*, **117**, 1181–1207, https://doi.org/10.1130/B25630.1.

Hambrey, M.J. and Harland, W.B. 1981. Criteria for the identification of glacigenic deposits. *In*: Hambrey, M. J. and Harland, W. B. (eds) *Earth's Pre-Pleistocene Glacial Record*. 14–21.

Hawco, J.B., Kenchington, C.G. and McIlroy, D. 2021. A quantitative and statistical discrimination of morphotaxa within the Ediacaran genus Palaeopascichnus. *Papers in Palaeontology*, **7**, 657–673, https://doi.org/10.1002/spp2.1290.

He, J., Zhu, W. and Ge, R. 2014. New age constraints on Neoproterozoic diamicites in Kuruktag, NW China and Precambrian crustal evolution of the Tarim Craton. *Precambrian Research*, **241**, 44–60, https://doi.org/10.1016/j.precamres.2013.11.005.

Hoffman, P.F., Abbot, D.S., et al. 2017. Snowball Earth climate dynamics and Cryogenian geology-geobiology. *Science Advances*, **3**, e1600983, https://doi.org/10.1126/sciadv.1600983.

Hofmann, H.J., Fritz, W.H. and Narbonne, G.M. 1983. Ediacaran (Precambrian) Fossils from the Wernecke Mountains, Northwestern Canada. *Science*, **221**, 455–457, https://doi.org/10.1126/science.221.4609.455.

Hofmann, H.J., O'Brien, S.J. and King, A.F. 2008. Ediacaran Biota on Bonavista Peninsula, Newfoundland, Canada. *Journal of Paleontology*, **82**, 1–36.

Högström, A., Jensen, S., Palacios, T. and Ebbestad, J.O.R. 2013. New information on the Ediacaran-Cambrian transition in the Vestertana Group, Finnmark, northern Norway, from trace fossils and organic-walled microfossils. *Norsk Geologisk Tidsskrift*, **93**, 95–106.

Hu, W. and McSaveney, M.J. 2018. A polished and striated pavement formed by a rock avalanche in under 90 s mimics a glacially striated pavement. *Geomorphology*, **320**, 154–161, https://doi.org/10.1016/j.geomorph.2018.08.011.

Huang, R. and Fan, X. 2013. The landslide story. *Nature Geoscience*, **6**, 325–326, https://doi.org/10.1038/ngeo1806.

Inglis, J.D., MacLean, J.S., Samson, S.D., D'Lemos, R.S., Admou, H. and Hefferan, K. 2004. A precise U–Pb zircon age for the Bleïda granodiorite, Anti-Atlas, Morocco: implications for the timing of deformation and terrane assembly in the eastern Anti-Atlas. *Journal of African Earth Sciences*, **39**, 277–283, https://doi.org/10.1016/j.jafrearsci.2004.07.041.

Jensen, S., Högström, A.E.S., et al. 2018. New occurrences of Palaeopascichnus from the Stáhpogieddi Formation, Arctic Norway, and their bearing on the age of the Varanger Ice Age. *Canadian Journal of Earth Sciences*, **55**, 1253–1261, https://doi.org/10.1139/cjes-2018-0035.

Johnson, S., McLeod, M. and Branscombe, L. 2019. A note on the location of diamictite in the Ratcliffe Brook Group on Hanford Brook, southern New Brunswick, Canada. *In*: *The Atlantic Geoscience Society (AGS) La Société Géoscientifique de l'Atlantique* – 45th Colloquium and Annual Meeting: Program with Abstracts. 35–36.

Keller, C.B., Husson, J.M., et al. 2019. Neoproterozoic glacial origin of the Great Unconformity. *Proceedings of the National Academy of Sciences*, **116**, 1136–1145, https://doi.org/10.1073/pnas.1804350116.

Kenchington, C.G., Harris, S.J., Vixseboxse, P.B., Pickup, C. and Wilby, P.R. 2018. The Ediacaran fossils of Charnwood Forest: Shining new light on a major biological revolution. *Proceedings of the Geologists' Association*, **129**, 264–277, https://doi.org/10.1016/j.pgeola.2018.02.006.

Kennedy, K. and Eyles, N. 2021. Syn-rift mass flow generated 'tectonofacies' and 'tectonosequences' of the Kingston Peak Formation, Death Valley, California, and their bearing on supposed Neoproterozoic panglacial climates. *Sedimentology*, **68**, 352–381, https://doi.org/10.1111/sed.12781.

Kennedy, K., Eyles, N. and Broughton, D. 2019. Basinal setting and origin of thick (1·8 km) mass-flow dominated Grand Conglomérat diamictites, Kamoa, Democratic Republic of Congo: Resolving climate and tectonic controls during Neoproterozoic glaciations. *Sedimentology*, **66**, 556–589, https://doi.org/10.1111/sed.12494.

Kocsis, Á.T., Reddin, C.J., Alroy, J. and Kiessling, W. 2019. The r package divDyn for quantifying diversity dynamics using fossil sampling data. *Methods in Ecology and Evolution*, **10**, 735–743, https://doi.org/10.1111/2041-210X.13161.

Kröner, A. 1981. A29. Late Precambrian diamictites of South Africa and Namibia. *In*: Hambrey, M. J. and Harland, W. B. (eds) *Earth's Pre-Pleistocene Glacial Record*. 167–177.

Kröner, A. and Germs, G.J.B. 1971. A re-interpretation of the Numees-Nama contact at Aussenkjer, southwest Africa. *Transactions of the Geological Soceity of South Africa*, **74**, 69–74.

Kühnemann, V., Meinhold, G., Schulz, B., Gilbricht, S., Weber, S. and Wemmer, K. 2024. The "greywacke problem" explored in the neoproterozoic of Saxo-Thuringia: new insights into sediment composition and metamorphic overprint. *International Journal of Earth Sciences*, https://doi.org/10.1007/s00531-024-02475-x.

Le Heron, D.P., Vandyk, T.M., Wu, G. and Li, M. 2018. New perspectives on the Luoquan Glaciation (Ediacaran-Cambrian) of North China. *The Depositional Record*, **4**, 274–292, https://doi.org/10.1002/dep2.46.

Le Heron, D.P., Vandyk, T.M., et al. 2019. Bird's-eye view of an Ediacaran subglacial landscape. *Geology*, **47**, 705–709, https://doi.org/10.1130/G46285.1.

Letsch, D., Large, S.J.E., Buechi, M.W., Winkler, W. and von Quadt, A. 2018. Ediacaran glaciations of the west African Craton – Evidence from Morocco. *Precambrian Research*, **310**, 17–38, https://doi.org/10.1016/j.precamres.2018.02.015.

Li, Z.-X., Liu, Y. and Ernst, R. 2023. A dynamic 2000—540 Ma Earth history: From cratonic amalgamation to the age of supercontinent cycle. *Earth-Science Reviews*, **238**, 104336, https://doi.org/10.1016/j.earscirev.2023.104336.

Linnemann, U., Pidal, A.P., et al. 2018. A ~565 Ma old glaciation in the Ediacaran of peri-Gondwanan West Africa. *International Journal of Earth Sciences*, **107**, 885–911, https://doi.org/10.1007/s00531-017-1520-7.

Linnemann, U., Ovtcharova, M., et al. 2019. New high-resolution age data from the Ediacaran–Cambrian boundary indicate rapid, ecologically driven onset of the Cambrian explosion. *Terra Nova*, **31**, 49–58, https://doi.org/10.1111/ter.12368.

Linnemann, U., Hofmann, M., et al. 2022. An Upper Ediacaran Glacial Period in Cadomia: the Granville tillite (Armorican Massif) – sedimentology, geochronology and provenance. *Geological Magazine*, **159**, 999–1013, https://doi.org/10.1017/S0016756821001011.

Liu, A.G. 2011. Reviewing the Ediacaran fossils of the Long Mynd, Shropshire. *Proceedings of the Shropshire Geological Society*, **16**, 31–43.

Liu, A.G., McIlroy, D. and Brasier, M.D. 2010. First evidence for locomotion in the Ediacara biota from the 565 Ma Mistaken Point Formation, Newfoundland. *Geology*, **38**, 123–126, https://doi.org/10.1130/G30368.1.

Liu, A.G., McIlroy, D., Matthews, J.J. and Brasier, M.D. 2014a. Confirming the metazoan character of a 565 Ma trace-fossil assemblage from Mistaken Point, Newfoundland. *PALAIOS*, **29**, 420–430, https://doi.org/10.2110/palo.2014.011.

Liu, A.G., Matthews, J.J., Menon, L.R., McIlroy, D. and Brasier, M.D. 2014b. *Haootia quadriformis* n. gen., n. sp., interpreted as a muscular cnidarian impression from the Late Ediacaran period (approx. 560 Ma). *Proceedings of the Royal Society B: Biological Sciences*, **281**, 20141202–20141202, https://doi.org/10.1098/rspb.2014.1202.

Liu, A.G., Kenchington, C.G. and Mitchell, E.G. 2015. Remarkable insights into the paleoecology of the Avalonian Ediacaran macrobiota. *Gondwana Research*, **27**, 1355–1380, https://doi.org/10.1016/j.gr.2014.11.002.

Mallmann, G., Chemale, F., Ávila, J.N., Kawashita, K. and Armstrong, R.A. 2007. Isotope geochemistry and geochronology of the Nico Pérez Terrane, Rio de la Plata Craton, Uruguay. *Gondwana Research*, **12**, 489–508, https://doi.org/10.1016/j.gr.2007.01.002.

Martin, H. 1965. *The Precambrian Geology of South West Africa and Namaqualand*.

Martin, M.W., Grazhdankin, D.V., Bowring, S.A., Evans, D.A.D., Fedonkin, M.A. and Kirschvink, J.L. 2000. Age of Neoproterozoic Bilaterian Body and Trace Fossils, White Sea, Russia: Implications for Metazoan Evolution. *Science*, **288**, 841–845.

Maslov, A., Meert, J., et al. 2013. New Constraints for the Age of Vendian Glacial Deposits (Central Urals). *Doklady Earth Sciences*, **449**, 303–308, https://doi.org/10.1134/S1028334X13030203.

Massey, C.I., Petley, D.N. and McSaveney, M.J. 2013. Patterns of movement in reactivated landslides. *Engineering Geology*, **159**, 1–19, https://doi.org/10.1016/j.enggeo.2013.03.011.

Matthews, J.J. 2015. *The Stratigraphical Context of the Ediacaran Biota of Eastern Newfoundland*. University of Oxford.

Matthews, J.J., Liu, A.G., Yang, C., McIlroy, D., Levell, B. and Condon, D.J. 2020. A Chronostratigraphic Framework for the Rise of the Ediacaran Macrobiota: New Constraints from Mistaken Point Ecological Reserve, Newfoundland. *GSA Bulletin*, **133**, 612–624, https://doi.org/10.1130/B35646.1.

McIlroy, D. and Brasier, M.D. 2017. Ichnological evidence for the Cambrian explosion in the Ediacaran to Cambrian succession of Tanafjord, Finnmark, northern Norway. *Geological Society, London, Special Publications*, **448**, 351–368, https://doi.org/10.1144/SP448.7.

McIlroy, D. and Walter, M.R. 1997. A reconsideration of the biogenicity of Arumberia banksi Glaessner & Walter. *Alcheringa: An Australasian Journal of Palaeontology*, **21**, 79–80, https://doi.org/10.1080/03115519708619187.

McMahon, W.J., Liu, A.G., Tindal, B.H. and Kleinhans, M.G. 2020. Ediacaran life close to land: Coastal and shoreface habitats of the Ediacaran macrobiota, the Central Flinders Ranges, South Australia. *Journal of Sedimentary Research*, **90**, 1463–1499, https://doi.org/10.2110/jsr.2020.029.

McMahon, W.J., Davies, N.S., Liu, A.G. and Went, D.J. 2022. Enigma variations: characteristics and likely origin of the problematic surface texture Arumberia, as recognized from an exceptional bedding plane exposure and the global record. *Geological Magazine*, **159**, 1–20, https://doi.org/10.1017/S0016756821000777.

Meinhold, G., Arslan, A., Jensen, S. and Kühnemann, V. 2025. Discovery of trace fossils in the Weesenstein Group, Elbe Zone, Germany, and its significance for revising the Ediacaran and Ordovician stratigraphy of Saxo-Thuringia. *Geological Magazine*, **162**, e10, https://doi.org/10.1017/S0016756825000032.

Menon, L. 2015. *Ediacaran Discoidal Impressions and Related Structures from Newfoundland, Canada and the Long Mynd, Shropshire, UK: Their Nature and Biogenicity*. http://purl.org/dc/dcmitype/Text, University of Oxford.

Menon, L.R., McIlroy, D. and Brasier, M.D. 2013. Evidence for Cnidaria-like behavior in ca. 560 Ma Ediacaran Aspidella. *Geology*, **41**, 895–898, https://doi.org/10.1130/G34424.1.

Menon, L.R., McIlroy, D., Liu, A.G. and Brasier, M.D. 2015. The dynamic influence of microbial mats on sediments: fluid escape and pseudofossil formation in the Ediacaran Longmyndian Supergroup, UK. *Journal of the Geological Society*, **173**, 177–185, https://doi.org/10.1144/jgs2015-036.

Menon, L.R., McIlroy, D. and Brasier, M.D. 2017. 'Intrites' from the Ediacaran Longmyndian Supergroup, UK: a new form of microbially-induced sedimentary structure (MISS). *Geological Society, London, Special Publications*, **448**, 271–283, https://doi.org/10.1144/SP448.12.

Merdith, A.S., Williams, S.E., et al. 2021. Extending full-plate tectonic models into deep time: Linking the Neoproterozoic and the Phanerozoic. *Earth-Science Reviews*, **214**, 103477, https://doi.org/10.1016/j.earscirev.2020.103477.

Miller, N., Johnson, P. and Stern, B. 2008. Marine versus non-marine environments for the Jibalah Group, NW Arabian shield: A sedimentologic and geochemical survey and report of possible metazoa in the Dhaiqa formation. *Arabian Journal for Science and Engineering*, **33**, 55–77.

Mills, A.J., Normore, L., Gomez, N., Dunning, G.R. and Lowe, D.G. 2024. A tale of two basins: juxtaposition of the Ediacaran fossil-bearing St. John's Basin against the Ediacaran glaciovolcanic Bonavista Basin on the Bonavista Peninsula, Avalon Zone, Newfoundland. *Atlantic Geoscience*, **60**, 131–150, https://doi.org/10.4138/atlgeo.2024.007.

Mills, B.J.W., Krause, A.J., Scotese, C.R., Hill, D.J., Shields, G.A. and Lenton, T.M. 2019. Modelling the long-term carbon cycle, atmospheric CO2, and Earth surface temperature from late Neoproterozoic to present day. *Gondwana Research*, **67**, 172–186, https://doi.org/10.1016/j.gr.2018.12.001.

Molén, M.O. 2023. Glaciation-induced features or sediment gravity flows – An analytic review. *Journal of Palaeogeography*, **12**, 487–545, https://doi.org/10.1016/j.jop.2023.08.002.

Moynihan, D.P., Strauss, J.V., Nelson, L.L. and Padget, C.D. 2019. Upper Windermere Supergroup and the transition from rifting to continent-margin sedimentation, Nadaleen River area, northern Canadian Cordillera. *GSA Bulletin*, **131**, 1673–1701, https://doi.org/10.1130/B32039.1.

Muscente, A.D., Bykova, N., et al. 2019. Ediacaran biozones identified with network analysis provide evidence for pulsed extinctions of early complex life. *Nature Communications*, **10**, 911, https://doi.org/10.1038/s41467-019-08837-3.

Narbonne, G.M. 1994. New Ediacaran Fossils from the Mackenzie Mountains, Northwestern Canada. *Journal of Paleontology*, **68**, 411–416.

Narbonne, G.M. 2005. The Ediacara Biota: Neoproterozoic Origin of Animals and Their Ecosystems. *Annual Review of Earth and Planetary Sciences*, **33**, 421–442, https://doi.org/10.1146/annurev.earth.33.092203.122519.

Narbonne, G.M. and Hofmann, H.J. 1987. Ediacaran biota of the Wernecke Mountains, Yukon, Canada. *Palaeontology*, **30**, 647–676.

Narbonne, G.M., Laflamme, M., Trusler, P.W., Dalrymple, R.W. and Greentree, C. 2014. Deep-Water Ediacaran Fossils from Northwestern Canada: Taphonomy, Ecology, and Evolution. *Journal of Paleontology*, **88**, 207–223, https://doi.org/10.1666/13-053.

Nelson, L.L., Ramezani, J., et al. 2022. Pushing the boundary: A calibrated Ediacaran-Cambrian stratigraphic record from the Nama Group in northwestern Republic of South Africa. *Earth and Planetary Science Letters*, **580**, 117396, https://doi.org/10.1016/j.epsl.2022.117396.

Niu, Y., Shi, G.R., Zhang, Q., Jones, B.G., Wang, X. and Zhao, G. 2024. Ediacaran Cordilleran-type mountain ice sheets and their erosion effects. *Earth-Science Reviews*, **249**, 104671, https://doi.org/10.1016/j.earscirev.2023.104671.

Noble, S.R., Condon, D.J., Carney, J.N., Wilby, P.R., Pharaoh, T.C. and Ford, T.D. 2015. U-Pb geochronology and global context of the Charnian Supergroup, UK: Constraints on the age of key Ediacaran fossil assemblages. *GSA Bulletin*, **127**, 250–265, https://doi.org/10.1130/B31013.1.

O'Connell, B., McMahon, W.J., et al. 2024. Transport of 'Nama'-type biota in sediment gravity and combined flows: Implications for terminal Ediacaran palaeoecology. *Sedimentology*, https://doi.org/10.1111/sed.13239.

Oyhantçabal, P., Siegesmund, S., Wemmer, K., Frei, R. and Layer, P. 2007. Post-collisional transition from calc-alkaline to alkaline magmatism during transcurrent deformation in the southernmost Dom Feliciano Belt (Braziliano–Pan-African, Uruguay). *Lithos*, **98**, 141–159, https://doi.org/10.1016/j.lithos.2007.03.001.

Palacios, T. 2024. The oldest fossil record in the Iberian Peninsula; lower Ediacaran acritarchs of the Tentudía Formation, Ossa-Morena Zone (OMZ), Southwest Iberian Massif. *Journal of Iberian Geology*, https://doi.org/10.1007/s41513-024-00266-6.

Pang, K., Wu, C., et al. 2021. New Ediacara-type fossils and late Ediacaran stratigraphy from the northern Qaidam Basin (China): Paleogeographic implications. *Geology*, **49**, 1160–1164, https://doi.org/10.1130/G48842.1.

Pauley, J.C. 1991. A revision of the stratigraphy of the longmyndian supergroup, welsh borderland, and of its relationship to the uriconian volcanic complex. *Geological Journal*, **26**, 167–183, https://doi.org/10.1002/gj.3350260209.

Pecoits, E. 2003. Sedimentología y consideraciones estratigráficas de la Formación Las Ventanas en su área tipo, Departamento de Maldonado, Uruguay. *Revista de la Sociedad Uruguaya de Geologia Publicacion Especial*, **1**, 124–140.

Pecoits, E., Gingras, M., Aubet, N. and Konhauser, K. 2008. Ediacaran in Uruguay: palaeoclimatic and palaeobiological implications. *Sedimentology*, **55**, 689–719, https://doi.org/10.1111/j.1365-3091.2007.00918.x.

Pecoits, E., Gingras, M.K. and Konhauser, K.O. 2011. Chapter 53 Las Ventanas and San Carlos formations, Maldonado Group, Uruguay. *Geological Society, London, Memoirs*, **36**, 555–564, https://doi.org/10.1144/M36.53.

Penn, J.L., Deutsch, C., Payne, J.L. and Sperling, E.A. 2018. Temperature-dependent hypoxia explains biogeography and severity of end-Permian marine mass extinction. *Science*, **362**, https://doi.org/10.1126/science.aat1327.

Perry, A.L., Low, P.J., Ellis, J.R. and Reynolds, J.D. 2005. Climate Change and Distribution Shifts in Marine Fishes. *Science*, **308**, 1912–1915, https://doi.org/10.1126/science.1111322.

Peters, S.E. and Gaines, R.R. 2012. Formation of the ‘Great Unconformity’ as a trigger for the Cambrian explosion. *Nature*, **484**, 363–366, https://doi.org/10.1038/nature10969.

Psarras, C., Donoghue, P.C.J., Garwood, R.J., Grazhdankin, D.V., Parry, L.A., Rogov, V.I. and Liu, A.G. 2023. Three-dimensional reconstruction, taphonomic and petrological data suggest that the oldest record of bioturbation is a body fossil coquina. *Papers in Palaeontology*, **9**, e1531, https://doi.org/10.1002/spp2.1531.

Pu, J.P., Bowring, S.A., et al. 2016. Dodging snowballs: Geochronology of the Gaskiers glaciation and the first appearance of the Ediacaran biota. *Geology*, **44**, 955–958, https://doi.org/10.1130/G38284.1.

Pyle, L.J., Narbonne, G.M., James, N.P., Dalrymple, R.W. and Kaufman, A.J. 2004. Integrated Ediacaran chronostratigraphy, Wernecke Mountains, northwestern Canada. *Precambrian Research*, **132**, 1–27, https://doi.org/10.1016/j.precamres.2004.01.004.

R Core Team. 2021. R: A Languange and Environment for Statistical Computing.

Reid, L.M., Holmes, J.D., Payne, J.L., García-Bellido, D.C. and Jago, J.B. 2020a. Taxa, turnover and taphofacies: a preliminary analysis of facies-assemblage relationships in the Ediacara Member (Flinders Ranges, South Australia). *Australian Journal of Earth Sciences*, **67**, 905–914, https://doi.org/10.1080/08120099.2018.1488767.

Reid, L.M., Payne, J.L., García-Bellido, D.C. and Jago, J.B. 2020b. The Ediacara Member, South Australia: Lithofacies and palaeoenvironments of the Ediacara biota. *Gondwana Research*, **80**, 321–334, https://doi.org/10.1016/j.gr.2019.09.017.

Retallack, G.J. 2022. Towards a glacial subdivision of the Ediacaran Period, with an example of the Boston Bay Group, Massachusetts. *Australian Journal of Earth Sciences*, **69**, 223–250, https://doi.org/10.1080/08120099.2021.1954088.

Rice, A.H.N., Edwards, M.B., Hansen, T.A., Arnaud, E. and Halverson, G.P. 2011. Chapter 57 Glaciogenic rocks of the Neoproterozoic Smalfjord and Mortensnes formations, Vestertana Group, E. Finnmark, Norway. *Geological Society, London, Memoirs*, **36**, 593–602, https://doi.org/10.1144/M36.57.

Rooney, A.D., Cantine, M.D., et al. 2020. Calibrating the coevolution of Ediacaran life and environment. *Proceedings of the National Academy of Sciences*, https://doi.org/10.1073/pnas.2002918117.

Runnegar, B., Gehling, J.G., Jensen, S. and Saltzman, M.R. 2024. Ediacaran paleobiology and biostratigraphy of the Nama Group, Namibia, with emphasis on the erniettomorphs, tubular and trace fossils, and a new sponge, Arimasia germsi n. gen. n. sp. *Journal of Paleontology*, **98**, 1–59, https://doi.org/10.1017/jpa.2023.81.

Sanchez Bettucci, L. and Linares, E. 1996. Primeras edades en Basaltos del Complejo Sierra de las Animas. *XIII Congreso Geológico Argentino y III Congreso de Exploración de Hidrocarburos, Actas*, **1**, 399–404.

Sandberg, C.G.S. 1928. The origin of the Dwyka Conglomerate of South Africa and other 'glacial' deposits. *Geological Magazine*, **65**, 117–139.

Sayles, S.D. 1914. The Squantum Tillite. *Museum of Comparative Zoology Bulletin*, **66**, 141–175.

Schwellnus, C. 1941. The Nama tillite in the Klein Karas Mountains. *Transactions Geologic Society of South Africa*, **44**, 19–33.

Scotese, C.R. 2016. PALEOMAP PaleoAtlas for GPlates and the PaleoData Plotter Program, PALEOMAP Project.

Scotese, C.R., Song, H., Mills, B.J.W. and van der Meer, D.G. 2021. Phanerozoic paleotemperatures: The earth's changing climate during the last 540 million years. *Earth-Science Reviews*, **215**, 103503, https://doi.org/10.1016/j.earscirev.2021.103503.

Segessenman, D.C. and Peters, S.E. 2024. Transgression–regression cycles drive correlations in Ediacaran–Cambrian rock and fossil records. *Paleobiology*, **50**, 150–163, https://doi.org/10.1017/pab.2023.31.

Shen, B., Xiao, S., Dong, L., Chuanming, Z. and Liu, J. 2007. Problematic macrofossils from Ediacaran successions in the North China and Chaidam blocks: implications for their evolutionary roots and biostratigraphic significance. *Journal of Paleontology*, **81**, 1396–1411, https://doi.org/10.1666/06-016R.1.

Shen, B., Xiao, S., Zhou, C., Kaufman, A.J. and Yuan, X. 2010. Carbon and sulfur isotope chemostratigraphy of the Neoproterozoic Quanji Group of the Chaidam Basin, NW China: Basin stratification in the aftermath of an Ediacaran glaciation postdating the Shuram event? *Precambrian Research*, **177**, 241–252, https://doi.org/10.1016/j.precamres.2009.12.006.

Shields, G.A., Mills, B.J.W., Zhu, M., Raub, T.D., Daines, S.J. and Lenton, T.M. 2019. Unique Neoproterozoic carbon isotope excursions sustained by coupled evaporite dissolution and pyrite burial. *Nature Geoscience*, 1–5, https://doi.org/10.1038/s41561-019-0434-3.

Socci, A.D. and Smith, G.W. 1990. Stratigraphic implications of facies within the Boston Basin. *In*: Socci, A. D., Skehan, J. W. and Smith, G. W. (eds) *Geology of the Composite Avalon Terrane of Southern New England*. 0., https://doi.org/10.1130/SPE245-p55.

Soldatenko, Y., El Albani, A., et al. 2019. Precise U-Pb age constrains on the Ediacaran biota in Podolia, East European Platform, Ukraine. *Scientific Reports*, **9**, 1675, https://doi.org/10.1038/s41598-018-38448-9.

Song, H., Huang, S., Jia, E., Dai, X., Wignall, P.B. and Dunhill, A.M. 2020. Flat latitudinal diversity gradient caused by the Permian–Triassic mass extinction. *Proceedings of the National Academy of Sciences*, **117**, 17578–17583, https://doi.org/10.1073/pnas.1918953117.

Środoń, J., Condon, D.J., et al. 2023. Ages of the Ediacaran Volyn-Brest trap volcanism, glaciations, paleosols, Podillya Ediacaran soft-bodied organisms, and the Redkino-Kotlin boundary (East European Craton) constrained by zircon single grain U-Pb dating. *Precambrian Research*, **386**, 106962, https://doi.org/10.1016/j.precamres.2023.106962.

Stein, C.L. and Smith, A.J. 1986. Authigenic Carbonate Nodules in the Nankai Trough, Site 583. *Initial Reports of the Deep Sea Drilling Project*, https://doi.org/10.2973/dsdp.proc.87.115.1986.

Stockey, R.G., Pohl, A., Ridgwell, A., Finnegan, S. and Sperling, E.A. 2021. Decreasing Phanerozoic extinction intensity as a consequence of Earth surface oxygenation and metazoan ecophysiology. *Proceedings of the National Academy of Sciences*, **118**, https://doi.org/10.1073/pnas.2101900118.

Suess, E., Balzer, W., Hesse, K.-F., Müller, P.J., Ungerer, C.A. and Wefer, G. 1982. Calcium Carbonate Hexahydrate from Organic-Rich Sediments of the Antarctic Shelf: Precursors of Glendonites. *Science*, **216**, 1128–1131, https://doi.org/10.1126/science.216.4550.1128.

Surprenant, R.L. and Droser, M.L. 2024. New insight into the global record of the Ediacaran tubular morphotype: a common solution to early multicellularity. *Royal Society Open Science*, **11**, 231313, https://doi.org/10.1098/rsos.231313.

Tang, F., Yin, C., Bengtson, S., Liu, P., Wang, Z. and Gao, L. 2008. Octoradiate Spiral Organisms in the Ediacaran of South China. *Acta Geologica Sinica - English Edition*, **82**, 27–34, https://doi.org/10.1111/j.1755-6724.2008.tb00321.x.

Tasistro-Hart, A.R. and Macdonald, F.A. 2023. Phanerozoic flooding of North America and the Great Unconformity. *Proceedings of the National Academy of Sciences*, **120**, e2309084120, https://doi.org/10.1073/pnas.2309084120.

Thomas, R.J., Chevallier, L.P., et al. 2002. Precambrian evolution of the Sirwa Window, Anti-Atlas Orogen, Morocco. *Precambrian Research*, **118**, 1–57, https://doi.org/10.1016/S0301-9268(02)00075-X.

Thompson, M.D. and Bowring, S.A. 2000. Age of the Squantum “tillite,” Boston Basin, Massachusetts; U-Pb zircon constraints on terminal Neoproterozoic glaciation. *American Journal of Science*, **300**, 630–655, https://doi.org/10.2475/ajs.300.8.630.

Thompson, M.D., Grunow, A.M. and Ramezani, J. 2007. Late Neoproterozoic paleogeography of the Southeastern New England Avalon Zone: Insights from U-Pb geochronology and paleomagnetism. *GSA Bulletin*, **119**, 681–696, https://doi.org/10.1130/B26014.1.

Tierney, F.L., Billings, M.P. and Cassidy, M.M. 1968. Geology of the city tunnel, Greater Boston, Massachusetts. *Boston Society of Civil Engineers*, **55**, 60–96.

Tindal, B. 2023. *Geological Constraints on Neoproterozoic Glacial Episodes*. PhD, University of Cambridge.

Vandyk, T.M., Kettler, C., Davies, B.J., Shields, G.A., Candy, I. and Le Heron, D.P. 2021. Reassessing classic evidence for warm-based Cryogenian ice on the western Laurentian margin: The “striated pavement” of the Mineral Fork Formation, USA. *Precambrian Research*, **363**, 106345, https://doi.org/10.1016/j.precamres.2021.106345.

Vernhet, E., Youbi, N., Chellai, E.H., Villeneuve, M. and El Archi, A. 2012. The Bou-Azzer glaciation: Evidence for an Ediacaran glaciation on the West African Craton (Anti-Atlas, Morocco). *Precambrian Research*, **196–197**, 106–112, https://doi.org/10.1016/j.precamres.2011.11.009.

Vickers-Rich, P., Ivantsov, A., et al. 2013. *Reconnaissance for an Ediacaran Fauna, Kingdom of Saudi Arabia*. Technical Report **SGS-TR-2013-5**.

Waggoner, B. 2003. The Ediacaran Biotas in Space and Time. *Integrative and Comparative Biology*, **43**, 104–113, https://doi.org/10.1093/icb/43.1.104.

Wang, C., Evans, D.A.D., et al. 2022. Proterozoic-Mesozoic development of the Quanji block from northern Tibet and the cratonic assembly of eastern Asia. *American Journal of Science*, **322**, 705–727, https://doi.org/10.2475/05.2022.03.

Wang, R., Shen, B., et al. 2023a. A Great late Ediacaran ice age. *National Science Review*, nwad117, https://doi.org/10.1093/nsr/nwad117.

Wang, R., Yin, Z. and Shen, B. 2023b. A late Ediacaran ice age: The key node in the Earth system evolution. *Earth-Science Reviews*, **247**, 104610, https://doi.org/10.1016/j.earscirev.2023.104610.

Wang, X., Zhang, X. and Liu, W. 2021a. Biostratigraphic constraints on the age of Neoproterozoic glaciation in North China. *Journal of Asian Earth Sciences*, **219**, 104894, https://doi.org/10.1016/j.jseaes.2021.104894.

Wang, X., Zhang, X., Zhang, Y., Cui, L. and Li, L. 2021b. New materials reveal *Shaanxilithes* as a *Cloudina*-like organism of the late Ediacaran. *Precambrian Research*, **362**, 106277, https://doi.org/10.1016/j.precamres.2021.106277.

Wang, X.-P., Chen, Z., Pang, K., Zhou, C.-M., Xiao, S., Wan, B. and Yuan, X.-L. 2021c. *Dickinsonia* from the Ediacaran Dengying Formation in the Yangtze Gorges area, South China. *Palaeoworld*, **30**, 602–609, https://doi.org/10.1016/j.palwor.2021.01.002.

Wang, Y., Zhuang, Q., Shi, C., Liu, J. and Zheng, L. 1980. Quanji Group along the northern border of Chaidamu Basin. *In*: Tianjin Institute of Geology and Mineral Resources (ed.) *Research on Precambrian Geology, Sinian Suberathem in China, Tianjin*. 214–230.

Wang, Z., Wang, J., Suess, E., Wang, G., Chen, C. and Xiao, S. 2017. Silicified glendonites in the Ediacaran Doushantuo Formation (South China) and their potential paleoclimatic implications. *Geology*, **45**, 115–118, https://doi.org/10.1130/G38613.1.

Wang, Z., Chen, C., et al. 2020. Wide but not ubiquitous distribution of glendonite in the Doushantuo Formation, South China: Implications for Ediacaran climate. *Precambrian Research*, **338**, 105586, https://doi.org/10.1016/j.precamres.2019.105586.

Wilby, P.R., Carney, J.N. and Howe, M.P.A. 2011. A rich Ediacaran assemblage from eastern Avalonia: Evidence of early widespread diversity in the deep ocean. *Geology*, **39**, 655–658, https://doi.org/10.1130/G31890.1.

Winterer, E.L. and Von der Borch, C.C. 1968. Striated pebbles in a mudflow deposit, South Australia. *Palaeogeography, Palaeoclimatology, Palaeoecology*, **5**, 205–211, https://doi.org/10.1016/0031-0182(68)90114-4.

Wong Hearing, T.W., Pohl, A., et al. 2021. Quantitative comparison of geological data and model simulations constrains early Cambrian geography and climate. *Nature Communications*, **12**, 3868, https://doi.org/10.1038/s41467-021-24141-5.

Wood, D.A., Dalrymple, R.W., Narbonne, G.M., Gehling, J.G. and Clapham, M.E. 2003. Paleoenvironmental analysis of the late Neoproterozoic Mistaken Point and Trepassey formations, southeastern Newfoundland. *Canadian Journal of Earth Sciences*, **40**, 1375–1391, https://doi.org/10.1139/e03-048.

Wood, R., Liu, A.G., et al. 2019. Integrated records of environmental change and evolution challenge the Cambrian Explosion. *Nature Ecology & Evolution*, **3**, 528–538, https://doi.org/10.1038/s41559-019-0821-6.

Wood, R., Bowyer, F.T., et al. 2023. New Ediacaran biota from the oldest Nama Group, Namibia (Tsaus Mountains), and re-definition of the Nama Assemblage. *Geological Magazine*, **160**, 1673–1686, https://doi.org/10.1017/S0016756823000638.

Woodhouse, A., Swain, A., Fagan, W.F., Fraass, A.J. and Lowery, C.M. 2023. Late Cenozoic cooling restructured global marine plankton communities. *Nature*, 1–6, https://doi.org/10.1038/s41586-023-05694-5.

Wu, C., Pang, K., et al. 2022. The rangeomorph fossil Charnia from the Ediacaran Shibantan biota in the Yangtze Gorges area, South China. *Journal of Paleontology*, 1–17, https://doi.org/10.1017/jpa.2022.97.

Xiao, Q., She, Z., et al. 2020. Terminal Ediacaran carbonate tempestites in the eastern Yangtze Gorges area, South China. *Palaeogeography, Palaeoclimatology, Palaeoecology*, **547**, 109681, https://doi.org/10.1016/j.palaeo.2020.109681.

Xiao, S., Bao, H., et al. 2004. The Neoproterozoic Quruqtagh Group in eastern Chinese Tianshan: evidence for a post-Marinoan glaciation. *Precambrian Research*, **130**, 1–26, https://doi.org/10.1016/j.precamres.2003.10.013.

Xiao, S., Chen, Z., Pang, K., Zhou, C. and Yuan, X. 2021. The Shibantan Lagerstätte: insights into the Proterozoic–Phanerozoic transition. *Journal of the Geological Society*, **178**, jgs2020-135, https://doi.org/10.1144/jgs2020-135.

Xiao, S.H. and Narbonne, G.M. 2020. Chapter 18 - The Ediacaran Period. *In*: Gradstein, F. M., Ogg, J. G., Schmitz, M. D. and Ogg, G. M. (eds) *Geologic Time Scale 2020*. 521–561., https://doi.org/10.1016/B978-0-12-824360-2.00018-8.

Yang, C., Rooney, A.D., et al. 2021. The tempo of Ediacaran evolution. *Science Advances*, **7**, eabi9643, https://doi.org/10.1126/sciadv.abi9643.

Yao, J., Xiao, S., Yin, L., Li, G. and Yuan, X. 2005. Basal Cambrian Microfossils from the Yurtus and Xishanblaq Formations (tarim, North-West China): Systematic Revision and Biostratigraphic Correlation of Micrhystridium-Like Acritarchs. *Palaeontology*, **48**, 687–708, https://doi.org/10.1111/j.1475-4983.2005.00484.x.

Youbi, N., Ernst, R.E., et al. 2020. The Central Iapetus magmatic province: An updated review and link with the ca. 580 Ma Gaskiers glaciation. *In*: Adatte, T., Bond, D. P. G. and Keller, G. (eds) *Mass Extinctions, Volcanism, and Impacts: New Developments*. 0., https://doi.org/10.1130/2020.2544(02).

Zhao, Y., Chen, M., et al. 2004. Discovery of a Miaohe-type Biota from the Neoproterozoic Doushantuo Formation in Jiangkou County, Guizhou Province, China. *Chinese Science Bulletin*, **49**, 2224–2226, https://doi.org/10.1007/BF03185792.

Zhou, C., Li, X.-H., Xiao, S., Lan, Z., Ouyang, Q., Guan, C. and Chen, Z. 2017. A new SIMS zircon U–Pb date from the Ediacaran Doushantuo Formation: age constraint on the Weng'an biota. *Geological Magazine*, **154**, 1193–1201, https://doi.org/10.1017/S0016756816001175.

Zhou, C., Yuan, X., Xiao, S., Chen, Z. and Hua, H. 2019. Ediacaran integrative stratigraphy and timescale of China. *Science China Earth Sciences*, **62**, 7–24, https://doi.org/10.1007/s11430-017-9216-2.

Zhou, X., Lu, Z., Rickaby, R.E.M., Domack, E.W., Wellner, J.S. and Kennedy, H.A. 2015. Ikaite Abundance Controlled by Porewater Phosphorus Level: Potential Links to Dust and Productivity. *The Journal of Geology*, **123**, 269–281, https://doi.org/10.1086/681918.

Zhu, M., Gehling, J.G., Xiao, S., Zhao, Y. and Droser, M.L. 2008. Eight-armed Ediacara fossil preserved in contrasting taphonomic windows from China and Australia. *Geology*, **36**, 867–870, https://doi.org/10.1130/G25203A.1.

Zieger-Hofmann, M., Zieger, J., et al. 2022. Correlation of Neoproterozoic diamictites in southern Namibia. *Earth-Science Reviews*, **233**, 104159, https://doi.org/10.1016/j.earscirev.2022.104159.